JOURNAL OF THE

AERONAUTICAL SCIENCES

VOLUME 25 APRIL, 1958 NUMBER 4

CONTENTS

Hypersonic Flight and the Re-Entry Problem (Twenty-First Wright Brothers Lecture) ..... H. JULIAN ALLEN 217

On Radial Deflection of a Cylinder of Finite Length With Various End Conditions... ..... L. TING AND S. W. YUAN 230

The Prospects for Magneto-Aerodynamics..... E. L. RESLER, JR., AND W. R. SEARS 235

Aeroelastic Instability at High Mach Number..... JAGANNATH P. CHAWLA 246

A Turbulent Analog of the Stewartson-Illingworth Transformation..... ..... FRED E. C. CULICK AND JACQUES A. F. HILL 259

Readers' Forum..... 263

Published by
INSTITUTE OF THE AERONAUTICAL SCIENCES, INC.

JOURNAL OF THE AERONAUTICAL SCIENCES

Editor: W. R. SEARS
Director, Graduate School of Aeronautical Engineering, Cornell University

Associate Editor: ROBERT R. DEXTER *Managing Editor:* RITA J. TURINO
Editorial Assistant: CAROLINE TAYLOR

Editorial Committee

Aerodynamics and Fluid Mechanics

Holt Ashley
H. Julian Allen
Dean R. Chapman
Francis H. Clauser
Hugh L. Dryden
John C. Evvard
Antonio Ferri
Alexander Flax
Wallace D. Hayes
R. T. Jones
Carl Kaplan
H. W. Liepmann
C. C. Lin
H. F. Ludloff
Harold Luskin
Clark B. Millikan
Henry T. Nagamatsu
H. J. E. Reid
George S. Schairer
G. B. Schubauer
John Stack
Theodore Theodorsen
Arthur N. Tifford
Th. von Kármán

Flight Testing

R. R. Gilruth
Melvin N. Gough
W. L. Howland
W. F. Milliken, Jr.

Rotating Wing Aircraft

F. B. Gustafson
K. H. Hohenemser
Bartram Kelley
R. B. Maloy
Ralph McClarren
R. H. Miller
R. H. Prewitt
Igor I. Sikorsky

Structures

John E. Duberg
R. R. Heldenfels
N. J. Hoff
Samuel Levy
J. F. McBrearty
W. Ramberg
E. E. Sechler
F. R. Shanley
C. R. Strang
S. Timoshenko

Meteorology

C. F. Brooks
D. M. Little
F. W. Reichelderfer
K. C. Spengler

Vibration and Flutter

Lee Arnold
M. A. Biot
R. L. Bisplinghoff
Harold A. Cheilek
I. E. Garrick
Martin Goland

Aircraft Design

W. E. Beall
E. H. Heinemann
Hall L. Hibbard
Richard Hutton
C. L. Johnson
A. A. Kartveli
F. K. Teichmann

Electronics

K. C. Black
M. V. Kiebert, Jr.
David S. Little
Paul Rosenberg
Giles J. Strickroth

Physiologic Problems

H. G. Armstrong
Louis H. Bauer
Robert J. Benford
W. Randolph Lovelace, II
Ross A. MacFarland

Flight Propulsion

William Bollay
George W. Brady
R. P. Kroon
Frank E. Marble
Abe Silverstein
E. S. Taylor

Instruments

Alan G. Binnie
Charles H. Colvin
Frank R. Cook
C. S. Draper
S. G. Eskin
C. F. Savage
R. C. Sylvander

SUBSCRIPTION RATES

JOURNAL OF THE AERONAUTICAL SCIENCES, Published Monthly. United States and Possessions: 1 Year, $15.00; Single Copies, $1.50. Foreign Countries Including Canada (American Currency Rates): 1 Year, $16.00; Single Copies, $1.50.

AERONAUTICAL ENGINEERING REVIEW, Published Monthly. United States and Possessions: 1 Year, $5.00; Single Copies, $0.50. Foreign Countries Including Canada (American Currency Rates): 1 Year, $6.00; Single Copies, $0.50.

Notices of change of address should be sent to the Institute at least 30 days prior to actual change of address.

Manuscripts for publication, proofs, and all correspondence should be addressed to the Editorial Office of the JOURNAL.

Publication Office, 20th and Northampton Sts., Easton, Pa. Correspondence regarding subscriptions may be addressed to the Editorial Office of the JOURNAL OF THE AERONAUTICAL SCIENCES, 2 East 64th Street, New York 21, N.Y.

© *Copyright, 1958, by the Institute of the Aeronautical Sciences, Inc.*

Second-Class Mail Privileges Authorized at Easton, Penna. Acceptance for mailing at a special rate of Postage provided for in the Act of August 24, 1912. Authorized April 29, 1937.

JOURNAL OF THE AERONAUTICAL SCIENCES

VOLUME 25 APRIL, 1958 NUMBER 4

Hypersonic Flight and the Re-Entry Problem

The Twenty-First Wright Brothers Lecture

H. JULIAN ALLEN*

Ames Aeronautical Laboratory, NACA

Introduction

Progress in transportation has been brought about more by revolutionary than by evolutionary changes in methods of propulsion. Over many centuries of use, sailing ships were greatly improved, yet they gave way to the steamship less than 100 years after the invention of this new means of propulsion. In less than 20 years the horse-drawn carriage was replaced by the automobile, and more recently, in this country, the steam locomotive has submitted to the Diesel engine.

Although these changes have often resulted in more economical transportation, they have not always done so. Speed improvement has also been an impetus. True, speed and economy often go hand in hand, but speed alone may constitute the sole reason for change, particularly when the vehicle has military usefulness. In the history of development of the airplane, speed has played a particularly prominent role.

At its inception, the airplane could hardly have been considered useful, militarily or otherwise. With its engine, which weighed 17 lbs. per hp., the first Wright brothers machine could barely fly. The initial success, in fact, is attributable to the knowledge and ingenuity of the inventors. They knew the vital need for providing their craft with a sufficiently great wing span to minimize the induced drag penalty imposed by the heavy engine. They then devised a biplane configuration which permitted the required long span to be realized with a minimum of structural weight. In spite of the marginal performance of the first Wright machine, the situation was clearly correctable. Charles Manly had already constructed, for the ill-fated Langley Aerodrome, an engine no heavier than the 12-hp. Wright engine which had produced, in three 10-hour tests, more than 50 hp.—a most remarkable achievement.

To the sagacious no doubt, while the general future of the airplane seemed bright, the military future seemed brilliant. Although the first Wright airplane had only reached 31 m.p.h., it was evident that high speed would be a particular virtue of the aircraft to come. This high speed would be unusually significant for the military airplane since it would provide an invulnerability to possible counterweapons. Progress in improvement was sufficient in the next 10 years to enable the airplane to play a supporting role in World War I, and, in the following 20 years to give it a decisive role in World War II. In spite of the fact that over this whole period the performance gains had been truly amazing, it then appeared that further significant increase in speed was unlikely. One cause was traceable to the propeller. As the aircraft speed had increased, the tip speed of the propeller had approached too close to the speed of pressure propagation in air. Thus compression shock losses occurred which seriously decreased the attainable lift-drag ratio of the blades, and the propulsive efficiency dropped accordingly. The use of thinner blade sections helped to delay the onset of the difficulty. However, this cure clearly was short-lived at best. Even presuming that the propeller difficulties could be circumvented, the increase in airplane drag to be anticipated at transonic and higher speeds would require such a large increase in power as to make the propulsion system again excessively heavy. The propeller-driven airplane powered by the piston engine had reached an impasse.

A drastic change was needed and it came. Before World War II was over, Sir Frank Whittle in England and engineers at the Junkers Company in Germany had developed turbojet engines that gave promise of providing the required high power at much lower weight

Presented before the Institute of the Aeronautical Sciences in the Natural History Building Auditorium, Smithsonian Institution, Washington, D.C.

* Chief, High-Speed Research Division.

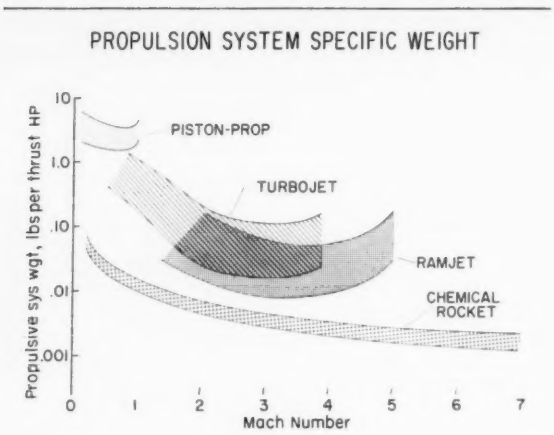

FIG. 1.

than could be attained with a piston engine and propeller combination. In the years since that war the promised performance of the turbojet engine has been realized. For the turbojet, higher speeds are not only desirable but necessary if high propulsive efficiency is to be achieved. It fell to the aerodynamicist to make the attainment of efficient transonic and, later, supersonic flight a reality. Thin wings of low aspect ratio provided one solution for reducing drag; swept wings, another; and means for promoting favorable interference between aircraft components, a third. The aerodynamic improvements, in general, brought new and severe structural problems. Nevertheless, in time the revolution was complete. The new breed of airplane did not provide the increased speed without penalty to range, for the aerodynamic efficiency had suffered a permanent setback from the wave drag which had been incurred on entering the supersonic regime. By careful aerodynamic design, however, the penalty incurred due to wave drag could be kept within acceptable bounds. The effect on range of the unavoidable decrease in lift-drag ratio could be minimized by the use of more efficient structures to provide a more favorable ratio of gross weight to empty weight.

Now that the sonic speed hurdle has been passed and truly supersonic flight has become commonplace, the quest for more speed continues, and it devolves upon the power plant to produce the increased thrust required for higher speed with a minimum increase in engine weight. Two engine types have received consideration in this regard. One is the ram-jet, which is a natural progression from the turbojet or turbojet with afterburner. The other is the rocket motor.

Fig. 1 shows the weights of the several power plants per unit thrust horsepower as a function of flight speed. The attractiveness of the rocket motor from this standpoint is obvious. It has a second advantage in having no maximum limit on speed as do the air-breathing engines. The limit of usefulness for the piston engine and propeller drive occurs when the speed is sufficiently high that the turbojet engine performs about as efficiently but with less weight. A similar limit occurs for the turbojet since at a sufficiently high speed (Mach Number of the order of 4) the compressor-turbine serves only to decrease the efficiency and increase the weight in comparison with the ram-jet. For the ram-jet the limit of usefulness as a heat engine occurs when, due to the heat of compression, the temperature of the air entering the combustor reaches the temperature for chemical equilibrium through combustion so no heat can be added. The problems of air-breathing engines have been[1] and are now the subject of much research. The limit speeds will certainly be increased but probably not indefinitely. A third advantage of the rocket motor is that since it does not require oxygen from the atmosphere it is not altitude limited. It performs best, in fact, *in vacuo*.

In spite of these advantages the rocket motor has the important disadvantage that it requires all of the chemicals needed for its operation to be carried aboard the vehicle it powers, while the other engines require only fuel. Fig. 2 shows the specific impulses in pounds thrust per pound per second of propellant for the several engines as a function of speed, and indicates the very inferior position of chemical rocket motors in this regard.

Clearly for high-speed short-range flight the rocket's advantage of light engine weight far outweighs its disadvantage of low specific impulse. However, for high-speed longer range flight the situation is not so obvious. It is the purpose in this paper to discuss such questions as: Can rocket vehicles compete with supersonic airplanes on an efficiency basis for long-range flight? What types of rocket vehicles, if any, appear attractive and under what circumstances? What new problems occur with these vehicles and do they appear surmountable?

PERFORMANCE

There are three types of long-range, high-speed vehicles which appear to be of particular interest—the ballistic, the glide, and the skip rocket. The typical flight trajectories of these rockets are shown in Fig. 3. The ballistic trajectory is so well known that no dis-

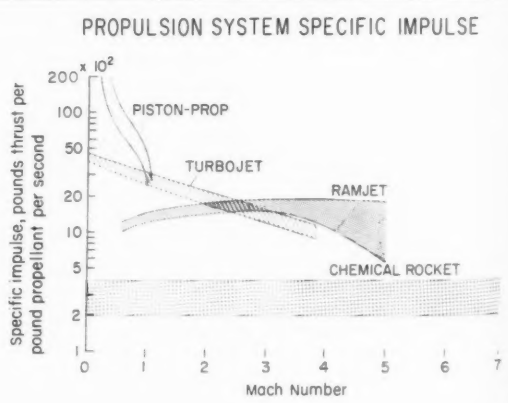

FIG. 2.

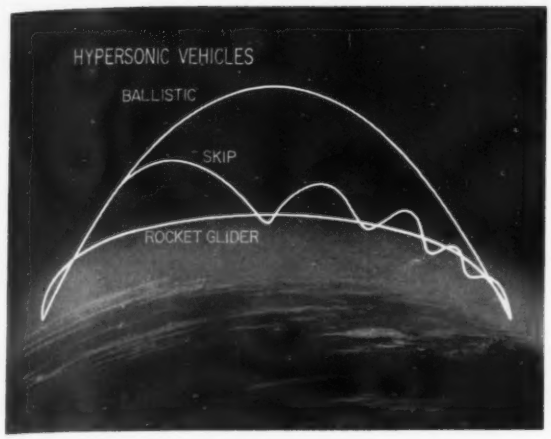

FIG. 3.

cussion of it is needed, but it is perhaps desirable to discuss the other two briefly.

The glide rocket is boosted by the rocket motor to an altitude and speed such that at the end of boost the dynamic pressure is that required for the vehicle to fly without power at some given lift coefficient. This altitude, which gradually decreases as the vehicle loses momentum due to drag, has been termed by Sänger[2, 3] the "equilibrium altitude." The aerodynamic lift required for flight is the weight less the centrifugal force resulting from the curved flight around the earth. Thus the aerodynamic lift, which equals the weight for low speed, becomes zero as satellite speed is approached. The equilibrium altitude as a function of speed, therefore, varies as shown in Fig. 4 for a range of wing loadings from 10 to 100 lbs. per sq.ft., and for a lift coefficient of 1/10. It is at first, I think, a little surprising that even for speeds closely approaching satellite speed the equilibrium altitudes remain below 250,000 ft. The glide path relative to the earth below it, therefore, remains very nearly flat at all supersonic speeds.

The skip-rocket trajectory is composed of a succession of ballistic paths each connected to the next by a "skipping phase" during which the vehicle enters the atmosphere, negotiates a turn at some given lift coefficient, and is then ejected from the atmosphere. In each skip the minimum altitude must be less, of course, than the equilibrium altitude at which the glide rocket would fly at the same lift coefficient and speed, since an increased lift is required to execute the turn.

For all three rocket vehicles we will be concerned only with those trajectories which yield the maximum range for a given energy input.[4] For the glide rocket and for the skip rocket, when in the atmosphere, the lift coefficient for maximum lift-drag ratio must be maintained to achieve this end. For the glide rocket, as noted earlier, the flight path angle during glide is the small angle required to maintain equilibrium altitude as speed decreases during flight. For the ballistic rocket the least-energy trajectory requires, as a function of range, the flight path angles at end of boost shown in Fig. 5. For the skip rocket having a very low lift-drag ratio the optimum angle at end of boost approaches that for the ballistic rocket. As the lift-drag ratio increases, the optimum angle will be less than that for the ballistic vehicle except at the longest ranges. This case is indicated in Fig. 5 for a skip rocket having a lift-drag ratio of 6.

It is a purpose of this paper not only to compare optimum performance of these three rocket vehicles with one another, but also with that of a typical supersonic airplane powered by air-breathing engines. The efficiency of flight is perhaps best measured by the cost of delivering a given payload a given distance—the higher the cost the lower the efficiency. It is clearly beyond the scope of this paper to actually compute this cost. Rather I will use as a measure of the efficiency the ratio of initial weight to payload. All the components which go to make up the initial weight (fuel, structure, engines, etc.) do not have the same unit cost nor, for a nonexpendable vehicle, is all this material wasted. Nevertheless, this ratio should provide a fair estimate of efficiency, particularly if the vehicle is considered expendable.

In the following, I will first discuss the ratio of initial weight to final ("empty") weight and then the ratio of

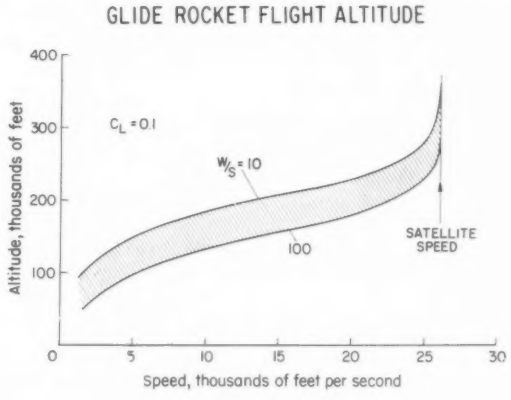

FIG. 4.

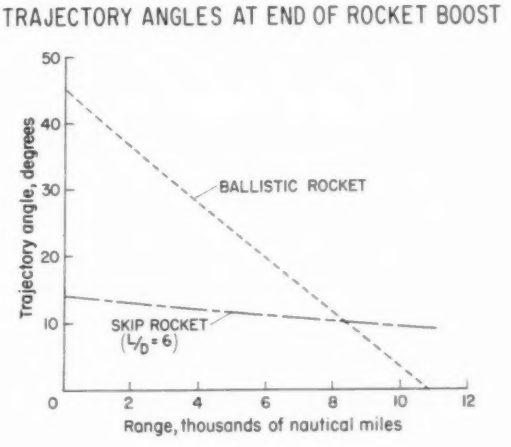

FIG. 5.

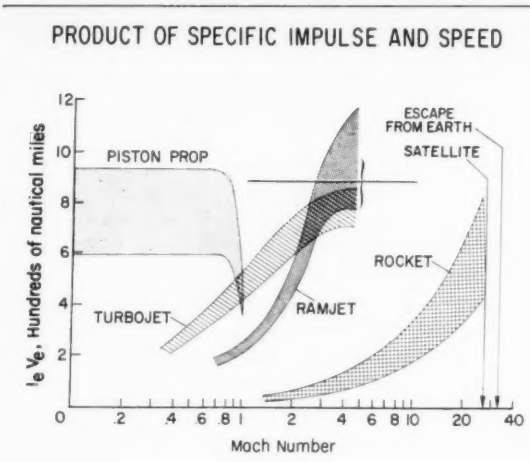

FIG. 6.

final weight to payload so that, lastly, some reasonably intelligent estimates, I hope, can be made of the relative flight efficiency.

For the aeronautical engineer the ratio of initial weight to final weight, and the range, are related by the Breguet equation. One form of this equation is

$$R = (L/D)IV \ln (W_i/W_f) \tag{1}$$

where

L/D = lift-drag ratio
W_i = take-off (initial) weight
W_f = landing (final) weight
I = specific impulse of the fuel
V = flight speed

The product IV is equal, of course, to the thermal propulsive efficiency times the heat value of a unit weight of fuel.

For the comparison of the several vehicles it would clearly be desirable to develop for rockets an equation corresponding to the Breguet equation. This was done in reference 4 in the following way. First, it should be noted that the speed at end of rocket boost can always be written

$$V_b = I_e g \ln (W_i/W_f) \tag{2}$$

where g = acceleration of gravity and I_e = effective specific impulse. The effective specific impulse would be the actual specific impulse of the propellant if the thrust were extremely large compared to the weight, and aerodynamic drag during boost were negligible. These conditions are not met in practice so the effective impulse must always be less than the actual, but for efficient designs the difference is not great.

Next we define an "effective drag" force in unpowered flight which, when multiplied by the range, equals the kinetic energy of the rocket vehicle—that is,

$$D_e R = (W_f/2g) V_b^2 \tag{3}$$

and an "effective lift" equal to the final weight

$$L_e = W_f \tag{4}$$

From Eqs. (3) and (4) it follows that

$$R = (L/D)_e (V_b^2/2g) \tag{5}$$

From Eqs. (2) and (5), then, a rocket equation similar in form to Breguet's equation is obtained,

$$R = (L/D)_e I_e V_e \ln (W_i/W_f) \tag{6}$$

where the effective velocity is

$$V_e = V_b/2 \tag{7}$$

With Eqs. (1) and (6) we will be able to make the first comparisons we desire, for it is the product

$$(L/D)IV$$

which constitutes our standard of excellence.

The power-plant characteristics of Fig. 2 may be replotted as $I_e V_e$ (which for airplane propulsion is IV) as a function of flight speed. These products are shown in Fig. 6. It is clear that this "propulsion product" is very low generally for the rocketcraft, for only at the highest flight speeds are they at all comparable with the

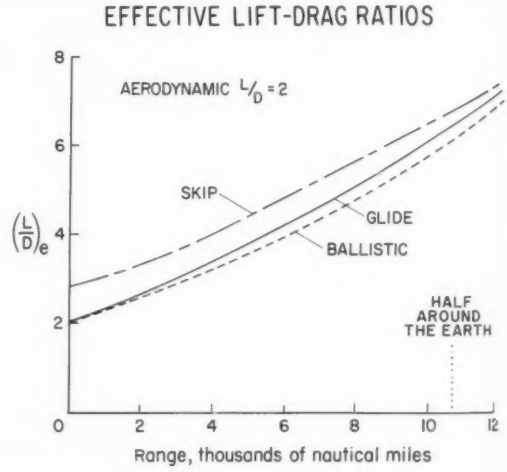

FIG. 7(a).

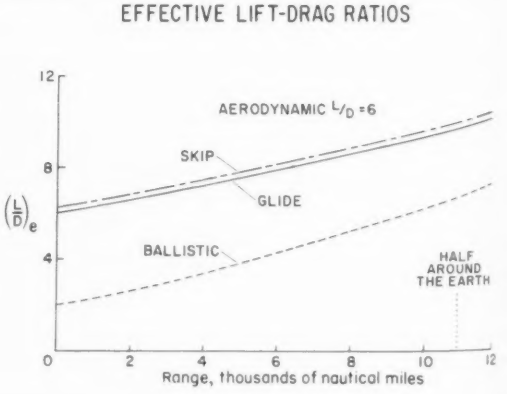

FIG. 7(b).

air-breathing engines. This, I think, is the dismal picture that has too often brought on the usual rejection of rocketcraft as reasonably efficient vehicles. However, it is not alone this propulsion product which determines the efficiency since it is also necessary to consider the effect of lift-drag ratio on the range-weight relation.

The effective lift-drag ratios for rockets have been determined in reference 4. In Fig. 7(a) are shown the effective lift-drag ratios for the ballistic rocket, and for the glide and skip rockets when the maximum aerodynamic lift-drag ratio has the low value of 2. The skip vehicle is best and, oddly enough, the glider is barely better than the ballistic rocket. In Fig. 7(b) is shown the effective lift-drag ratio for the ballistic rocket, again, and for the glide and skip rockets having the moderately high aerodynamic lift-drag ratio of 6. Here, the glide and skip vehicles are very nearly equal and, of course, the ballistic vehicle is much inferior. The most striking and important feature to be noted in both these Figures is that for all the rocketcraft the effective lift-drag ratio continuously increases with increasing range. One physical explanation for this increase for the ballistic rocket is the following. When the range is half the circumference of the earth, the speed at end of boost is required to be just satellite speed and for greater range no increase in energy input is required. Thus the effective drag, by definition, continuously decreases with increasing range. For the glide rocket a physical explanation that may perhaps be more apparent is that, as speed is increased to obtain longer range, the centrifugal force increases. Thus, less of the weight must be supported by aerodynamic lift, so that the aerodynamic drag is less.

If one now combines the results of Figs. 6 and 7, the ratio of initial-to-final weight can be obtained. These ratios are shown in Figs. 8(a) and 8(b) for the rockets and the airplane. The assumptions here are that the effective specific impulse for the rockets is a presently obtainable value (300) in Fig. 8(a) and twice this value (600), which might be obtainable in the future, in Fig. 8(b). It is also assumed that the IV product for the air-breathing, hydrocarbon-burning engine is slightly more than 800 nautical miles (see Fig. 6) and the aerodynamic lift-drag ratio for the airplane, the glide rocket, and the skip rocket is 6.

It is seen that when the range is sufficiently great, the improvement in effective lift-drag ratio offsets the disadvantageous propulsion characteristics of the rocket so that the rocket vehicles on the basis of weight ratio become competitive with the airplane.

It is next in order to consider the component weights, other than payload, that go to make up the final weight. As regards the propulsion system weight, the advantage here is, as we have seen, with the rocketcraft. For the structural weight the situation is not so clear. The ballistic vehicle would appear to have the advantage since it has no wings; however, it will tend to have the largest tankage weight. Consideration must also be given to the fact that it may experience large aerodynamic loads on entering the atmosphere which may adversely affect structural weight. The skip rocket will be similarly affected. A factor of primary significance for all of the long-range rocketcraft is that they are subject to intense aerodynamic heating as a result of the high speeds attained. Even if the heat can be radiated away, the high surface temperature must adversely affect structural weight. If the heat cannot all be radiated, then the final weight must be increased by the required weight of coolant needed to protect the vehicle. It is fitting, then, to discuss in some detail several of the more important factors which influence final weight in an effort to gain insight into the relative ratios of final weight to payload.

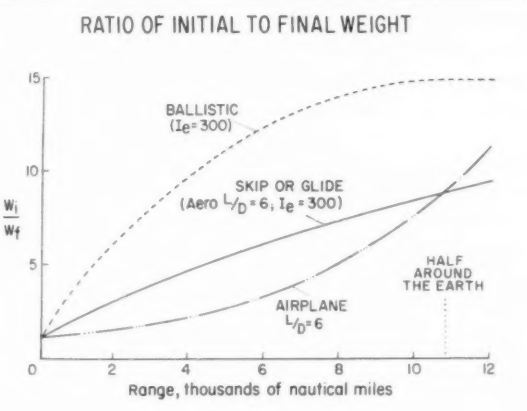

FIG. 8(a).

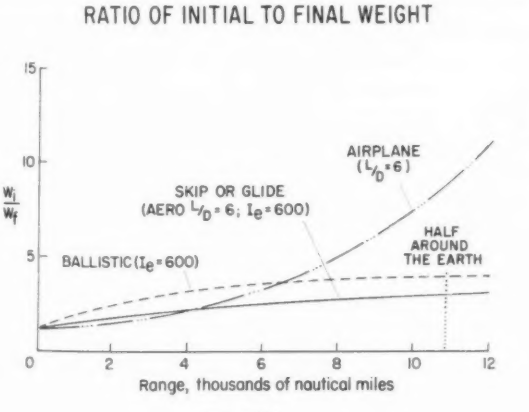

FIG. 8(b).

AERODYNAMIC HEATING

Before discussing the detailed heating problems associated with each of the rocket types it is well to review the nature of the problem from a general point of view. First, as indicated in Fig. 9, for long-range rockets the speeds at rocket burnout are generally 10,000 ft. per sec. or greater. In the usual case, the speed at landing will be very small compared to burnout speed so that virtually all of the kinetic energy imparted to

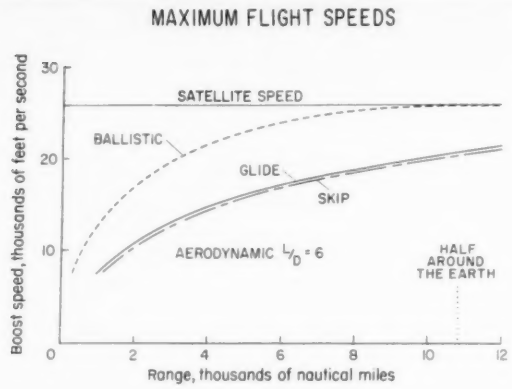

FIG. 9.

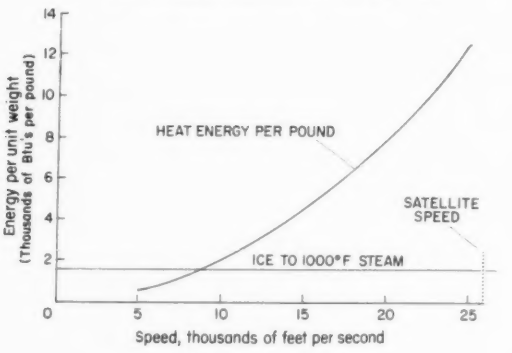

FIG. 10.

these craft must appear as heat. The heat equivalent per pound of weight as a function of flight speed is shown in Fig. 10. Also shown is the heat required to convert one pound of ice to steam at 1,000°F. as a "measuring stick" of what a fairly good coolant can handle. It is evident that if all of the kinetic energy appeared as heat within the vehicle and if the time rate of heat addition were so great that little of this heat could be radiated away, the problem might well be insurmountable even for some cooling system far better than this ice-to-steam system. To make this point clear, consider a ballistic vehicle having a flight range of 1,500 nautical miles which requires (see Fig. 9) speed at end of boost of something over 15,000 ft./sec. If the coolant to absorb the kinetic energy were three times as effective as the ice, all of the final weight would be in coolant (see Fig. 10) so that no payload could be carried. A practical vehicle could obviously not be built if the coolant weight required became even a large fraction of the final weight.

How can this situation be avoided? One of two solutions to the problem may be applied. If the rate of heat input is extremely high so that only a small part of the heat convected to the vehicle can be radiated away, then it is mandatory that a minimum fraction of the total kinetic energy appear as heat within the vehicle. On the other hand, if an excessively large fraction of the kinetic energy must be convected as heat to the vehicle, the time rate of this convective heating must be sufficiently slow that a large fraction of the heat can be radiated away at a surface temperature that is structurally permissible. Let us now consider, in light of the above, the heating problems of the ballistic, glide, and skip vehicles.

The ballistic vehicle requires the first method of solution for the heating problem since the convective heat input rates will usually be several orders of magnitude greater than the rate at which surfaces at temperatures near the melting point of metals can radiate. Fortunately,[5] the total convective heat input can be kept satisfactorily low since the fraction of the total kinetic energy change which must be accepted as convected heat to the vehicle is approximately

$$C_f S / 2C_D A$$

where C_f = the frictional drag coefficient per unit of the wetted area S and C_D = the total drag coefficient based on the reference area A.

That is to say, by making the friction drag small compared to the total drag, a large fraction of the heat developed is given to the atmosphere (wasted in shock waves, etc.), and the heat convected to the vehicle is kept small. Thus for ballistic vehicles the solution to the heating problem is to employ blunt shapes which have high pressure-drag coefficients.* In this way the heat convected can be kept to a per cent or so of the kinetic energy change so that the weight of coolant required may be correspondingly small.

For the glide vehicle, this solution of the heating problem is not possible since, for the glider to be superior to the ballistic vehicle, it must develop a high aerodynamic lift-to-drag ratio which is incompatible with a small ratio of frictional to total drag. However, the glider gradually converts its kinetic energy into range so that, unlike the ballistic vehicle, the time rate of convective heating is not large, as has been shown.[4] Hence for the glider there is a possibility of radiating all or nearly all the convected heat with surface temperatures which are structurally permissible. Eggers has shown, as indicated in Fig. 11 taken from reference 6, that the maximum temperature for radiation equilibrium of an average surface element for a conical glide vehicle could be about 1,600°F., which is within that allowable for some presently available materials. The radiation equilibrium temperature is adversely affected by increasing the wing loading and accordingly satisfactory values of loading will generally be low ones. Moreover, while the use of coolants at such "hot spots" as the bow of the body or wing leading edges, when present, would probably be required,[6, 7] the weight of the coolant should not necessarily be excessive.

* This idea has no doubt occurred to many. It has been brought to my attention, for example, that Dr. H. H. Nininger, Director of the American Meteorite Museum, had suggested the possible advantage of blunt shapes for missile re-entry bodies as a result of examination of the shape and surface condition of many metallic meteorites.

For the skip rocket, the heating problem appears to be much more formidable. As with the glider, high lift-drag ratios must be developed if it is to be a useful type, so that a low ratio of frictional to total drag cannot be realized. A large fraction of the kinetic energy change in the first skip, which is, in itself, a fairly large fraction of the total kinetic energy at burnout, must be convected to the vehicle. On the other hand, the time spent in the atmosphere is so small during this skip that the rate of convective heating is high. Eggers,[6] again, has indicated that a conical skip rocket during the first skip would reach the very high radiation equilibrium temperatures shown in Fig. 11. These temperatures would require the extensive use of coolant. Thus the weight penalty would probably be so excessive as to rule out this vehicle as impractical or even impossible except for short-range flights.

Aerodynamic Loads

The effects of aerodynamic loads on rocketcraft are more complex than they are for more conventional aircraft since when loads are high aerodynamic heating is usually intense. Thus rocket structures when subjected to high stress due, say, to bending moments may simultaneously be subjected to additional localized stress resulting from severe temperature differences within the structure. For hypersonic vehicles, in fact, thermal stress may easily be a principal cause for structural failure as is evidenced by the explosive spalling types of failures which, fortunately for us, occur with many meteors.[8]

By astute choice of materials and ingenuity in arrangement, however, the designer of a rocketcraft can keep these thermal stresses from reaching untenable values. Much work is, of course, in progress by structural engineers to find solutions to these thermal stress problems[9] and much more will be required before the same confidence in design can be provided that has been attained in the conventional structural design of airplanes. The time well may come when our knowledge of these thermal aspects will have advanced to the degree that only small penalty in weight will have to be paid for these complicating effects. On the other hand, the direct aerodynamic load will always be a vital factor in determining the weight of structure, and it is about these loads that we will be concerned here.

Since the aerodynamic loads are directly proportional to the dynamic pressure and hence the air density, it is well to note that the density variation in the atmosphere, over the range which is important from the load standpoint,[4, 5, 10] can be approximated by the exponential relation

$$\rho = \rho_0 e^{-\beta y}$$

where ρ_0 is sea-level density, β a constant, and y the altitude.

This particular functional relationship leads to some singularly interesting simplifications.[5] The variations with altitude of the deceleration experienced by a ballistic missile in its flight down through the atmosphere is a case in point. The velocity can be expressed as

$$V = V_E e^{-[C_{D\rho_0}Ag/(2\beta W \sin\theta_E)]e^{-\beta y}}$$

where

θ_E = trajectory angle below the horizontal
V_E = velocity on entrance to the atmosphere
C_D = drag coefficient
g = acceleration of gravity
W = weight
A = reference area on which the drag coefficient is based

and the deceleration in terms of g is

$$(dV/dt)/g = -(C_D\rho_0 A V_E^2/2W) \times e^{-\beta y} e^{-[C_{D\rho_0}Ag/(\beta W \sin\theta_E)]e^{-\beta y}}$$

If the speed at impact is less than about 61 per cent of entrance speed, which will usually be the case, then it can be shown that the maximum deceleration is simply

$$[(dV/dt)/g]_{max} = -(\beta V_E^2 \sin\theta_E)/2ge$$

where e is the Naperian logarithm base. That is to say, the maximum deceleration that can be experienced is

RADIATION EQUILIBRIUM TEMPERATURES

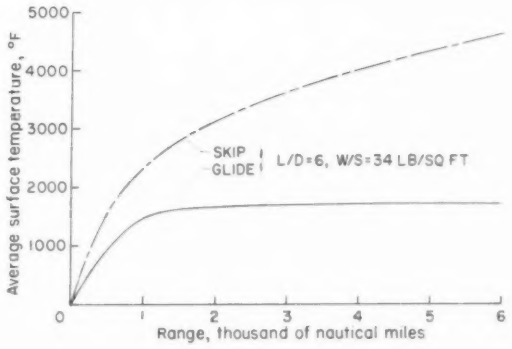

FIG. 11.

EFFECT OF SIZE ON DECELERATION OF IRON SPHERES

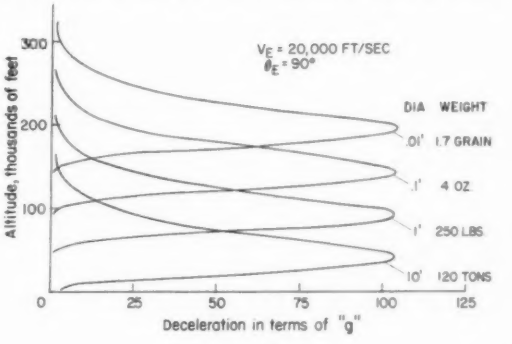

FIG. 12.

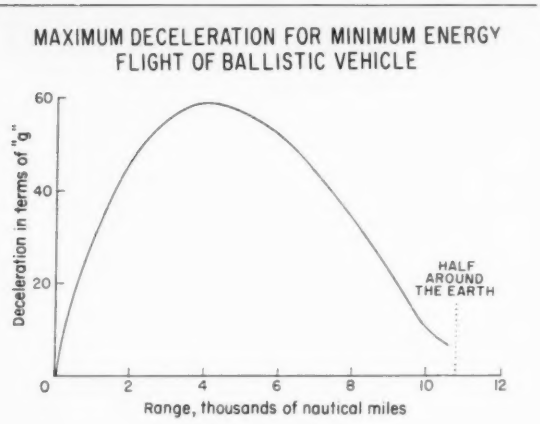

FIG. 13.

independent of the drag coefficient and, hence, of the vehicle's shape. This deceleration is also independent of the weight.

As an arbitrary example consider a series of solid iron spheres which have diameters ranging from 1/100 ft. to 10 ft. and for which the entrance velocity is 20,000 ft. per sec. and flight path is vertical ($\theta_E = 90°$). These spheres range in weight from less than 2 grains to over 100 tons. The decelerations for each is shown in Fig. 12. It is seen that not only is the maximum deceleration the same for all, but the functional relation of the deceleration with altitude is also identical. The deceleration curve is simply shifted to higher altitudes the lighter the sphere. Moreover, even for the heaviest sphere the maximum deceleration is reached prior to impact, so it is to be expected that for any ballistic vehicle which employs a high-drag shape to minimize the heating problem the maximum deceleration will similarly be reached before impact. It is also important to note that for each of the iron spheres the decelerations are large compared to gravity over a range of altitude of about 100,000 ft. This is also the range over which the heating rates are high.

For a ballistic vehicle which for a given range has the least kinetic energy at rocket burnout, both the velocity and trajectory are determined so that the deceleration can be calculated. This deceleration is given in Fig. 13. It is seen that the worst deceleration occurs for a range of 4,000 nautical miles when it is something less than 60 times gravitational acceleration. The maximum deceleration falls off with increasing range in spite of the fact that the burnout speed is increasing because the angle of approach to the earth becomes more flattened and so the time rate of density change is decreasing enough to more than offset the speed increase.

In any event, for the nose portion of a ballistic vehicle which is of bluff shape, necessitated by aerodynamic heating considerations, the decelerations shown in Fig. 13 are not so high as to seriously increase the structural weight. In fact for ranges of half the earth circumference and greater, the decelerations are within human tolerance so that return of a manned satellite in the form of a ballistic-type vehicle seems reasonable[4] even when aerodynamic lift is not employed to minimize the re-entry forces experienced.[6, 11]

For the glide rocket, the aerodynamic load problem is, in the main, the same as that for the conventional airplane with the exception that we must deal, in whole or in part, with a hot structure. Moreover, the gust load problem is as yet not well defined.

For the skip rocket, the aerodynamic loads, in contrast with aerodynamic heating, do not appear to present too severe a problem. The normal accelerations which occur in the first skip are shown as a function of total range in Fig. 14. The aerodynamic lift-drag ratio assumed is 6. It is seen that these normal accelerations generally are of the order we have become accustomed to in fighter airplane design. Even aside from aerodynamic heating consideration, however, the structural problem is far more serious than for the glide rocket.

STABILITY

The aerodynamic stability of rocketcraft presents some unusual problems which can influence both structure and guidance importantly.

For the ballistic missile, Friedrich and Dore[12] have given a general method for the analysis of the stability. In reference 13, this method was used with certain simplifying assumptions to describe the oscillatory behavior of a ballistic body at supersonic speeds. The general solution for the angle of attack, α, is

$$\alpha = e^{k_1 e^{-\beta y}} [C_1 J_0(2\sqrt{k_2}\, e^{-(\beta y/2)} + C_2 Y_0(2\sqrt{k_2}\, e^{-(\beta y/2)})]$$

In this equation $J_0(\,)$ and $Y_0(\,)$ are the zero-order Bessel functions of the first and second kinds, respectively. The "dynamic stability" factor is

$$k_1 = [g\rho_0 A/(4\beta W \sin\theta_E)]\,[C_D - C_{L_\alpha} + (C_{m_q} + (C_{m_{\dot\alpha}})\,(l/\sigma)^2]$$

while the "static stability" factor is

$$k_2 = -[g\rho_0 A/(2\beta^2 W l \sin^2\theta_E)]\,[C_{m_\alpha}(l/\sigma)^2]$$

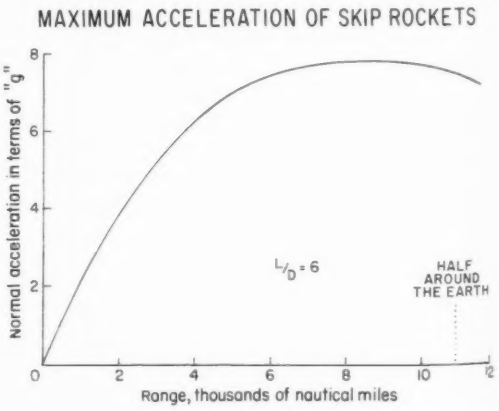

FIG. 14.

and

C_D = the drag coefficient
$C_{L\alpha}$ = the rate of change of lift coefficient with angle of attack
C_{mq} = the rate of change of moment coefficient with angular velocity
$C_{m\dot{\alpha}}$ = the rate of change of moment coefficient with time rate of change of angle of attack
$C_{m\alpha}$ = rate of change of moment coefficient with angle of attack
l/σ = ratio of the characteristic length to the radius of gyration
C_1, C_2 = constants of integration

The other symbols are as previously defined.

If the body on entering the atmosphere has its axis misaligned by an angle α_E with respect to the flight path but has no angular velocity, then C_2 is zero and the solution becomes

$$\alpha/\alpha_E = e^{k_1 e^{-\beta y}} J_0(2\sqrt{k_2}\, e^{-(\beta y/2)})$$

Then to illustrate the typical oscillatory behavior, suppose k_2 has a value of 10^5, which is a likely one, and k_1 has in turn the values -10 (damped), 0, $+10$ (undamped). The angle of attack variations with altitude would then be those shown in Fig. 15. If we look first at the oscillations when the dynamic stability factor is zero, it will be seen that during the descent as the air density increases the missile responds by pitching about zero angle with decreasing amplitude. The motion, thus, is a damped one, as seen by the envelope curve, but not damped in the usual sense that energy has been removed from the system. Rather, this behavior is akin to the motion that would occur with an oscillating mass on a spring if the spring constant were to increase continually. The effect of the dynamic stability factor on the amplitude, in fact, only becomes significant in decreasing ($k_1 = -10$) or increasing ($k_1 = +10$) the amplitude at altitudes below about 100,000 ft. where the amplitude has already been reduced to one-tenth the original value.

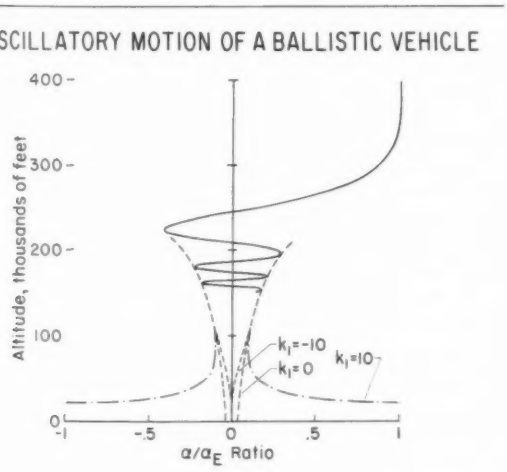

FIG. 15.

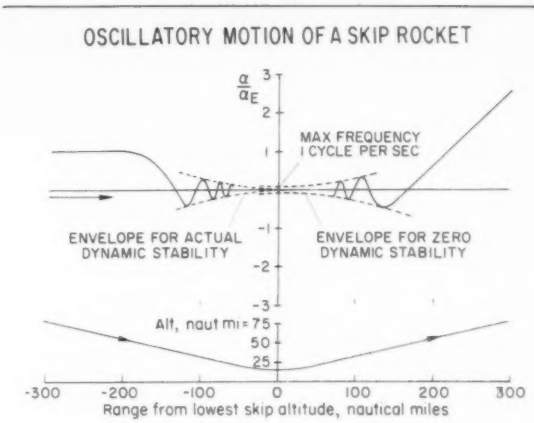

FIG. 16.

The effect of the oscillations that occur must be allowed for in the design of whatever cooling system is used to protect the vehicle from the aerodynamic heating that is experienced, since the local heat input rate will be changed by the motion from what they would be for the case when α is zero.

The frequency can also be determined by the method of reference 13. It increases with decreasing altitude until the altitude for maximum deceleration is reached—i.e., where the velocity is 61 per cent of the entrance speed—and then decreases. The frequency, in a typical case, may easily become as high as 10 cycles per sec. and hence may introduce important stresses due to inertial loads which must be considered in the structural design. Proper orientation of the vehicle by reaction controls prior to the entrance to the atmosphere can, of course, prevent the occurrence of such additional problems.

For the long-range glide rocket which properly follows the "equilibrium" trajectory, the stability problems are generally those for conventional airplanes except that, at the highest speeds, when a sizable part of the vehicle's weight may be offset by the centrifugal force due to the curved path around the earth, the dynamic pressure is less than at slower speeds so the frequency of all oscillatory motions is correspondingly lower.

The angular motion of a skip rocket during the first part of the skip when the vehicle is approaching the earth resembles the behavior noted for ballistic vehicles. During the second part of a skip when the vehicle leaves the atmosphere some interesting motions are possible and the behavior during a complete skip for a typical vehicle is thus worth some discussion. As an example, consider a skip rocket which consists essentially of a triangular plan-form wing with large leading-edge-sweep angle and with a root-chord length of about 50 ft. For an assumed wing loading of about 20 lbs. per sq. ft., a lift-drag ratio of 6, and a flight range of about 4,000 nautical miles, the speed on entering the

atmosphere will be 14,500 ft. per sec. before the first skip at a flight path angle, θ, of about 12° below the horizontal. The path during the first skip is shown in the lower part of Fig. 16. Suppose on the approach to the earth the vehicle has no angular velocity but is pitched an angle α_E away from the correct trim angle. If the static margin is 5 per cent of root chord, then the initial angular response to the increasing dynamic pressure, which, as with the ballistic vehicle, is mathematically expressible as a Bessel function of the first kind (zero order), is that shown on the left in the upper part of Fig. 16. The amplitude of the oscillation diminishes and frequency increases as the bottom of the skip is approached. The maximum frequency reached is slightly less than one cycle per sec. If the dynamic stability were zero the motion would diverge as the vehicle left the atmosphere. Now, curiously enough, while the motion during the outgoing flight could be represented by the reverse of the same Bessel function, it might not be the same since the general solution is of the form

$$\alpha = C_1 J_0(\ ) + C_2 Y_0(\ )$$

and it is possible that C_1 may be zero rather than C_2. In the event that this is the case, the Bessel function of the second kind (zero order) gives the motion shown on the right in the upper part of the Figure—that is, the vehicle is left with an angular velocity as it leaves the atmosphere. This tumbling would not present a serious problem since the angular rate is only 1/10 r.p.m. which could be checked readily by reaction controls. Fortunately, it appears that the dynamic stability would actually be so stabilizing for the case assumed as to well damp the motion as the bottom of the skip was approached, as is also indicated in the Figure.

In the flight of a glide rocket, the flight path at rocket burnout may accidentally be higher or lower than the equilibrium altitude or the flight path angle may accidentally be higher or lower than that required to follow the equilibrium trajectory. In either event, the vehicle will follow a skip path before recovery to the equilibrium path may be effected. In this event it follows, from what has been said about the skip-rocket stability problem, that if the glide rocket oscillates, it will do so at lower frequency than it would at equilibrium altitude when above this altitude, and at higher frequency when below it. The amplitude variation would, of course, be the opposite of this behavior.

Comparison of Flight Efficiencies

In the section on performance it was pointed out that the measure of efficiency for long-range flight of the three types of rockets and of the supersonic airplane would be chosen as the ratio of the initial weight to payload. It is in order, now, in the light of the discussion of aerodynamic heating, loading, and stability, to adjudge the relative efficiencies of these vehicles. To review, on the basis of the ratios of initial to final weight given in Fig. 8(a), it was noted that for ranges less than half the circumference of the earth, the supersonic airplane was the most attractive and the ballistic vehicle the least. The glide and skip rockets are not only intermediate in this regard but have approximately equal weight ratios.

On the other hand, for the ballistic vehicle the payload will generally be a larger fraction of the final weight than for the other vehicles since (1) by using a high drag shape for the re-entry body the coolant weight to protect it from aerodynamic heating will generally be small; (2) the re-entry body is relatively small and robust so that its structural weight should be low in spite of the large drag and side forces that may be experienced; (3) if, then, the payload is a large fraction of the re-entry body weight, the propellant tankage weight, which is directly geared to this weight, can be kept small through clever design; and (4) the motor weight, as for all the rocketcraft, will be low (see Fig. 1).

For the glide rocket in comparison with the airplane the ratio of payload to final weight has a chance of being superior by virtue of the engine weight advantage. However, it was noted that low wing loading appears to be a necessity for these vehicles if little or no coolant is to be required, and thus this rocketcraft does not have the natural robustness of the ballistic re-entry body. Rather, the structural problem is more nearly that for the conventional airplane with the exception that the surface, at least, must be able to withstand high temperatures. Success or failure of glide rockets is clearly to be determined by the state of the metallurgical and structural arts and the ingenuity of the designer.

The skip rocket is certainly unattractive for the present at least. Its coolant requirements are severe. Moreover, the structural loads are fairly large and occur when aerodynamic heating is intense. Thus, it is to be expected that the disadvantage of high coolant and structural weight will far more than offset the very marginal advantage it has as regards initial-to-final-weight ratio when compared with the glide rocket.

In short, it is my opinion that the ballistic vehicle can compare very favorably with the supersonic airplane for long range as well as short range flight and the glide rocket may also prove to be attractive, but not so the skip rocket.

New Problems of Hypervelocity Vehicles

Up to this point the discussion of the problems of rocket vehicles has been confined to the effects of phenomena which have in the past been important ones for lower speed aircraft and will continue to be important for aircraft of all speeds. Now with considerable extension of both speed and altitude, other phenomena also become important. The nature of some problems will be altered, as a result, and new problems, of course, will be encountered.

First, it is well to note that our interest in bluff bodies for ballistic vehicles in particular, and in rounded-nosed bodies generally, has changed our emphasis in aerody-

namics. The detached bow waves which occur with such bodies at high supersonic speeds complicate the calculations of the flow-field characteristics. In the present period, much attention is being given to such studies.[14] In addition, at the very high altitudes attained by most of the rocketcraft, the mean free path of air molecules can be of the same order, or long, compared to the dimensions of the vehicles. Thus, slip-flow and free-molecule-flow studies are of interest, particularly for satellite vehicles.[10] The aerodynamicist must deal with air having unfamiliar states and properties.

Second, at hypersonic speeds where, for example, air is greatly decelerated, it may undergo considerable change in composition,[15] the degree of change depending upon many factors. Dissociation of oxygen and nitrogen molecules can occur and, in addition, thermal ionization of many of the constituents. It is naturally to be expected that the convective heat transfer will, as a result, be altered from what it was for the "perfect" gas, and this has been the subject of much recent research effort.[16] Moreover, the decelerated gas becomes capable of radiating energy and the radiative heat transfer must generally be considered for hypersonic vehicles, particularly for long-range ballistic rockets. It is not only the aerodynamic heating problems that are affected. The fact that at very high air temperature the gas becomes electrically conductive[16] introduces new problems in radio wave transmission and reception. In addition, a conducting gas flow can, of course, be influenced by a magnetic field. The study of such flows, which has been termed "magneto gas dynamics," is still in too primitive a state to indicate how important a role it can play, but many interesting possibilities suggest themselves.[17]

Third, our experience with airplanes powered by air-breathing engines has naturally been restricted to the stratosphere, or lower. Our ignorance increases with altitude. For rockets, literally, "the sky's the limit," and it is not surprising that a great emphasis has now been placed on obtaining a more thorough understanding of the whole atmosphere.[10] These studies are not aimed at an understanding of the chemical and physical characteristics alone, but also of the occurrence of high-energy particles, from meteors to cosmic rays, and the nature of the problems they will promote.

This discussion of new problems has only touched upon a few of the known phenomena which become of interest in consideration of high-speed rockets. Certainly numerous others will appear as the conquest of space progresses. Faced with such a nebulous state of affairs it is not surprising that our approach to these new problems is a cautious one. It is well to note, however, that in this regard the present situation is certainly analogous to that which the Wright brothers faced at the turn of the century. If we give the same painstaking and intelligent treatment to our problems as they gave to theirs a half century ago, our success seems assured.

References

[1] Silverstein, Abe, *Research on Aircraft Propulsion Systems*, The Twelfth Wright Brothers Lecture, Journal of the Aeronautical Sciences, Vol. 16, No. 4, pp. 197–226, April, 1949.

[2] Sänger, Eugen, *Raketen-flugtechnik;* R. Oldenbourg, Berlin, 1933.

[3] Sänger, E., and Bredt, I., *A Rocket Drive for Long Range Bombers*, BuAer Navy Dept., Trans. CGD-32, 1947.

[4] Eggers, Alfred J., Jr., Allen, H. Julian, and Neice, Stanford E., *A Comparative Analysis of the Performance of Long Range Hypervelocity Vehicles*, NACA TN 4046, 1957 (supersedes NACA RM A54L10).

[5] Allen, H. Julian, and Eggers, A. J., Jr., *A Study of the Motion and Aerodynamic Heating of Missiles Entering the Earth's Atmosphere*, NACA TN 4047, 1957 (supersedes NACA RM A53D28).

[6] Eggers, A. J., Jr., *Performance of Long Range Hypervelocity Vehicles*, Jet Propulsion, Vol. 27, No. 11, pp. 1147–1151, November, 1957.

[7] Stalder, Jackson R., *A Survey of Heat Transfer Problems Encountered by Hypersonic Aircraft*, Jet Propulsion, Vol. 27, No. 11, pp. 1178–1184, November, 1957.

[8] Nininger, H. H., *Out of the Sky; An Introduction to Meteoritics*, University of Denver Press, 1952.

[9] Batdorf, Samuel B., *Structural Problems in Hypersonic Flight*, Jet Propulsion, Vol. 27, No. 11, pp. 1157–1161, November, 1957.

[10] Hansen, C. Frederick, *Some Characteristics of the Upper Atmosphere Pertaining to Hypervelocity Flight*, Jet Propulsion, Vol. 27, No. 11, pp. 1151–1156, November, 1957.

[11] Ferri, Antonio, Feldman, Lewis, and Daskin, Walter, *The Use of Lift for Re-entry From Satellite Trajectories*, Jet Propulsion, Vol. 27, No. 11, pp. 1184–1191, November, 1957.

[12] Friedrich, Hans R., and Dore, Frank J., *The Dynamic Motion of a Missile Descending Through the Atmosphere*, Journal of the Aeronautical Sciences, Vol. 22, No. 9, pp. 628–632, 638, September, 1955.

[13] Allen, H. Julian, *Motion of a Ballistic Missile Angularly Misaligned With the Flight Path Upon Entering the Atmosphere, and Its Effect Upon Aerodynamic Heating, Aerodynamic Loads, and Miss Distance*, NACA TN 4048, 1957 (supersedes NACA RM A56F15).

[14] Lees, Lester, *Recent Developments in Hypersonic Flow*, Jet Propulsion, Vol. 27, No. 11, pp. 1162–1178, November, 1957.

[15] Hansen, C. Frederick, *Approximations for the Thermodynamic and Transport Properties of High-Temperature Air*, NACA TN 4150, 1958.

[16] Rose, P. N., *Physical Gas Dynamics Research at the AVCO Research Laboratories*, AVCO Res. Rep. No. 9, May, 1957.

[17] Sears, William, *The Prospects for Magneto Aerodynamics*, paper presented at the IAS National Summer Meeting, June 17–20, 1957.

(Discussion of the Lecture follows)

Discussion of the Lecture

Antonio Ferri, Director, Aerodynamics Laboratory, Polytechnic Institute of Brooklyn: I was very pleased to be invited to comment on this excellent and stimulating paper which treats the subject of long-range high-speed flight since I am extremely interested in this field. I agree completely with the speaker on his concluding remark that the rocket glider appears attractive for long-range flight, and I concur in general with many of the technical analyses presented.

I shall limit my comments to two topics. First, I believe that the comparison presented between the heating problems encountered by using a skip trajectory and a glider trajectory is not necessarily indicative of the relative merits of the two solutions because the comparison has been made on the basis of maximum

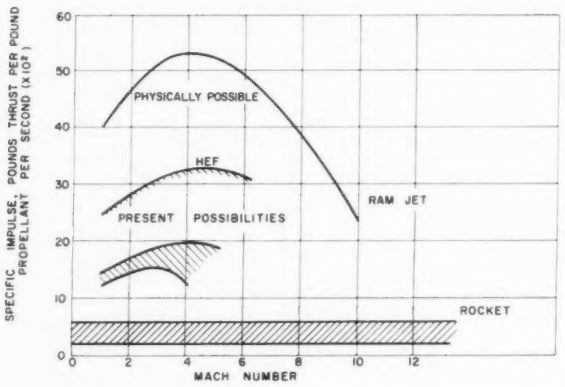

FIG. 1.

temperature for radiation equilibrium. The skip vehicle can take advantage of transient effects in order to reduce the surface temperature by utilizing the heat capacity of the vehicle structure. These effects if used to their best advantage can be important and therefore must be considered. In reference 1, a skip trajectory has been analyzed for a different application and it was shown that the transient effects due to the presence of the small heat sink represented by the structure of the vehicle can keep the surface temperature much below the value corresponding to the maximum temperature of radiation equilibrium.

The second comment is related to the comparison between ballistic vehicles, gliders, and airplanes with air breathing engines. I have a somewhat different opinion on the relative possibilities of rocket and jet engines and of airplanes with continuous propulsion and rocket glider vehicles when compared only from the point of view of long-range flight possibilities.

I am much more optimistic on the possibilities of air breathing engines and airplanes for the application considered. As an example, I do not find any physical reason why, in this analysis, we should not consider high energy fuels as described in the technical literature

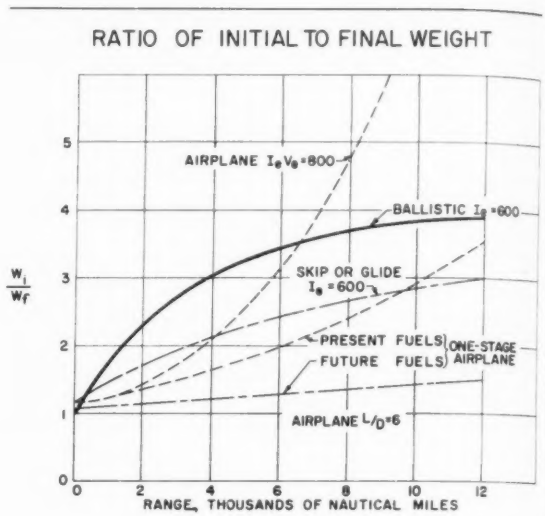

FIG. 2.

(see, for example, reference 2). Then much larger impulses can be obtained in ram-jets than assumed by the speaker (see Fig. 1). These improvements alone affect strongly the terms of the comparisons between airplanes and gliders, as shown in Fig. 2.

In connection with the high-speed long-range airplane configurations, I firmly believe that for fuels considered today, a multistage airplane has much better possibilities than the single-stage airplane. In this scheme the first stage is used for take-off and acceleration to supersonic speed, and uses turbojets. The second and possibly third stages are used for the long-range high-speed flight. We have investigated these solutions in some detail.* The two-stage solution appears very attractive for high-speed transport flight. The first stage is the largest part of the system, and is attached to a given airport. Therefore it can be used

* This work has been performed with the cooperation of L. Feldman and W. Daskin of the Gruen Applied Science Laboratories, Inc.

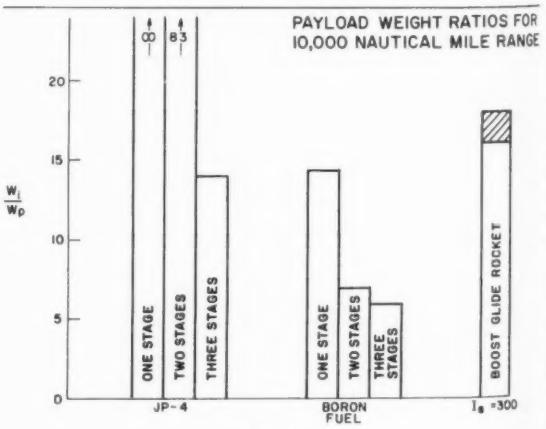

FIG. 3.

for several flights scheduled at very small intervals of time. The second stage which travels the distance is much smaller than the first and therefore is less expensive. The three-stage solution requires dropping the second stage; therefore in this respect it corresponds qualitatively to the solution of a rocket glider where a new booster is required for each flight. A comparison of the possibilities of such configurations with the others mentioned before for a range of 10,000 miles is presented in Fig. 3. Here as parameter the ratio of initial weight of the system to the payload weight is presented. A probable consistent value of this ratio for a rocket glider is also shown. It can be seen that the airplane compares very favorably with the glider.

References

[1] Ferri, Antonio, Feldman, Lewis, and Daskin, Walter, *The Use of Lift for Re-entry from Satellite Trajectories*, Jet Propulsion, Vol. 27, No. 11, pp. 1184–1191, November, 1957.

[2] Anonymous, *Gasoline to Kerosene to 'Zip'—With Energy Calling the Signals*, Jet Propulsion, Vol. 27, No. 6, p. 682, June, 1957.

Wallace D. Hayes, Professor of Aeronautical Engineering, Princeton University: I want to extend my congratulations to Mr. Allen for his excellent review of hyperballistic flight, with his clear presentation of the most important factors involved. Of particular interest to me is the final demise of the skip vehicle, whose attractiveness I have felt to have a nostalgic rather than a logical basis. It appears likely that space or security has cramped Mr. Allen's style somewhat, in that he has not discussed particularly novel or unconventional ideas for solving some of the serious problems in the field. We should like, but of course are not permitted, to see what we might be using in hyperballistic flight ten years from now. Perhaps an idea must have been published in *Life* magazine before it can be declassified for a Wright Brothers Lecture.

The considerations which have been presented are for relatively inanimate, suitably engineered payloads for which the large re-entry decelerations of the ballistic missile may be tolerated. With a human or canine payload the considerations would be different and would appear to preclude the use of a purely ballistic missile. The question of maneuverability also lies outside the scope which has been chosen by Mr. Allen for his lecture. In this respect we may note that the conventional concept of maneuverability is inapplicable at hypersonic speeds. Busemann noted in 1944 that with a fixed L/D and a speed of $1/\sqrt{2}$ of satellite speed the same amount of energy must be expended to fly an airplane around a pylon as to fly it around the world. And, of course, a true satellite outside the atmosphere is completely unmaneuverable by aerodynamic means.

Mr. Allen's use of the Brequet formula is perhaps the most logical compromise to make in comparing the performance of completely dissimilar vehicles. The results for the range of the ballistic missile and the glide vehicle have had to be forced into the Brequet formula, which is a natural formula only for the airplane. Some such compromise was necessary in order to obtain a comparison. However, it is essential for us to keep in mind that the application to the ballistic missile is arbitrary with respect to the definitions of $(L/D)_e$ and of $I_e V_e$, and that the only valid comparison which may be made must be on the product of these two factors. Hence, neither Fig. 6 nor either of Figs. 7(a) and 7(b) has any meaning taken alone, and they acquire meaning only when taken together.

The question of possible multiple staging of airplane configurations has already been raised by Professor Ferri. With regard to the comparison between the ballistic missile and the glide vehicle, the performance of both would presumably be equally improved by equivalent suitable staging. Thus, with such equivalent staging Mr. Allen's comparison would not be changed. However, the design problems associated with multiple staging may be considerably different for the two types of vehicles, and it may be appreciably easier to design multistage ballistic missiles than multistage glide vehicles, or vice versa. Different staging for the two types of vehicles would alter the comparison.

I am in complete agreement with Mr. Allen on the very great importance of rarefied gas flows in the design of hyperballistic vehicles. However, we should note that it may be very difficult to develop appreciable lift on a body which is in a flow so rarefied that it may be considered a free-molecule flow. In the limiting case of free-molecule flow at infinite Mach Number on a body at zero absolute temperature with unit accommodation coefficients, the lift given by the theory is strictly zero, independent of the shape. The drag, of course, is finite, so that the lift-drag ratio is zero.

Again, I want to thank Mr. Allen for a most interesting and stimulating lecture.

H. H. Kurzweg, Associate Technical Director for Aeroballistic Research, U.S. Naval Ordnance Laboratory: I suppose you are all, as I am, confronted with the same problem—to find a good way to keep adequately informed on the rapid and continuous progress in the thinking about fast flying missiles and aircraft. Every day piles of papers and reports appear and disappear on our desks and it becomes more and more difficult timewise to find the grains of gold in the sand. Our system of communication seems to become outdated. We must find new ways to increase the amount of thoughts per unit time to be transplanted from one brain to the other. One step in the direction is the condensation of the results on latest investigations in a brief, logical, and easily understandable system. The lecture we have just heard is an excellent example of how it should be done. The wide scatter of opinions on the usefulness of various types of long-range vehicles has been focused to a few clear lines which makes all further discussions on the subject so much easier and more profitable.

Years ago, before the ICBM's and IRBM's entered the newspaper stage, when we measured heat transfer

(*Continued on page 262*)

On Radial Deflection of a Cylinder of Finite Length With Various End Conditions†

L. TING* AND S. W. YUAN**

Polytechnic Institute of Brooklyn

SUMMARY

By a method different from that given in references 1 and 2, the radial deformations of a thin-walled circular cylindrical shell subjected to a pair of equal and opposite concentrated radial loads are obtained in the present paper for the cases of cylinders of finite length with built-in, simply supported, and free ends. When the length of the cylinder is not too large compared to its radius, the solutions for different end conditions differ from each other considerably. The solutions for cylinders with both ends free agree with Rayleigh's inextensional solution,[3] while the solutions for cylinders with both ends simply supported agree with Odqvist's solution[4] and also that in reference 1. When the length of the cylinder is large compared to its radius, the solutions corresponding to different end conditions approach that for the cylinder of infinite length, as expected. Rayleigh's inextensional solution, Odqvist's solution, and the solution in reference 1 are no longer valid in this range.

SYMBOLS

a	= radius of cylinder
h	= wall thickness
k	= $[3(1-\nu^2)(a/h)^2]^{1/4}$
n	= integer
q	= radially distributed load
x	= axial coordinate
w	= radial displacement
A_{1n}, A_{2n}	= real part of complex roots of characteristic equation
B_{1n}, B_{2n}	= imaginary part of complex roots of characteristic equation
C_{1n}, C_{2n}, G_{1n}, G_{2n}	= amplitudes defined under Eq. (7)
$D = Eh^3/[12(1-\nu^2)]$	= bending rigidity of wall of shell per unit length
E	= Young's modulus of elasticity
L, L_1, L_2	= length of shell
0	= of the order of
P	= concentrated radial load
$\bar{w} = (w/h)/(P/Eh^2)$	= nondimensional radial deflection
λ_{jn}	= complex roots of characteristic equation
ν	= Poisson's ratio
φ	= circumferential coordinate, rad.
ρ	= u, v, or w (see Fig. 1)

INTRODUCTION

IN REFERENCES 1 AND 2, the solutions for cylinders of finite length are constructed from the corresponding solution for cylinders of infinite length by the method of images. The solutions so obtained are correct only if both ends of the cylinder are simply supported. For cylinders with different end conditions, such as those with free or built-in ends, the method of images cannot be applied. It is necessary to use a different method.

In the present paper, the solution for cylinders of infinite length is employed as the particular integral while the end conditions are fulfilled by finding the proper solutions to the homogeneous differential equation. The additional work in finding the proper solution is the onus inherent in solving a wider class of problems than the method of images affords.

In reference 2, it was pointed out that the leading terms $n = 2, 4, \ldots$, in the Fourier series in φ obtained in reference 1 for the radial deformation of cylinders of infinite length are inaccurate and that therefore the expressions based upon the Flügge equation[2] should be used. If a combination of expressions from the Flügge equation and from that in reference 1 are used as the particular integral, the task of finding the proper solution to the homogeneous Flügge equation is extremely tedious. It is necessary to simplify the Flügge equation.

It was shown by a careful analysis of order of magnitude that the Flügge equation can be simplified to the complete Donnell equation,[5]

$$\nabla^8 w + [12(1-\nu^2)/a^2h^2](\partial^4 w/\partial x^4) + (2/a^8)(\partial^6 w/\partial\varphi^6)(+1/a^8)(\partial^4 w/\partial\varphi^4) - (1/D)\nabla^4 q = 0 \quad (1)$$

It is called the complete Donnell equation in order to differentiate it from the one derived in reference 6 and quoted in references 1 and 2.

Based upon Eq. (1), simplified expressions for radial deformation of cylinders of infinite length are obtained in the present paper. The results agree with those based upon the Flügge equation.[2] This is also a confirmation of the accuracy of the complete Donnell equation in addition to the analytic proof in reference 5.

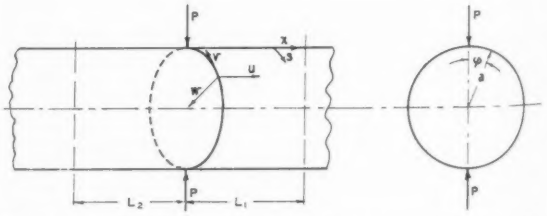

FIG. 1. Loads and components of displacements of a circular cylinder.

Received May 15, 1957.

† This investigation was partially sponsored by the Foster Wheeler Corporation, New York. The authors wish to express their gratitude to A. H. Egsieker for permission to publish this paper.

* Formerly, Research Associate. Now, Research Assistant Professor.

** Formerly, Professor of Aeronautical Engineering. Now, Canadair Professor of Fluid Mechanics, Université Laval, Canada.

With the simplified expressions as the particular integral, the corresponding solutions to the homogeneous equation of Eq. (1) are obtained for cylinders of finite length with built-in, simply supported, and free ends (see Fig. 1).

Simplified Solutions for the Radial Deformation of Cylinders of Infinite Length

When the complete Donnell equation,[5] Eq. (1), is used as the governing differential equation for the radial displacement, the solution can be obtained by the same method as in reference 1,

$$\left.\begin{aligned}\bar{w}_x &= Ehw/P \\ &= \frac{k}{2\pi}\exp\left(\frac{-k|x|}{a}\right)\left[\cos\left(kx/a\right)+\sin\left(k|x|/a\right)\right]+\frac{k^4}{\pi}\sum_{n=2,4}^{\infty}\frac{\cos n\varphi}{n^3}\times \\ &\qquad \sum_{j=1,2,3,4}\frac{i(\lambda_{jn}^2+1)^2\exp\left(-in|x|\lambda_{jn}/a\right)}{\lambda_{jn}[(\lambda_{jn}^2+1)^3+2(k/n)^4\lambda_{jn}^2]}\end{aligned}\right\} \tag{2}$$

where $\lambda_{1n}=-\lambda_{3n}=(\lambda_{1n}+iB_{1n})/n$ and $\lambda_{2n}=-\lambda_{4n}=(\lambda_{2n}+iB_{2n})/n$

are the four complex roots with positive imaginary part of the characteristic equation,

$$(\lambda^2+1)^4+4(k/n)^4\lambda^4-2n^{-2}+n^{-4}=0 \tag{3}$$

The last two terms in Eq. (3), $-2n^{-2}+n^{-4}$, are the extra terms as compared to the corresponding equation in reference 1. It is obvious that they are negligible for $n \gg 1$ as compared to the term $(\lambda^2+1)^4$, therefore, the terms in reference 1 for $n \gg 1$ are correct. This agrees with the conclusion in reference 2.

Since the terms in reference 1 for $n = 2, 4, 6 \ldots$, i.e., for $n^2 \ll k^2$, are incorrect, it is desirable to evaluate the terms in Eq. (2) for $n^2 \ll k^2$ only.

The roots can be expressed as power series of $(n/k)^2$, and the coefficients of the power series are determined by equating the coefficients of like powers of $(n/k)^2$ in Eq. (3),

$$\left.\begin{aligned}\lambda_{1n} &= -\bar{\lambda}_{2n}=(\lambda_{1n}+iB_{1n})/n \\ &=\frac{1}{2}\left(\frac{n}{k}\right)(1-n^{-2})^{1/2}\left\{1-\frac{1}{2(1-n^{-2})}\left(\frac{n}{k}\right)^2-\frac{1}{8}\left[3+\frac{1}{(1-n^{-2})^2}\right]\left(\frac{n}{k}\right)^4+\cdots\right\}+ \\ &\qquad \frac{i}{2}\left(\frac{n}{k}\right)(1-n^{-2})^{1/2}\left\{1+\frac{1}{2(1-n^{-2})}\left(\frac{n}{k}\right)^2-\frac{1}{8}\left[3+\frac{1}{(1-n^{-2})^2}\right]\left(\frac{n}{k}\right)^4+\cdots\right\}\end{aligned}\right\} \tag{4}$$

and

$$\left.\begin{aligned}\lambda_{2n} &= -\bar{\lambda}_{4n}=(\lambda_{2n}+B_{2n})/n \\ &=\left(\frac{k}{n}\right)\left\{1-\frac{1}{2}\left(\frac{n}{k}\right)^2+\frac{1}{4}\left(\frac{n}{k}\right)^4+\cdots\right\}+i\left(\frac{k}{n}\right)\left\{1+\frac{1}{2}\left(\frac{n}{k}\right)^2+\frac{1}{4}\left(\frac{n}{k}\right)^4+\cdots\right\}\end{aligned}\right\} \tag{5}$$

Since $k=[4\sqrt{3(1-\nu^2)}\,(a/h)^{1/2}] \gg 1$, there exists a set of values of n such that $n^2 \gg 1$ and also $(n/k)^2 \ll 1$. This implies that when $n^2 \gg 1$ but $(n/k)^2$ is still small enough for the power series in Eqs. (4) and (5) to converge with sufficient rapidity, the results given by the expressions (4) and (5) match with those given in reference 1, with accuracy not less than that of the approximate differential equation, Eq. (1).

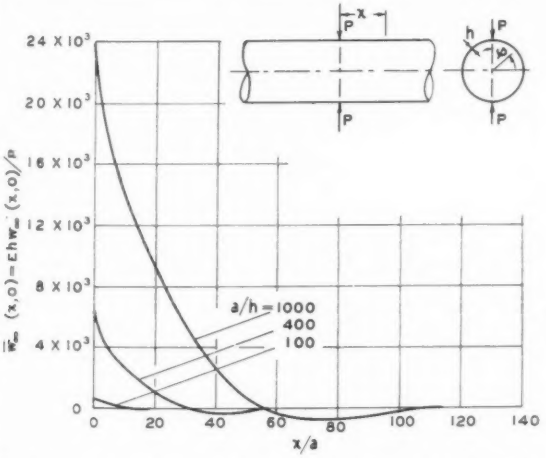

Fig. 2. Radial deflections of infinitely long cylinders along the generatrix.

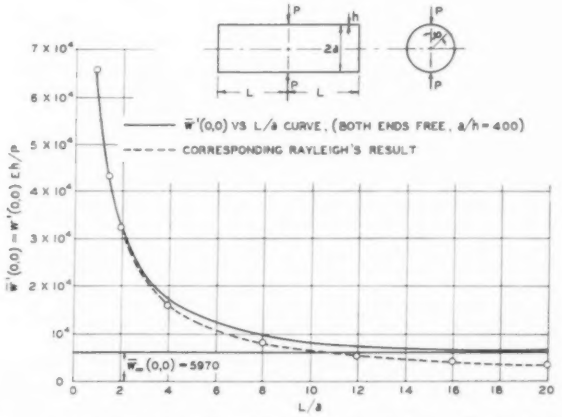

Fig. 3. Maximum radial deflection of cylinders with various length-radius ratio (free ends).

After substituting the expressions for λ_j, Eqs. (4) and (5), into Eq. (2), the expressions for $\bar{w}_\infty$ can be simplified:

$$\bar{w}_\infty = \frac{k}{2\pi}\exp\left(\frac{-k|x|}{a}\right)\left[\cos\left(\frac{k|x|}{a}\right)+\sin\left(\frac{k|x|}{a}\right)\right]+\sum_{n=2,4}^{\infty}\exp\left(\frac{-B_{1n}|x|}{a}\right)\left[C_{1n}\cos\left(\frac{A_{1n}|x|}{a}\right)+G_{1n}\sin\left(\frac{A_{1n}|x|}{a}\right)\right]\cos n\varphi+\sum_{n=2,4}^{\infty}\exp\left(\frac{-B_{2n}|x|}{a}\right)\left[C_{2n}\cos\left(\frac{A_{2n}|x|}{a}\right)+G_{2n}\sin\left(\frac{A_{2n}|x|}{a}\right)\right]\cos n\varphi \quad (6)$$

where, for $(n/k)^2 \ll 1$,

$$\left.\begin{aligned} C_{1n} &= \frac{2k}{\pi}\left(\frac{k}{n}\right)^2\frac{1}{(1-n^{-2})^{3/2}}\left\{1+\left(\frac{n}{k}\right)^2\left[(1-n^{-2})-\frac{1}{2(1-n^{-2})}\right]-\frac{1}{8}\left(\frac{n}{k}\right)^4\left[7+2(1-n^{-2})^2-\frac{3}{(1-n^{-2})^2}\right]+\cdots\right\}\\ G_{1n} &= \frac{2k}{\pi}\left(\frac{k}{n}\right)^2\frac{1}{(1-n^{-2})^{3/2}}\left\{1-\left(\frac{n}{k}\right)^2\left[(1-n^{-2})-\frac{1}{2(1-n^{-2})}\right]-\frac{1}{8}\left(\frac{n}{k}\right)^4\left[7+2(1-n^{-2})^2-\frac{3}{(1-n^{-2})^2}\right]+\cdots\right\}\\ C_{2n} &= \frac{k}{\pi}\left\{1-\frac{3}{2}\left(\frac{n}{k}\right)^2-\frac{5}{2}\left(\frac{n}{k}\right)^4+\cdots\right\}\\ G_{2n} &= \frac{k}{\pi}\left\{1+\frac{3}{2}\left(\frac{n}{k}\right)^2-\frac{5}{2}\left(\frac{n}{k}\right)^4+\cdots\right\} \end{aligned}\right\} \quad (7)$$

for $n \gg 1$; the corresponding results in reference 1 can be used.

For practical purposes, the infinite series can be approximated by the first few terms, $n = 2, 4, \ldots, m$ with $m \ll k$, and the constants C_{1n}, G_{1n}, and A_{1n}, B_{1n} can be approximated, respectively, by the leading term in their power series of $(n/k)^2$, [see Eqs. (4), (5), and (7)]. Hence Eq. (6) is further simplified to

$$\bar{w}_\infty\left(\frac{|x|}{a},\varphi\right)=\sum_{n=2,4}^{m\ll k}\left(\frac{2k}{\pi}\right)\left(\frac{k}{n}\right)^2\frac{1}{(1-n^{-2})^{3/2}}\left\{\cos\left(\mu_n|x|/a\right)+\sin\left(\mu_n|x|/a\right)\right\}\exp\left(\frac{-u_n|x|}{a}\right)\cos n\varphi \quad (8)$$

where $\mu_n = (1/2)\,n(n^2-1)^{1/2}/k$. The first and the third terms in Eq. (6) are neglected, because the coefficients C_{1n} and G_{1n} in the second term of Eq. (6) are of the order of $(k/n)^2$ as compared to those of the first and the third terms.

The counterpart of Eq. (8) in reference 1 can be obtained,

$$\bar{w}_{\infty Y}\left(\frac{|x|}{a},\varphi\right)=\sum_{n=2,4}^{m\ll k}\left(\frac{2k}{\pi}\right)\left(\frac{k}{n}\right)^2\left\{\cos\left(\bar{\mu}_n|x|/a\right)+\sin\left(\bar{\mu}_n|x|/a\right)\right\}\exp\left(\frac{-\bar{\mu}_n|x|}{a}\right)\cos n\varphi \quad (9)$$

where $\bar{\mu}_n = (1/2)n^2/k$.

The ratio of the amplitudes of the corresponding terms in Eqs. (9) and (8) is 1 to $(1-n^{-2})^{-3/2}$. The percentage error of the terms in Eq. (9), the solution of reference 1, as compared to that of Eq. (8) is $1-(1-n^{-2})^{3/2}$, i.e., 35, 9, 4, and 2 per cent for $n = 2$, 4, 6, 8, respectively. This result is independent of the ratio of a/h. It agrees with the one in Table 1 in reference 2, which was obtained for the special values of $a/h = 100$. It can also be concluded that the results from the complete Donnell equation will differ from those from the Flügge equation by less than one per cent.

Fig. 2 shows the radial deflection for $a/h = 100$, 400, and 1,000.

Radial Deformation for Cylinders of Finite Length

The solution, w_∞, developed in the previous section for an infinite cylinder can be used as a particular integral—i.e.,

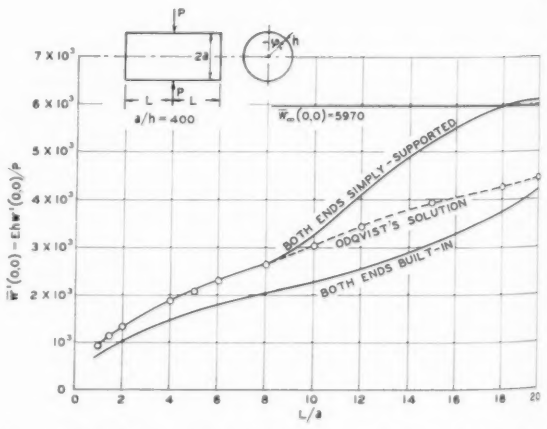

FIG. 4. Maximum radial deflection of cylinders with various length-radius ratio (simply supported and built-in end).

$$w(x, \varphi) = w_\infty(x, \varphi) + w_c(x, \varphi)$$

where w_c is the solution of the homogeneous differential equation of Eq. (1). In many problems, the leading terms in w_∞ and w_c cancel each other; therefore, Eq. (6) should be used for w_∞ in the evaluation of $w(x, \varphi)$. However, $w_c(x, \varphi)$ is determined by the values of $w_\infty(x, \varphi)$ and its derivative at the two ends $x = L_1$ and $x = -L_2$, where w_∞ can be approximated by Eq. (8), because in all the other terms the exponential factor diminishes very rapidly as $|x|/a$ increases. (It is assumed that L_1 and L_2 are at least of the order of magnitude of the radius.) From Eq. (8), it is clear that $w_c(x, \varphi)$ can be represented by a finite trigonometric series,

$$w_c(x, \varphi) = \sum_{n=2,4}^{m \ll k} w_n(x) \cos n\varphi \tag{10}$$

Since $n \leqq m \ll k$, the complementary integral $w_c(x, \varphi)$ can be split into two parts w_I and w_{II} (see reference 7), i.e.,

$$w_c(x, \varphi) = w_I[(kx/a), \varphi] + w_{II}[(\mu_n x/a), \varphi]$$

where

$$w_I\left(\frac{kx}{a}, \varphi\right) = \sum_{n=2,4}^{m \ll k} \left\{ \left[F_{1n} \cos \frac{k(L_1 - x)}{a} + F_{2n} \sin \frac{k(L_1 - x)}{a} \right] \exp \frac{-k(L_1 - x)}{a} \cos n\varphi + \left[F_{3n} \cos \frac{k(L_2 + x)}{a} + F_{4n} \sin \frac{k(L_2 + x)}{a} \right] \exp \frac{-k(L_2 + x)}{a} \cos n\varphi \right\} \tag{11}$$

$$w_{II}\left(\frac{\mu_n x}{a}, \varphi\right) = \sum_{n=2,4}^{m \ll k} \left\{ \left[H_{1n} \cos \frac{\mu_n(L_1 - x)}{a} + H_{2n} \sin \frac{\mu_n(L_1 - x)}{a} \right] \exp \frac{-\mu_n(L_1 - x)}{a} \cos n\varphi + \left[H_{3n} \cos \frac{\mu_n(L_2 + x)}{a} + H_{4n} \sin \frac{\mu_n(L_2 + x)}{a} \right] \exp \frac{-\mu_n(L_2 + x)}{a} \cos n\varphi \right\} \tag{12}$$

w_I represents the solution for the edge effect.[8] The influence of the first term on the right-hand side of Eq. (11) is confined to the vicinity of the end $x = L_1$, while that of the second term to the vicinity of $x = -L_2$. Since μ_n's are not large numbers, the effect of w_{II} is not localized. The radial deflection of the finite cylinder, $w = w_\infty + w_I + w_{II}$, can be represented by $w' = w_\infty + w_{II}$ for the part of the cylinder not too close to the ends. The four sets of constants H_{1n}, H_{2n}, H_{3n}, and H_{4n} in w_{II} can be determined uniquely by two boundary conditions at each end. The question now is which two of the four boundary conditions should be prescribed on w_{II}. This can be settled by a careful examination of the relative orders of magnitude of the different terms in the boundary conditions, while w_I and w_{II} obey the following relationship:

$$\partial w_I/\partial x = k0(w_I/a) = (k/n)\, 0[(1/a)(\partial w_I/\partial \varphi)] \gg \partial w_I/a\partial\varphi \tag{13}$$

$$\partial w_{II}/\partial x = 0(n^2 w_{II}/ka) = (n/k)\, 0[(1/a)(\partial w_{II}/\partial \varphi)] \ll \partial w_{II}/a\partial\varphi \tag{14}$$

The two boundary conditions for $w'(x, \varphi)$ are summarized as follows. (1) Built-in edges,

$$w_{II} = -w_\infty \quad \text{and} \quad \partial w_{II}/\partial x = -(\partial w_\infty/\partial x) \tag{15}$$

(2) Simply supported edges,

$$w_{II} = -w_\infty \quad \text{and} \quad \partial^2 w_{II}/\partial x^2 = -(\partial^2 w_\infty/\partial^2 x) \tag{16}$$

(3) Free edges,

$$\partial^2 w_{II}/\partial x^2 = -(\partial^2 w_\infty/\partial x^2) \quad \text{and} \quad \partial^3 w_{II}/\partial x^3 = -(\partial^3 w_\infty/\partial x^3) \tag{17}$$

The application of $w_{II}(x, \varphi)$ to solve unsymmetrical problems in the shells can be found in reference 9 where boundary conditions for built-in edges and free edges equivalent to those in this paper are given.

If the concentrated loads are applied at the center of the cylinder—i.e., $L_1 = L_2 = L$—and both ends are subjected to the same set of boundary conditions, the radial deformation of the cylinder at the point of application of the concentrated load can be expressed as:

$$w'(0, 0) = w_\infty(0, 0) + 2Pk^3(Eh\pi)^{-1} \times \sum_{n=2,4}^{m \ll k} \frac{nJ_n}{(n^2 - 1)^{3/2}} \tag{18}$$

where $w_\infty(0, 0)$ = the corresponding radial displacement of the cylinder of infinite length,

$$J_n = \frac{-2 \exp(-2\mu_n L/a)\,[2 + \sin(2\mu_n L/a) - \cos(2\mu_n L/a) - \exp(-2\mu_n L/a)]}{1 + 2\exp(-2\mu_n L/a)\sin(2\mu_n L/a) - \exp(-4\mu_n L/a)} \tag{18a}$$

for built-in ends,

$$J_n = \frac{-2 \exp(-2\mu_n L/a)\,[\cos(2\mu_n L/a) + \sin(2\mu_n L/a) + \exp(-2\mu_n L/a)]}{1 + 2\exp(-2\mu_n L/a)\cos(2\mu_n L/a) + \exp(-4\mu_n L/a)} \tag{18b}$$

for simply supported edges,

$$J_n = \frac{2 \exp(-2\mu_n L/a)\,[2 + \cos(2\mu_n L/a) - \sin(2\mu_n L/a) + \exp(-2\mu_n L/a)]}{1 + 2\exp(-2\mu_n L/a)\sin(2\mu_n L/a) + \exp(-4\mu_n L/a)} \tag{18c}$$

for free edges.

It is clear that J_n tends to zero when L/a tends to infinity. This means that, regardless of the kind of boundary conditions, the solution for the cylinders of finite length approaches the solution for cylinders of infinite length when L/a approaches infinity.

The radial displacement $w'(0, 0)$ is plotted against L/a for a cylinder with $a/h = 400$ in Fig. 3 for free ends and in Fig. 4 for simply supported and fixed ends.

The Rayleigh solution[3] which fulfills the boundary conditions for free edges, Eq. (17), gives

$$w_R(0, 0) = 0.149Pa^3/(4DL)$$

or $$\bar{w}_R(0, 0) = w_R(0, 0)Eh/p = 0.149k^4(a/L)$$

When the value of a/h is fixed, $\bar{w}_R(0, 0)$ is in inverse proportion to L/a and tends to zero as L/a tends to infinity. It is clear that the Rayleigh solution cannot be applied when $L/a \gg 1$. When $L/a = 0(1)$, the results obtained in this paper for cylinders with free ends agree with the Rayleigh results (see Fig. 3).

Discussion

Although in this paper only a special unsymmetrical problem has been treated, a general remark can be made regarding the accuracy of many approximate equations.

The complete Donnell equation, Eq. (1), is accurate enough for unsymmetrical problems, for engineering purposes.

If the cylindrical shell deforms into many circumferential waves, i.e.,

$$\partial\rho/\partial\varphi \gg \rho \tag{19}$$

where ρ stands for u, v, or w, Eq. (1) reduces to the equation in references 1 and 6,

$$\nabla^8 w + [12(1 - \nu^2)/a^2h^2](\partial^4 w/\partial x^4) = (1/D)\nabla^4 q$$

The latter equation was also obtained by Green and Zerna.[10]

If it is known that

$$\partial\rho/a\partial\varphi \gg \partial\rho/\partial x \tag{20}$$

Eq. (1) degenerates to (the homogeneous part)

$$[(\partial^2/\partial\varphi^2) + 1]^2(\partial^4\rho/a^4\partial\varphi^4) + 12(1 - \nu^2)(a^2/h^2)(\partial^4\rho/\partial x^4) = 0 \tag{21}$$

Eq. (21) is equivalent to Finsterwalder's equation for M_φ (see reference 3), because condition (20) is necessary and sufficient to justify Finsterwalder's assumption that $\partial M_x/\partial x$ and $\partial M_{x\varphi}/\partial x$ are negligible in the equations of equilibrium. Both Eq. (21) and Finsterwalder's equation are fourth order in x instead of eighth order. The "solutions due to edge effect," w_1, are eliminated.

If both conditions (19) and (20) are valid, Eq. (21) is further simplified to Schorer's equation,[11]

$$(\partial^8\rho/\partial\varphi^8) + [12(1 - \nu^2)a^6/h^2](\partial^4\rho/\partial x^4) = 0$$

For "short" cylinders with $L/a \ll \sqrt{2}\pi k$, and with both ends fixed or simply supported, the leading terms in $w_{II}(x, \varphi)$ cancel with the corresponding terms in $w_\infty(x, \varphi)$ and the radial displacement can be written as

$$w'(x, \varphi) = w_\infty(x, \varphi) + w_{II}(x, \varphi) = \sum_{n=2p,2p+2}^{\infty} w_n'(x) \cos n\varphi \tag{22}$$

where p is an integer much greater than unity. Eq. (22) implies condition (19), therefore solutions in reference 1 are accurate for "short" cylinders with simply supported ends.

Since w_{II} in Eq. (12) and the predominant terms in w_∞ also fulfill condition (20), Odqvist's solution,[4] which was based upon Schorer's equation, is also accurate for "short" cylinders with $L/a \ll \sqrt{2}\pi k$ [see Fig. 4].

For a thin cylindrical shell with flat heads, the end conditions prescribed on the shell due to the existence of the flat heads are equivalent to those of the simply supported ends, because the flat plate is much stiffer than the shell in resisting radial and circumferential displacements, i.e., $w = 0$, $v = 0$, and is much weaker than the shell in resisting lateral deflection and rotation, i.e., $N_x = 0$ and $M_x = 0$.

Finally, it is worthwhile to point out that, for the case,

$$\partial\rho/\partial\varphi = 0(\rho) = 0(a\partial\rho/\partial x)$$

the differential equation (1) degenerates to the membrane equation.[5]

References

[1] Yuan, S. W., *Thin Cylindrical Shells Subjected to Concentrated Loads*, Quarterly of Applied Mathematics, Vol. IV, No. 1, pp. 13–26, April, 1946.

[2] Yuan, S. W., and Ting, L., *On Radial Deflections of a Cylinder Subjected to Equal and Opposite Concentrated Radial Loads—Infinitely Long Cylinder and Finite-Length Cylinder with Simply Supported Ends*, Journal of Applied Mechanics, Vol. 24, No. 2, pp. 278–282, June, 1957.

[3] Timoshenko, S. P., *Theory of Plates and Shells*, (1st Ed.), pp. 427–440, 446–449, McGraw-Hill Book Company, New York, 1940.

[4] Odqvist, F. K. G., *Action of Forces and Moments Symmetrically Distributed Along a Generatrix of a Thin Cylindrical Shell*, Journal of Applied Mechanics, Trans. ASME, Vol. 68, pp. 106–108, 1946.

[5] Donnell, L. H., *A Discussion of Thin Shell Theory*, Proceedings of the Fifth International Congress of Applied Mechanics, pp. 66–70, Cambridge, Mass., 1938.

[6] Donnell, L. H., *Stability of Thin-Walled Tubes under Torsion*, NACA Report No. 479, 1933.

[7] Flügge, W., *Statik und Dynamik der Schalen*, p. 118, pp. 126–127, Julius Springer, Berlin, Germany, 1934.

[8] Love, A. E. H., *The Mathematical Theory of Elasticity*, 4th Ed., pp. 564–583, Dover Publications, New York, 1944.

[9] Gruber, E., *Die Berechnung Zylindrischer, biegungssteifer Schalen unter beliebigem Lastangriff*, Internat. Vereinig. Brücken- u. Hochbau Abh. 2, p. 196, 1934.

[10] Green, A. E., and Zerna, W., *Theoretical Elasticity*, 1st Ed., p. 422, Oxford University Press, Oxford, England, 1954.

[11] Schorer, H., *Line Load Action on Thin Cylindrical Shells*, Trans. ASCE, Vol. 61, pp. 281–316, 1935.

The Prospects for Magneto-Aerodynamics†

E. L. RESLER, JR.,* AND W. R. SEARS**
Cornell University

Summary

The equations describing the flow of an electrically conducting fluid in the presence of electric and magnetic fields are written down with the aid of certain simplifications appropriate to aeronautical applications. In order to estimate the probable significance of magneto-aerodynamic effects, some data on conductivity of pure and "seeded" air are first examined. Dimensionless quantities representing the ratios of forces and of currents are then formed and their values studied for conditions of flight in the atmosphere.

Some examples of magneto-hydrodynamic and magneto-gasdynamic effects in simple flows are given. These include two cases of Poiseuille flow of conducting liquids with applied magnetic fields and the case of quasi-one-dimensional gas flow with applied electrical and magnetic fields. In the last case, attractive possibilities are found for controlled acceleration or deceleration of gas at subsonic and supersonic speeds, even in constant-area channels. The behavior of the flow is characteristically different in different regimes of Mach Number and flow speed relative to certain "significant speeds" that are dependent on the ratio of electrical to magnetic field strengths. These are studied, and a chart is constructed to relate the length to the speed ratio of a maximum-acceleration constant-area channel.

It is concluded that the advantages that may accrue from magneto-aerodynamic methods are sufficiently attractive to justify the considerable research and engineering development that will be required. Among the unsolved engineering problems are the reduction of surface resistance of electrodes in contact with a conducting gas, development of techniques for seeding, and provision of the required magnetic fields in flight.

Symbols

a	= half-width of channel in cases of Figs. 4 and 5
a	= $\sqrt{\gamma p/\rho}$ in compressible flow
A	= cross-section area of channel
c	= speed of light
c_p	= specific heat for constant pressure
c_v	= specific heat for constant volume
D	= channel cross-section dimension [Eq. (15)]
$\mathbf{E}$	= electric field vector (magnitude E)
$\mathbf{F}$	= body force
$\mathbf{j}$	= current density vector (magnitude j)
$\mathbf{H}$	= magnetic field vector (magnitude H)
Ha	= Hartmann Number
$\mathbf{h}$	= perturbation magnetic field vector (magnitude h)
h_0	= stagnation enthalpy
K_B	= breakdown-potential constant [Eq. (50)]
L	= typical body length
M	= Mach Number
m	= mass flow per unit area
P	= constant pressure gradient in Eq. (28)
p	= static pressure
$\mathbf{q}$	= fluid velocity vector (magnitude q)
Q	= heat added by dissipation and/or other effects excluding Joule heating
R	= resistance per unit length of channel (Fig. 5)
Re	= Reynolds Number
R_m	= magnetic Reynolds Number
t	= time
T	= temperature
u	= flow speed (average) in channel
u_1, u_2, u_3	= significant speeds in channel flow
V	= typical flow speed; speed of flight
$\mathcal{V}$	= electrical potential
x, y, z	= Cartesian coordinates
α	= fractional ionization
γ	= c_p/c_v
ξ	= $(1/m)\int_{x_0}^{x} \sigma H^2 dx$
μ	= viscosity coefficient
ρ	= mass density
σ	= conductivity

Subscripts

x, y, z	= components of vectors, along x, y, z axes
0	= constant, especially initial conditions in channel flow

Introduction

If a fluid is a conductor of electricity, the possibility arises that an *electric body force* may be produced in it that will affect the fluid flow pattern in a significant way. To be sure, we are not unaccustomed to dealing with fluid flows with body forces—e.g., the gravitational force and the inertial, centrifugal, and Coriolis forces in moving coordinate systems—but all of these are examples where the body force is more or less outside of our control. The attractive thing about the electric body force (which we will call the e.b.f.) is that it can be controlled, insofar as the current and the magnetic field can be controlled, and perhaps made to serve useful purposes such as acceleration or deceleration of flow, prevention of separation, and the like.

A body force in fluid mechanics is any force that is applied by an external agency directly to the fluid elements, as distinguished from the pressure, for example, which is a force between adjacent particles. The e.b.f. involved here is the counterpart of the force that drives an electric motor; it is given by the vector product of the current and the magnetic field strength and is therefore perpendicular to both of these vectors. In the case of a fluid, we expect electric-current flow through a volume rather than along a wire and are

Presented at the Aerodynamics Session, National Summer Meeting, IAS, Los Angeles, June 17–20, 1957. Received November 26, 1957.

† This work was carried out at the Graduate School of Aeronautical Engineering under the sponsorship of the Mechanics Branch, Office of Naval Research. Reproduction in whole or in part is permitted for any purpose of the United States Government.

* Associate Professor of Aeronautical Engineering.

** Director, Graduate School of Aeronautical Engineering.

therefore concerned with the current-density vector $\mathbf{j}$, measured in amperes per unit area, for example. Similarly, the strength of the magnetic field $\mathbf{H}$ is measured in lines-of-force per square centimeter, usually called "gauss." Then the body force per unit volume is given by the vector equation

$$\mathbf{F} = \mathbf{j} \times \mathbf{H} \tag{1}$$

It is assumed here that the fluid is nonmagnetic—i.e., that it has the same permeability as empty space; this permeability has been taken equal to 1, since we propose to formulate our problem in electromagnetic units.

This force can be used to pump a conducting fluid, such as mercury, through pipes.[1] Recently it has been used in gasdynamics laboratories to help drive shock tubes;[2] here the conducting fluid is air or another gas heated to high temperature by discharge of a condenser through it. Astrophysicists also have a current interest in magneto-hydrodynamics because there are at least two different situations in their field where this body force apparently acts: (1) in the sun and stars where gases are highly ionized by the extreme temperatures, and (2) in nearly empty space where the temperatures of gas clouds are not high but the ionization is nevertheless sufficient, because of the low densities, to make them good conductors.

The possibility of these effects becoming important in aeronautics has naturally arisen, since the temperatures that occur in flight at high speeds are sufficient to ionize air appreciably. If, as predicted, these temperatures approximate the temperatures of electric arcs, it is clear that the air becomes a conductor and that the e.b.f. can be important aerodynamically.

The purpose of the present paper is to make an assessment of these aeronautical possibilities. How large are the effects likely to be, and under what conditions? What are some of the engineering problems posed?

Before proceeding to this task, however, we should notice another basic phenomenon of magneto-aerodynamics, equal in importance to the e.b.f. and even, in some cases, overshadowing it—namely, the Joule heating. This is one of the most familiar phenomena of electricity. We are used to it in metallic conductors, and it may be even more significant in magneto-aerodynamics, since the conductivities of gases are so much less. The electricians' familiar formula I^2R becomes, in this application,

$$\text{heat released per unit volume per unit time} = j^2/\sigma \tag{2}$$

where σ denotes the conductivity or the reciprocal of the specific resistance. The unit of conductance is the mho; here σ is a material property, the conductance of a unit cube. The conductance of such a sample is proportional to its cross-sectional area and inversely to its length. Thus σ has the units mho per unit length.

The Equations of Motion

To summarize what has been written above, the presence of electrical currents in a fluid introduces essentially two new effects, the e.b.f., $\mathbf{j} \times \mathbf{H}$; and Joule heating, j^2/σ. The only change required in the equations of fluid motion is the introduction of these new terms in the equations of momentum and energy. The equation of continuity remains unaltered. We have then

Continuity:

$$(\partial\rho/\partial t) + \operatorname{div}(\rho\mathbf{q}) = 0 \tag{3}$$

Momentum:

$$(D\mathbf{q}/Dt) + (1/\rho)\nabla p = (\mu/\rho)\{\nabla^2\mathbf{q} + (1/3)\nabla\nabla\cdot\mathbf{q}\} + (1/\rho)\mathbf{j} \times \mathbf{H} \tag{4}$$

Energy:

$$c_v(DT/Dt) + p(D\rho^{-1}/Dt) = (j^2/\rho\sigma) + Q \tag{5}$$

Here ρ, $\mathbf{q}$, p, μ, T, and σ are the density, velocity, pressure, viscosity, temperature, and electrical conductivity of the fluid; c_v is its specific heat at constant volume; and t is the time. The symbol Q denotes all heat added to the fluid except Joule heat, thus Q includes heat conduction, viscous dissipation, etc. One simplification has been made, for brevity, in writing Eq. (4)—namely, the viscous term has been written for the special case of constant μ—but this will not affect what is done below. It should be remembered however that μ is actually dependent upon T. The symbols $\mathbf{j}$ and $\mathbf{H}$ represent the current density and magnetic field strength defined above. The derivative D/Dt is the convective derivative—i.e., the rate of change for a fluid particle.

Eq. (5) is an expression of the fact that as heat is added to, or subtracted from, the fluid medium it appears either in internal energy or in mechanical work done. This is the simple expression of the First Law of Thermodynamics that applies when the thermodynamic and mechanical forms of energy are the only ones concerned. Eq. (5) does not attempt to include electrical forms of energy in the statement of the First Law. It is therefore useful only if there is no interchange of energy except what has been described above—i.e., Joule heating. In more complicated cases, for example, where the magnetic permeability of the fluid is a function of temperature or of the field strength, a more sophisticated formulation of the energy equation from the first law of thermodynamics is required.

Assuming that this is not the case in most aeronautical applications, the simple statement Eq. (5) is all that is needed. It takes on an interesting form if it is added to Eq. (4) after scalar multiplication of the latter with the velocity vector (thus changing Eq. (4) to a statement involving work done by forces). This form is, assuming the perfect-gas equation of state,

$$c_v(\partial T/\partial t) + (1/2)(\partial q^2/\partial t) + p(\partial \rho^{-1}/\partial t) + \mathbf{q}\cdot\nabla h_0 = (1/\rho)\mathbf{q}\cdot\mathbf{j}\times\mathbf{H} + (j^2/\rho\sigma) + \mu\{\nabla^2\mathbf{q} + (1/3)\nabla\nabla\cdot\mathbf{q}\}\cdot\mathbf{q} + Q \quad (6)$$

where h_0 denotes the stagnation enthalpy, $c_pT + q^2/2$. This form is useful for steady-flow problems, since the first three left-hand terms are then absent, and the left-hand side of Eq. (6) becomes the rate of increase of the stagnation enthalpy of a fluid particle. This rate involves two magneto-aerodynamic terms, one being the mechanical work done by the e.b.f., the other being the Joule heating. As we shall see below, it is possible for these two to oppose one another.

Ohm's Law

In Eqs. (3) to (5) we have introduced two new unknowns into the already complicated equations of gasdynamics—viz., $\mathbf{j}$ and $\mathbf{H}$ (assuming σ to be a known property of the fluid). We must provide additional equations concerning these. One of these is Ohm's Law:

$$\mathbf{j} = \sigma\{\mathbf{E} + \mathbf{q}\times\mathbf{H}\} \quad (7)$$

This should be thought of as an empirical result, describing in a macroscopic way how the electric current flows through a volume of conducting matter under the influence of an electric field $\mathbf{E}$ and the electromotive force $\mathbf{q}\times\mathbf{H}$ that is set up by motion relative to a magnetic field. The process of electrical conduction in gases in the presence of a magnetic field is really somewhat involved. Basically, a force acts on any charged particle that is moved across a magnetic field. In our case the charged particles are the electrons and ions of the gas, and, in relatively dense gases, they are constrained to move with the gas velocity $\mathbf{q}$. The electromotive force on them causes them to drift across the flow, their motion being impeded by frequent collisions with the other particles, and a net flux results that is described by the second term of Eq. (7). The first term represents a similar drift of charged particles, but here caused by the electric field $\mathbf{E}$.

The symbol $\mathbf{E}$ represents the total electric field strength (e.g., volts per unit length) due to external effects, such as the field set up by charged boundaries of the flow, and internal effects—i.e., separation of charges or *polarization*.[3] $\mathbf{E}$ is measured in the frame relative to which $\mathbf{q}$ is measured. In our approximation ($q \ll c$ = speed of light), $\mathbf{H}$ is not a function of $\mathbf{q}$. One can think of the term $\mathbf{q}\times\mathbf{H}$ as representing a tiny generator or source of e.m.f. at any point in the moving fluid; the effect of its e.m.f. is divided between driving a current through the gas and separating the positive and negative charges. If no current can flow, because of the presence of insulators, for example, the whole e.m.f. must be opposed by the field $\mathbf{E}$—i.e., by charge separation. More generally, the current density $\mathbf{j}$ cannot always be distributed like $\mathbf{q}\times\mathbf{H}$, so that a net field $\mathbf{E}$ will generally result, in magneto-aerodynamics. A calculation shows that the distance through which the positive and negative charges are moved in a gas to set up any reasonable field strength $\mathbf{E}$ is extremely small. It is a good approximation, therefore, to consider any infinitesimal sample of the gas to be neutral in charge, thus the field $\mathbf{E}$ appears to be produced by doublets—i.e., the gas is polarized. This is the approximation usually made for dielectrics, but it is also appropriate here. It does not imply that $\mathbf{E}$ is zero or negligibly small.

The importance of the quantity $\mathbf{E}$ is illustrated by combining Eqs. (6) and (7). The first two right-hand terms combine as follows:

$$\left.\begin{aligned}\mathbf{q}\cdot\mathbf{j}\times\mathbf{H} + (j^2/\sigma) &= \mathbf{q}\cdot\mathbf{j}\times\mathbf{H} + (\mathbf{E}+\mathbf{q}\times\mathbf{H})\cdot\mathbf{j}\\ &= \mathbf{E}\cdot\mathbf{j}\end{aligned}\right\} \quad (8)$$

where the rule of signs of a scalar triple product has been used. Thus the net magneto-aerodynamic contribution to the energy is seen to involve directly the electric field $\mathbf{E}$.

Maxwell's Equations

The introduction of Ohm's Law has related $\mathbf{j}$ to $\mathbf{q}$ and $\mathbf{H}$, but only with the involvement of a new unknown, $\mathbf{E}$. The set of equations is rendered determinate by means of Maxwell's field equations:

$$4\pi\mathbf{j} = \operatorname{curl}\mathbf{H} \quad (9)$$

$$\operatorname{curl}\mathbf{E} = -(\partial\mathbf{H}/\partial t) \quad (10)$$

As before, we have assumed the fluid to have the same magnetic permeability as empty space and have used electromagnetic units. We have neglected "displacement currents" in writing Eq. (9).[7]

Relative Magnitudes of Terms

Having written down the equations of motion, we are now able to investigate the relative magnitudes of the terms that appear, and in this way make some prediction of the importance of magneto-aerodynamic effects. There is an equally important reason for making this investigation—namely, that the set of equations is formidable and will require simplification. Aerodynamicists have had little success in trying to solve the equations of compressible viscous gas flow without drastic approximations, and it is even less likely that they can be handled with the added complexity of electro-magnetic terms. It will be necessary to approximate in the same rational way—i.e., to retain the most significant effects while discarding others in appropriate areas and types of flow. One may ask in this spirit, will there be any application of the magneto-aerodynamics of ideal fluids? Will the boundary-layer approximation still apply? Will the same approximations that the astrophysicists make in magneto-hydrodynamics (which will be described below) be permissible in aeronautics?

To begin this part of the study, we need, first of all, some estimate of the probable magnitudes of the conductivity σ and the magnetic field strength $\mathbf{H}$.

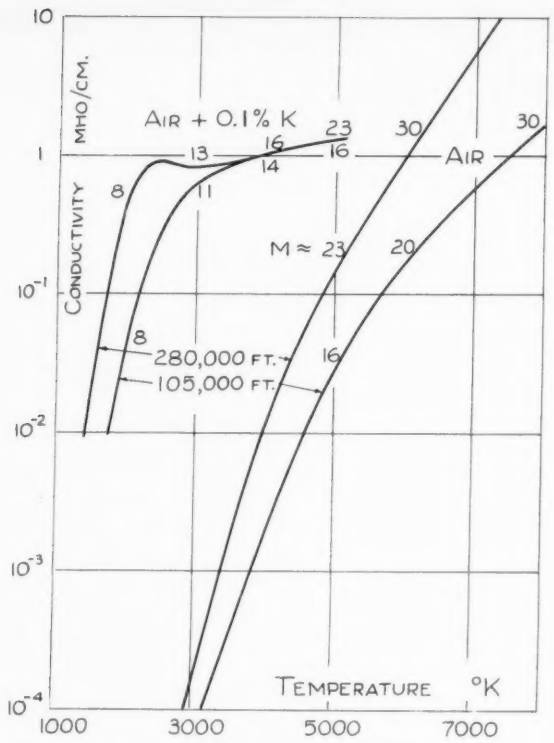

FIG. 1. Calculated conductivity of air and of air seeded with 0.1 per cent potassium (by weight) as functions of temperature for two altitudes. Corresponding Mach Numbers M giving approximately these stagnation temperatures are indicated. (From references 4 and 5.)

In the light of Ohm's Law, Eq. (7), we might also ask about the probable magnitude of $\mathbf{E}$, but we shall answer this question by specifically assuming that it has the same order of magnitude as $\mathbf{q} \times \mathbf{H}$. This assumption implies that the only electric fields present in the air are those induced by magneto-gasdynamic phenomena.

Conductivity

As has already been pointed out, electrical conduction in a gas is accomplished by a drift of charged particles. Conductivity is therefore increased by increasing the number of charged particles and reduced by increasing the probability of their collisions with impeding particles—i.e., atoms, molecules, and charged particles.

Let α denote the "fractional ionization" of the gas, defined as the number of original particles ionized. Thus α is nearly zero for air at room temperature, and $\alpha = 1$ represents a completely ionized gas, in which each original particle has given up one electron. Although α can exceed 1, the state of complete ionization represents a relatively large value for most applications, attained only at very high temperature. When α is small, so that charged particles in the main collide with neutral molecules, one arrives at the result

$$\sigma \sim \alpha T^{-1/2} \tag{11}$$

This regime is probably typical of aeronautical cases, but, in general, relation (11) is misleading in form since α itself is strongly dependent on the temperature T. Thus even in this regime, σ varies rapidly with T.

At the other extreme, when collisions between charged particles are dominant, the conductivity becomes independent of α, and relation (11) is replaced by

$$\sigma \sim T^{3/2} \tag{12}$$

There is an important case, however, in which the strong dependence of σ on T may be minimized, namely the case where conductivity is achieved by *seeding*. This means that an easily ionizable substance, such as potassium or sodium, is introduced into the air. The air temperature may be high enough to ionize completely this seeding substance, though it is insufficient to ionize the air itself appreciably. The result is then to remove the temperature dependence of α on T in Eq. (10), making σ relatively insensitive to temperature. The effects of seeding with various substances have been studied by R. Rosa in a Cornell University thesis.[4]

Some data on conductivity of air with and without seeding, from references 4 and 5, are presented in Fig. 1. The Mach Numbers spotted along the curves are only approximate and are intended to orient the reader as regards the relationship of stagnation temperature to flight speed. It is seen that σ for atmospheric air does not exceed about 0.1 mho/cm. even at the temperature corresponding to satellite speeds. On the other hand, one may obtain values near 1.0 mho/cm. by seeding, even at Mach Numbers contemplated for manned aircraft.

For purposes of orientation, it might be helpful to list the conductivities of other similar substances, in the same units. For example,

Copper	600,000 mho/cm.
Mercury	10,800 mho/cm.
Salt water (saturated at 25°C.)	0.25 mho/cm.
Pure water	0.0000002 mho/cm.

On the basis of Fig. 1, we shall adopt the value $\sigma = 1.0$ mho/cm. as a standard for certain numerical comparisons below. This value has the virtue that it is easy to change in any numerical result by appropriate multiplication.

Magnetic Field Strength

For the magnetic field strength H, on the other hand, there is no completely rational basis of estimation. Nevertheless, some milestones can be identified. A field strength of about 20,000 gauss saturates an iron core at room temperature. It is not certain that iron cores can be utilized in aeronautics in view of their weight; still, we can be sure that if they are used the saturation value will be the maximum field. This would seem to set only a very high upper limit even though in principle an air-core magnet could be made stronger.

Another indication of practical field strengths may be suggested by the value available in a permanent magnet. This runs to perhaps 1,500 or 2,000 gauss for good modern materials.

It seems probable that in aeronautical applications magnetic fields will be produced by air-core electromagnets whose currents are generated magneto-aerodynamically. The dimensions of such solenoids can be estimated in terms of vehicle dimensions, but since the number of turns will be determined by such matters as weight and resistance, one still does not have an estimate of H. In some simple computations carried out below we shall adopt rather arbitrarily the value $H = 1000$ gauss. Once again, its main virtue may be that it affords easy correction to other values for those who do not concur.

Dimensionless Ratios

In fluid mechanics it is useful to compare the magnitudes of dynamic (inertial) and viscous effects by forming their ratio, assuming that geometrically similar patterns of flow are being compared. The result, of course, is the Reynolds Number. It often has values of hundreds of thousands if the typical length is taken to be body diameter or wing chord, and one concludes that the viscosity can be ignored throughout most of the flow field. It is only a slight refinement of this procedure to introduce the boundary-layer thickness as the typical length (or, conversely, to inquire what typical length is required to make viscosity important) and to show thereby that inertial and viscous effects are comparable in magnitude in a boundary layer.

Let us undertake to apply this method to compare the e.b.f. with the dynamic force—i.e., the first and last terms of Eq. (4). In order of magnitude, the ratio is

$$\frac{\text{e.b.f.}}{\text{dynamic force}} = \frac{jH}{(1/2)\rho V^2/L} = \frac{\sigma V H^2 L}{(1/2)\rho V^2} \quad (13)$$

where V is the typical speed, say the flight speed, and L the scale-determining length. Here we assume, as mentioned above, that the electric field $\mathbf{E}$ has the same order of magnitude as $\mathbf{q} \times \mathbf{H}$; in other words, that the current density j is of order σVH. If L is put equal to an aircraft or missile length (or diameter), one is comparing the total force per unit cross section of the flow, which can be applied over this length, to the dynamic pressure of flight. Some values are plotted in Fig. 2, where altitude and Mach Number are the variables and the assumptions are stated. It appears that the e.b.f. will be big enough to affect the flow appreciably at high altitudes and high speeds.

Naturally, if we form the ratio of body force to viscous force we obtain the product of this number and the Reynolds Number:

$$\text{e.b.f./viscous force} = (\text{e.b.f./dynamic force}) \times Re \quad (14)$$

where $Re = \rho VL/\mu$. Thus, this ratio is many times as large as the one plotted in Fig. 2, except in boundary layers, wakes, etc., where the significant Reynolds Number is much smaller. The immediate conclusion is that an inviscid theory of magneto-aerodynamics is generally useful but must be interpreted in the light of boundary-layer theory. In other words, boundary layers and similar viscous regions have their common significance, in magneto-aerodynamic flows as well.

The number calculated in Eq. (14) becomes twice the square of the Hartmann Number[6] when the significant length is the diameter or breadth, D, of a pipe or channel:

$$2Ha^2 = [\sigma VH^2 D/(1/2)\rho V^2] \times [\rho VD/\mu] = 2\sigma H^2 D^2/\mu \quad (15)$$

A third interesting ratio is obtained by comparing electrical currents rather than forces. Let us compute the ratio of motion-induced current to the current necessary to produce the field $\mathbf{H}$. In doing so, we shall assume again that the current density j is of order σVH. The current to produce $\mathbf{H}$, on the other hand, depends on the dimension and the number of turns in the coils of the electromagnet. Dimensionally, this current $\approx H/L$, but a large factor, the number of turns, may be involved. Ignoring this omission, one has

$$\sigma VH/(H/L) = \sigma VL = R_m \quad (16)$$

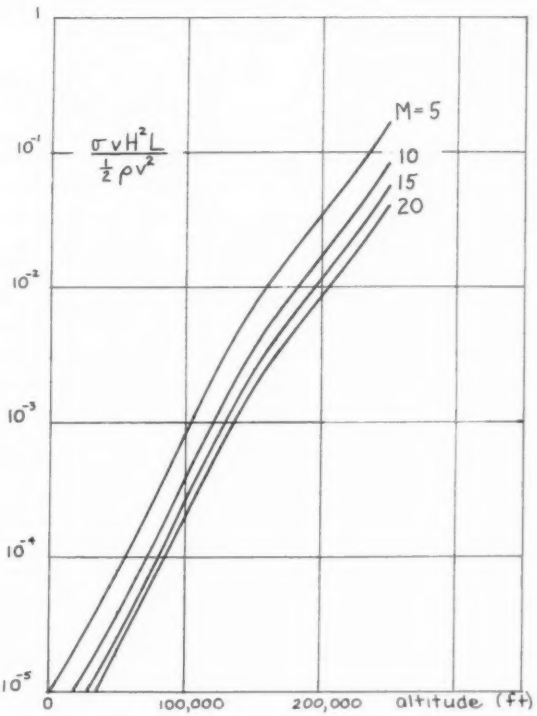

FIG. 2. Values of the ratio of typical electric body force to dynamic force as function of Mach Number and altitude, assuming $\sigma = 1$ mho/cm., $H = 1{,}000$ gauss, and $L = 1$ m.

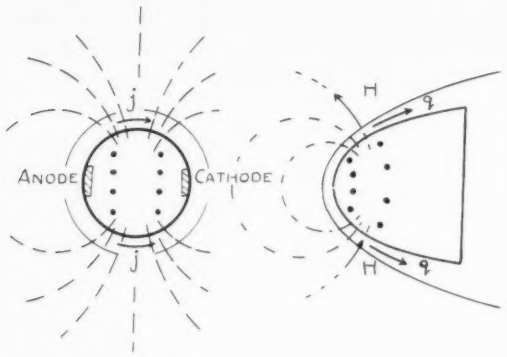

FIG. 3. Sketches of proposed device using magneto-aerodynamic effects to decelerate or control re-entry missiles.

Because of its resemblance to a Reynolds Number, this ratio has been called the "magnetic Reynolds Number."[7] It can also be interpreted as the ratio of motion-induced magnetic field to applied magnetic field. In this sense, one recognizes that the currents generated involve their own magnetic fields, in accordance with Eq. (9). This can be thought of as a perturbation of an applied magnetic field. The magnitude of the perturbation would follow from Eq. (9) by a process of integration equivalent to the calculation of the velocity field of a vortex; the result would certainly be of magnitude σVHL. Thus the ratio of induced to applied magnetic field strengths is equal to the magnetic Reynolds Number. This may be a more satisfactory interpretation of R_m since it does not involve the number of coil-turns mentioned above.

In astrophysical and similar problems involving either high conductivities and/or very large dimensions, the magnetic Reynolds Number may be so large as to show that the motion-induced magnetic field is many times as large as the applied field. In such cases, the applied field may sometimes be neglected entirely. This leads to the concept of a fluid of infinite conductivity. For such a fluid the differential Eqs. (3) to (10) are much simplified. For example, Eq. (7) requires that $\mathbf{E} + \mathbf{q} \times \mathbf{H}$ be zero, since $\mathbf{j}$ must remain finite. It can be shown that under these conditions the magnetic field is convected with the fluid. Since $\mathbf{j}$ is finite, the Joule heating disappears. There is a considerable body of literature pertaining to this case, especially because of its astrophysical importance, as has been mentioned.

Returning to aeronautics, let us investigate the probable values of our magnetic Reynolds Numbers. Suppose that $\sigma = 1.0$ mho/cm. and $L = 1.0$ m. as before, then

$$R_m = \sigma V L = 10^{-5} V(\text{m./sec.}) \qquad (17)$$

where the factor 10^{-5} has been introduced to relate the present units to electromagnetic units. Thus R_m is less than 1/10 even at satellite speeds, and the approximation of infinite conductivity seems not to be appropriate for aeronautics. On the other hand, considering the missing factor related to coil-terms, the values of R_m in Eq. (17) may be large enough to make an aeronautical system self-powered—i.e., the currents induced by flow of seeded air may be sufficient to power the electromagnets that produce the field.

EXAMPLES

In this section we propose to present a few examples of magneto-aerodynamic flows, chosen to illustrate some of the effects discussed above and some of the difficulties of solving the equations.

Deceleration of Flow

Consider the body force $\mathbf{j} \times \mathbf{H}$ with the current density given by Ohm's Law (Eq. (7)):

$$\mathbf{j} \times \mathbf{H} = \sigma\{\mathbf{E} \times \mathbf{H} + (\mathbf{q} \times \mathbf{H}) \times \mathbf{H}\} \qquad (18)$$

The force $\sigma(\mathbf{q} \times \mathbf{H}) \times \mathbf{H}$ always has a component *opposing* the flow—i.e., tending to decelerate the flow.

A possible application of this effect occurs in missile re-entry where it is sometimes desirable to increase the missile drag. This might be accomplished as sketched in Fig. 3. A missile nose is shown enveloped by a layer of hot, ionized air. It is proposed that a magnetic field $\mathbf{H}$ be provided and that the current generated, $\mathbf{j}$, be made to flow through electrodes, as sketched. Inside the missile, the current generated would activate the electromagnet. In this situation, as is mentioned again below, the electric field strength due to polarization, $\mathbf{E}$, would be small if substantially two-dimensional conditions occur in the ionized layer. Thus the vectors representing the e.b.f. are shown in Fig. 3 to be opposite to the flow direction everywhere.

The result would be a considerable drag on the missile; the force would be applied to the structure of the electromagnets. From an energy viewpoint, one recognizes that kinetic energy is being converted to electrical form and then being dissipated in Joule heating of both the ionized air and the coils of the electromagnets.

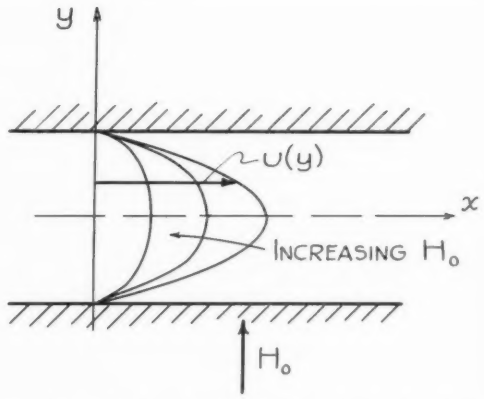

FIG. 4. Poiseuille flow of a conducting liquid, I. Magnetic field applied in plane of flow.

We have not made a detailed study of this device. A device based on similar principles was studied in detail by R. M. Patrick in a Cornell thesis.[5] Patrick's objective was to produce lift rather than drag, so that he considered the device at angles of attack.

In applications of this kind it is clear that the distribution of the e.b.f. across the ionized layer is nonuniform because the distribution of $\mathbf{q}$ is nonuniform. In view of the usual boundary-layer profile, it appears that the decelerating force must increase in magnitude with distance from the body surface. The result must then be a tendency to alter the boundary-layer profile in a sense that would diminish both heat transfer and skin friction. These tendencies have been recognized by Rossow,[8] whose work will be mentioned again in connection with the next example.

Two-Dimensional Channel Flow (I)

A classical case of magneto-hydrodynamic flow is the one sketched in Fig. 4, namely two-dimensional steady flow between infinite, parallel, insulating walls (Poiseuille flow) with a uniform magnetic field $\mathbf{H}_0$ applied normal to these walls. This case was treated by Hartmann[1] for an incompressible fluid. Under the hypothesis stated it can be assumed that all physical quantities are functions of y only (excepting, of course, the pressure p, which can vary linearly with x).

Eq. (10) implies div $\mathbf{H} = 0$, and, in the present problem, this means that the y-component of $\mathbf{H}$ is constant and equal to H_0. Similarly, Eq. (9) states div $\mathbf{j} = 0$, and this means that the y-component of $\mathbf{j}$ is constant; it must therefore be equal to zero since the top and bottom walls are insulators. For incompressible flow, then, Eq. (4) becomes

$$P = \mu(d^2u/dy^2) - j_zH_0 \tag{19}$$

where P denotes the constant pressure gradient $\partial p/\partial x$ and j_z is the z-component of $\mathbf{j}$.

The equation for the z-component of momentum now states that no current flows in the x direction—i.e., $\mathbf{j}$ has only a z-component. The remaining equation of momentum then becomes

$$\partial p/\partial y = H_x j_z \tag{20}$$

where H_x is the x-component of $\mathbf{H}$. Further consequences of the single-component nature of $\mathbf{j}$ follow from Eq. (9)—namely, that H_z, the z-component of $\mathbf{H}$, must be constant and

$$4\pi j_z = -\partial H_x/\partial y \tag{21}$$

According to the hypotheses of the present problem, the constant H_z must be equal to zero, but in any case it does not affect the dynamics of the flow—i.e., the solution is the same if the applied magnetic field has a z-component.

An analysis of the electric field vector $\mathbf{E}$ is accomplished by means of Eq. (10), which states curl $\mathbf{E} = 0$ in this problem. This leads to the conclusion that both the x- and z-components of $\mathbf{E}$ are constants. But Ohm's Law, Eq. (7), now states that the x-component is zero, that the y-component is equal to uH_z, and that j_z is given by

$$j_z = \sigma\{E_0 + uH_0\} \tag{22}$$

where E_0 is the constant z-component of the electric field, determined by boundary conditions at the extremities of the flow. Combining Eqs. (19) and (22), we have the differential equation for $u(y)$,

$$\mu(d^2u/dy^2) - \sigma H_0^2 u = P + \sigma E_0 H_0 \tag{23}$$

the solution of which is

$$u = -\frac{P + \sigma E_0 H_0}{\sigma H_0^2}\left\{1 - \frac{\cosh(\sqrt{\sigma/\mu}\, H_0 y)}{\cosh(\sqrt{\sigma/\mu}\, H_0 a)}\right\} \tag{24}$$

where a is the channel half-width as shown in Fig. 4. The familiar parabolic profile of Poiseuille flow is obtained from Eq. (24) by carrying out the limiting process $\sigma \to 0$.

It is interesting that in this case the velocity profile shape does not depend on E_0, although the current density certainly does, as well as the Joule heating.

The profiles in Fig. 4 are sketched from Hartmann's paper. They show how the parabolic profile of Poiseuille flow is flattened by the magneto-hydrodynamic effect. The flow of fluid for given pressure gradient $\partial p/\partial x$ is reduced.

The solution is completed by integration of Eq. (21) for H_x, j_z being given by Eqs. (22) and (24). Also, one can combine Eqs. (20) and (21) and integrate, yielding

$$\begin{aligned} p &= -(1/8\pi)H_x^2 + \text{function of } x \\ &= -(1/8\pi)H_x^2 + Px + \text{constant} \end{aligned}\Big\} \tag{25}$$

This type of result has led to the terminology "magnetic pressure" for terms like $H_x^2/8\pi$. It is clear that in the present problem the pressure gradients across the channel arise from the interaction of the induced current with the accompanying induced magnetic field.

The alteration of profiles by magneto-hydrodynamic effects in this problem suggests that a similar effect may occur in the analogous boundary-layer problem. This leads to the problem studied by Rossow[8] (the case of two-dimensional incompressible flow over an infinite flat plate with a normal magnetic field). Rossow's results show changes of profile analogous to those of Hartmann, as predicted above. Rossow proceeds to calculate the alteration of temperature profiles, accounting for Joule heating, heat conduction, and viscous dissipation. He concludes that heat transfer to the wall may be appreciably reduced by magneto-hydrodynamic effects.

Rossow's paper involves two interesting extensions of this problem. One is a calculation of the analogous case with magnetic field fixed to the undisturbed fluid stream. This represents, for example, the case of a plate moving through the atmosphere and the earth's magnetic field. The second is an investigation of the

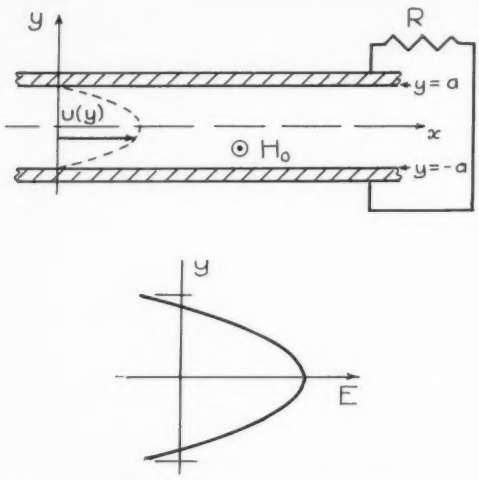

FIG. 5. Poiseuille flow of a conducting liquid, II. Magnetic field applied normal to plane of flow. Top and bottom walls of channel are conducting.

effects of variable σ. It has already been pointed out that σ varies rapidly with temperature; accordingly, Rossow writes

$$\sigma = \text{constant } [(u_\infty - u)/u_\infty] \tag{26}$$

where u_∞ denotes the stream speed. Although Eq. (26) is rather arbitrary, it should give an indication of the reduction of magneto-aerodynamic effects when conductivity drops off to a negligible value at the edge of a boundary layer. This is not quite the case sketched in Fig. 3, to be sure, for there the ionized layer is bounded by a shock wave, and the approximation of constant σ does not seem so objectionable.

Two-Dimensional Channel Flow (II)

A slightly different modification of Poiseuille flow is sketched in Fig. 5; this represents the same case as in Fig. 4, but with the uniform magnetic field directed along the z-axis—i.e., normal to the plane of the flow. This problem has the virtue of illustrating how an electric field **E** is induced by the motion; it also shows how relatively complicated a seemingly simple flow may become with magneto-hydrodynamic effects present. We shall treat it only in the approximation of first-order perturbations. Specifically, we assume that the magnetic field vector is made up of the uniform applied component $\mathbf{H}_0$ plus a much smaller perturbation **h**.

$$\mathbf{H} = \mathbf{H}_0 + \mathbf{h}, \quad h \ll H_0 \tag{27}$$

The principal effect of the magnetic field is then the production of a current-density component j_y in the y direction, and the x-component of Eq. (4) becomes, approximately,

$$P = \partial p/\partial x = \mu(\partial^2 u/\partial y^2) + j_y H_0 \tag{28}$$

Now Eq. (9) requires div **j** = 0. As in Hartmann's problem above, we postulate that conditions do not vary with the streamwise coordinate x, but we cannot also require independence of z. For the existence of a component j_y implies, according to Eq. (9), that the induced magnetic field varies with z—i.e.,

$$j_y = \partial h_x/\partial z \neq 0 \tag{29}$$

Thus the flow can be only quasi-two-dimensional. Eq. (29) implies that a streamwise component h_x is induced and that it varies with z. This variation signifies that the magnetic lines of force are actually curved whereas in our approximation we consider them to lie straight across the flow in the z direction. The current-density component j_y is then approximately constant and the term $j_y H_0$ in Eq. (28) represents an additional pressure gradient. The solution of Eq. (28) is the parabolic profile of Poiseuille flow, only the flow quantity for given pressure gradient being changed.

The approximate evaluation of j_y follows from Eq. (7):

$$j_y \approx \text{constant} = \sigma\{E_y - uH_0\} \tag{30}$$

If the top and bottom channel walls are insulators, or if the circuit connecting them is open, the only solution is $j_y = 0$. Suppose, however, that the circuit is closed, as sketched, by a conductor of resistance R per unit length and breadth of channel. Integrating Eq. (30) with respect to y, one has, for constant σ,

$$2aj_y = -\sigma\Delta\mathcal{U} - \sigma H_0 \int_{-a}^{a} u\,dy \tag{31}$$

where the top and bottom walls are at $y = \pm a$ and $\Delta\mathcal{U}$ denotes the voltage difference between these walls—i.e.,

$$\int_{-a}^{a} E_y\,dy = -\mathcal{U}(a) + \mathcal{U}(-a) \equiv -\Delta\mathcal{U} \tag{32}$$

But the same current must flow through the exterior circuit—i.e.,

$$j_y = \Delta\mathcal{U}/R \tag{33}$$

Thus, combining Eqs. (31) and (32),

$$j_y = \frac{-H_0 \int_{-a}^{a} u\,dy}{R + (2a/\sigma)} \tag{34}$$

The distribution of electric field is given by

$$E_y = (j_y/\sigma) + uH_0 \tag{35}$$

as sketched in Fig. 5.

It is interesting to note that the current density is proportional to the quantity of flow through the channel. We are informed that flowmeters operating on this principle are available. It is also interesting to consider the energy balance in this case. For this purpose we use Eqs. (6) and (8). The only alteration of Eq. (6) for the case of an incompressible fluid is the deletion of the term $p\partial\rho^{-1}/\partial t$. (To be sure, it

is not common to use the concept of stagnation enthalpy for an incompressible fluid because the total head, $p + \rho q^2/2$, is equally convenient and there is ordinarily no coupling between temperature and velocity. In magneto-hydrodynamics, however, there is such coupling by virtue of Joule heating.)

Thus, the rate at which stagnation enthalpy is being increased is given by Eq. (8). This rate is $\mathbf{j}\cdot\mathbf{E}$, or in our present approximation, $j_y E_y$. By integration of this quantity from wall to wall, this rate is easily found to be

$$j_y \int_{-a}^{a} E_y dy = -j_y^2 R \tag{36}$$

In other words, energy is being extracted from the fluid at a rate equal to the Joule heating of the external resistance. Another check on the energy balance can also be made—namely, that the total work done by the pressure gradient $\partial p/\partial x$ appears in heating of the fluid and the external resistance.

The induced streamwise component h_x of the magnetic field is not negligible, as Eq. (29) indicates. Thus the body-force component $j_y h_x$ in the equation of z-momentum is also appreciable, and there must be a pressure gradient $\partial p/\partial z$ of the same magnitude. To complete this solution by calculating to a better approximation all of the components set up by the motion is a complicated process. This problem has been treated, though not by the perturbation process suggested here, by Shercliffe.[9]

Although this sample does illustrate a case where the electric field is not originally known and must be calculated, it is a particularly simple case in the approximation employed here because the directions of the vectors $\mathbf{j}$, $\mathbf{E}$, and $\mathbf{q} \times \mathbf{H}$ are determined by the hypotheses of the problem. In general, in two- and three-dimensional problems, this is not the case; in fact, these vectors may have three different directions. The technique then employed is to eliminate $\mathbf{j}$ from Eq. (4) means of Eq. (9), and to obtain an auxiliary partial differential equation by combination of Eqs. (7), (9), and (10)—viz.,

$$(1/4\pi)\ \mathrm{curl}^2\ \mathbf{H} = \sigma\{-(\partial \mathbf{H}/\partial t) + \mathrm{curl}\ (\mathbf{q} \times \mathbf{H})\} \tag{37}$$

One-Dimensional Channel Flow—Acceleration of a Gas

Let us consider here a problem of more immediate aeronautical interest—namely, the acceleration of a gas flow in a channel such as a nozzle or tail-pipe. If the Reynolds Number is large and the channel cross-section A changes relatively slowly, one can neglect viscosity and treat the problem by the familiar methods of one-dimensional channel flow. In other words, one can consider the flow speed u to be a function of the coordinate x measured along the channel length only. Thus it is really an average speed. The same approximation can be made for the pressure p, density ρ, etc. The equations of motion, Eqs. (3), (4), and (8), become, for steady flow,

$$\textit{Continuity:} \qquad \rho u A = \text{constant} \tag{38}$$

$$\textit{Momentum:} \quad \rho u u' + p' = \sigma\{E - uH\}H \tag{39}$$

$$\textit{Energy:} \quad \rho u c_p T' + u^2 u' = \sigma\{E - uH\}E \tag{40}$$

where the prime denotes differentiation with respect to the coordinate x.

We recall that, in ordinary flow problems without magneto-aerodynamical effects, Eq. (40) becomes a statement of conservation of stagnation enthalpy. Eq. (38), together with this statement, leads to the familiar results of one-dimensional gasdynamics such as nozzle flow and choking. These appear as special cases in what follows.

Suppose now that not only $A(x)$ but also the field strengths $E(x)$ and $H(x)$ are given. Our point of view is therefore somewhat different from that adopted in our earlier examples, for here we do assume that an electric field is applied by a device exterior to the channel. We imagine, for example, that this field might be generated magneto-aerodynamically by motion of an aircraft and applied across an interior duct or tailpipe. Thus, within reasonable limits, we assume both E and H to be under control of the designer.

In general, for given $A(x)$, $E(x)$, and $H(x)$, Eqs. (38)–(40) cannot be integrated, but the acceleration u' and the derivative of the Mach Number, M', can be calculated. (The Mach Number that appears here is the conventional ratio u/a, where a denotes $\sqrt{\gamma p/\rho}$, $\gamma = c_p/c_v$.) The results are

$$u' = \frac{1}{M^2 - 1}\left\{\frac{u}{A} A' - \frac{\sigma H^2}{p}(u - u_3)(u - u_1)\right\} \tag{41}$$

and

$$M' = \frac{1 + [(\gamma - 1)/2]M^2}{M^2 - 1} \times \left\{\frac{M}{A} A' - \frac{\sigma H^2}{ap}(u - u_3)(u - u_2)\right\} \tag{42}$$

where the significant velocities u_1, u_2, and u_3 are defined as follows:

$$u_1 = [(\gamma - 1)/\gamma](E/H) \tag{43}$$

$$u_2 = \{(1 + \gamma M^2)/[2 + (\gamma - 1)M^2]\}u_1 \tag{44}$$

$$u_3 = E/H \tag{45}$$

The terms involving $A'(x)$ in Eqs. (41) and (42) are familiar to gasdynamicists; they state that the velocity and Mach Number decrease in an expanding channel at subsonic speeds and increase in an expanding channel at supersonic speeds.

The signs of the magneto-gasdynamic terms, on the other hand, depend on the magnitude of u relative to the significant velocities u_1, u_2, and u_3. In particular, u' can be made positive even in constant-area channels at supersonic speeds provided only that u lies in the interval between u_1 and u_3. Furthermore, M' can be made positive in a constant-area supersonic channel if $u_2 < u < u_3$. This is in sharp contrast

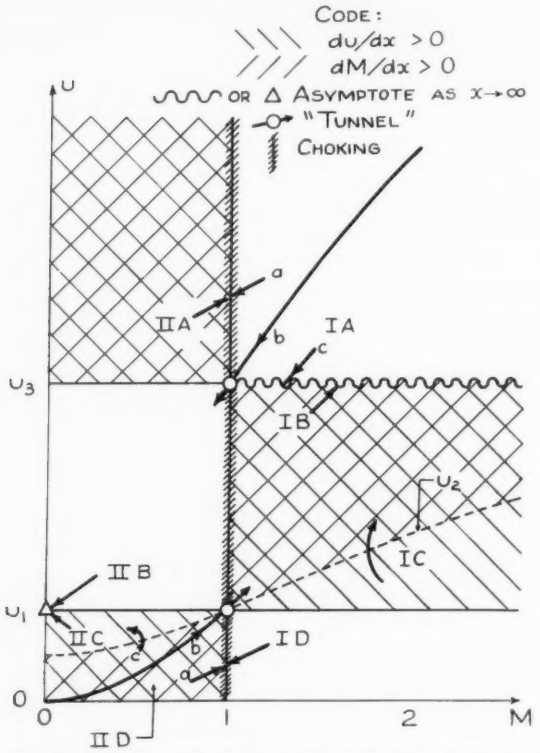

FIG. 6. Magneto-gasdynamic acceleration of one-dimensional flow in a constant-area channel. Regimes of positive acceleration and increasing Mach Number are designated by cross-hatching as shown. u_1, u_2, and u_3 are the "significant speeds" defined in this paper. Arrows denote typical behaviors of flows in the various regimes; arrowheads show direction of increasing x (downstream). *1A*, *1B*, etc. denote areas of different behaviors as indicated.

to the effects of pure heat addition, which always decelerates a supersonic constant-area flow and drives its Mach Number toward 1.

A summary of the various possibilities for constant-area flow is presented in Fig. 6, where the signs of u' and M' in a u, M plane are indicated. There are eight distinct regions in the u, M plane, in which different behaviors of $u(x)$ and $M(x)$ can be predicted from Eqs. (41) and (42). These are identified in Fig. 6 as follows:

(I) $M > 1$	(II) $M < 1$
(A) $u_3 < u$	(A) $u_3 < u$
(B) $u_2 < u < u_3$	(B) $u_1 < u < u_3$
(C) $u_1 < u < u_2$	(C) $u_2 < u < u_1$
(D) $u < u_1$	(D) $u < u_2$

In general, a "barrier" exists at $M = 1$, where the phenomenon of choking occurs: the denominators of both Eqs. (41) and (42) disappear. That this represents choking is evident, from the fact that the curve of u versus x turns back upon itself and becomes double valued after reaching the barrier. Thus the sonic speed can never actually be attained in such a channel, and the phenomenon would have to occur, if at all, at the open end of a channel.

There are, however, two exceptional cases, denoted "tunnels" in Fig. 6. These are two one-way tunnels through the barrier at sonic speed. For these special combinations of parameters (I*Ab* and II*Db*) the numerators and denominators of both Eqs. (41) and (42) disappear simultaneously, and, as can be verified, finite and continuous deceleration and acceleration, respectively, occur. The curves that lead to these tunnels have been plotted in Fig. 6, as they always separate choking from nonchoking channels and represent the special combinations that permit smooth passage through the sonic speed.

Maximum-Acceleration Constant-Area Duct, Supersonic Flow

According to Eq. (41), the acceleration of a supersonic stream in a constant-area channel can be made a maximum by choosing a certain value of E/H—i.e., the value that maximizes the product $-(u - u_3)\times(u - u_1)$. This value is

$$E/H = [(2\gamma - 1)/2(\gamma - 1)]u \tag{46}$$

The maximum acceleration is obtained by substituting this value in Eq. (41); the result is

$$u_{max}' = [1/(\gamma - 1)](\sigma H^2/4m)[M^2u/(M^2 - 1)] \tag{47}$$

where m denotes the constant ρu (the mass flow per unit cross-section area).

As an indication of the possible velocities to be achieved magneto-aerodynamically, we have integrated Eq. (47) for constant γ. In other words, we assume that E/H is varied with x so as to maintain u' always at its maximum value. This calculation involves, first, integration of M as a function of u, which can be carried out using Eqs. (41), (42), and (47). The results are

$$u = \text{constant} \times \left| \frac{M^2}{[(2\gamma + 1)/\gamma] - M^2} \right|^{1/(2\gamma+1)} \tag{48}$$

and finally,

$$(1/m)\int_{x_0}^{x} \sigma H^2 dx \equiv \xi = \frac{4\gamma(\gamma - 1)}{2\gamma + 1}\left\{\frac{\gamma + 1}{\gamma}\ln\frac{u}{u_0} - \frac{\gamma M_0^2 - (2\gamma + 1)}{(2\gamma + 1)\gamma M_0^2}\left[\left(\frac{u_0}{u}\right)^{2\gamma+1} - 1\right]\right\} \tag{49}$$

Here the quantities with subscript 0 denote values at an initial station of the channel. If σH^2 is constant, Eq. (49) permits an easy calculation of the channel length $x - x_0$ for velocity ratio u/u_0. Eq. (49) is plotted in Fig. 7 for several values of M_0, for $\gamma = 1.4$. It is interesting to note that the curve of u/u_0 against ξ becomes practically independent of M_0 for $M_0 > 5$, making u/u_0 a function of ξ only.

The corresponding Mach Numbers are not plotted, but could be determined from Eq. (48). Since u always increases with x in this case, the form of Eq. (48) indicates that M tends toward the value

$\sqrt{(2\gamma + 1)/\gamma}$, or, for $\gamma = 1.4$, $M \rightarrow 1.65$. Numerical calculations show that this approach is very rapid; M is nearly equal to 1.65 when u/u_0 reaches 3 for any initial Mach Number greater than 1. It is clear from this result that there is considerable heating of the gas in a typical case, and that appreciable further increase of flow speed might be achieved by expanding in a supersonic nozzle.

The present results (Eq. (49) and Fig. 7) must not be used when $E - uH$ is greater than the "breakdown" potential of the gas. This critical potential (where arcing occurs and therefore the assumptions of the present studies are violated) varies directly with density in the range of densities anticipated here; i.e., the restriction on our results may be written as

$$E - uH < K_B\rho \tag{50}$$

where K_B has the value of about 2×10^7 volt cm.^{2}/gm. for air.* Thus the restriction can easily be expressed by combining Eq. (46) and inequality (50) to give a maximum permissible value for u, above which Eq. (46) will lead to a violation of (50). It is

$$u < \sqrt{2(\gamma - 1)10^8 K_B m/H} \tag{51}$$

where H is measured in gauss, m in gm. cm.$^{-2}$ sec.$^{-1}$, and u in cm./sec. This does not mean that speeds greater than this cannot be achieved, but only that they cannot be achieved under the maximum-acceleration conditions of Eqs. (46)–(49). For greater velocities, acceleration might have to be accomplished under conditions of constant potential $E - uH$, for example. We are studying further the consequences of this limitation in practical cases.

Conclusions

The studies reported here suggest that electromagnetic effects may become important in aerodynamics, especially if seeding can be used to increase the conductivity of the air. Here we understand "aerodynamics" to mean the realm of flight where the continuum approximation is relatively useful. There are, for example, possibilities of decelerating re-entry missiles, controlling the skin friction and heat transfer in boundary layers, and accelerating or decelerating channel flows magneto-aerodynamically.

The last mentioned of these possibilities appears especially interesting to the present authors, since it permits some significant departures from the restrictions of conventional gasdynamics, such as acceleration of supersonic flows in straight tubes.

There are, however, some formidable practical obstacles in the path of engineering applications of the principles mentioned here. One of these may be the complexity of the equations of motion, since this will hamper the theoretical studies that might lead to significant and efficient applications. More serious,

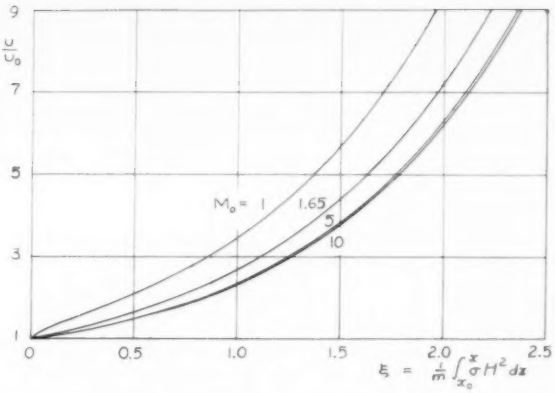

FIG. 7. Magneto-gasdynamic channel flow. Flow speed ratio as function of the channel-length variable ξ for a maximum-acceleration channel of constant area for several initial Mach Numbers.

however, is the problem of the development of magnets powerful enough to provide the required fields and yet light enough for use in flight. Techniques for rendering gases conducting by means of seeding must also be made practical.

Another engineering problem of particular significance seems to be posed by the need for electrodes in all the magneto-aerodynamic devices suggested in the present paper. Hartmann[1] mentioned the high surface resistance of electrodes in contact with mercury in his early experiments. Brogan[10] found a similar phenomenon in a shock tube, where the overall resistance of a circuit including cold copper electrodes in contact with ionized argon was many times the calculated resistance of the gas alone. The solution of this rather basic problem is certainly not obvious at present.

Thus, successful achievement of magneto-aerodynamic effects in flight must be preceded by considerable research and engineering development. The possible benefits to be obtained seem to justify such efforts.

References

[1] Hartmann, J., *Hg-Dynamics I, Theory of the Laminar Flow of an Electrically Conductive Liquid in a Homogeneous Magnetic Field*, Kgl. Danske Videnskabernes Selskab, Math.-fys, Meddelelser XV, 6, Copenhagen, 1937.

[2] Landshoff, R. K. M., (Ed.), *Magnetohydrodynamics, A Symposium*, Kolb, A. C., Kash, S. W., and Petschek, H. E., "Magnetically Driven Shock Waves," pp. 74–100, Stanford University Press, Stanford, 1957.

[3] Sears, F. W., *Principles of Physics II*, "Electricity and Magnetism," p. 187; Cambridge, Mass., 1947.

[4] Rosa, R. J., *Engineering Magneto-Hydrodynamics*, Part 2 of Ph.D. Thesis, Cornell University, June, 1956. (Available from University Microfilms, Ann Arbor, Mich.)

[5] Patrick, R. M., *Magneto-Hydrodynamics of Compressible Fluids*, Ph.D. Thesis, Cornell University, 1956. (Available from University Microfilms, Ann Arbor, Mich.)

[6] Cowling, T. G., *Magnetohydrodynamics*, p. 10; Interscience Publishers, Inc., New York, 1957.

(*Continued on page 258*)

* We can expect the same value to apply for seeded air.

Aeroelastic Instability at High Mach Number†

JAGANNATH P. CHAWLA*

Hughes Aircraft Company

SUMMARY

A brief discussion of the limitations of the piston theory is given. Using Lighthill's approach, the aerodynamic forces on oscillating airfoils are derived in a slightly different form to conform to the NACA practice and the familiar nondimensional flutter coefficients are tabulated for general double and single wedge and parabolic biconvex profiles. Extensive parametric studies are included for preliminary design to aid in estimating the effect on flutter speed and frequency of airfoil thickness and profile, initial angle of attack, modal shape, changes in elastic and inertial properties of the wing, and altitude of flight.

SYMBOLS

a	= velocity of sound
$A_i (i = 1, 2, 3)$	= constants defined in Eq. (23) and Table 1
c	= airfoil chord
h	= subscript for altitude
$\bar{h}$	= amplitude of airfoil oscillation in vertical translation
$h(t)$	= vertical oscillation of airfoil (see Fig. 2)
$I_i (i = 1, 2, 3)$	= integrals defined in Eq. (29)
I_α	= moment of inertia of wing about elastic axis per unit span
k	= reduced frequency $= (1/2)(\omega c/U)$
K_h	= wing stiffness in flexure
K_α	= wing stiffness in torsion
L	= lift force on the airfoil
L_i, M_i $(i = 1, 2, 3, 4)$	= nondimensional flutter coefficients defined in Eqs. (15), (16), and (17).
$\bar{L}_2$	= $L_2(Mk)$
$\bar{L}_4$	= $L_4(Mk)$
$\bar{M}_4$	= $M_4(Mk)$
m	= wing mass per unit span
M	= Mach Number of undisturbed stream $= U/a_\infty$
$\mathfrak{M}$	= moment (positive nose up) per unit span about the axis of pitching oscillations (see Fig. 2)
0	= subscript for sea level
p	= pressure at point on airfoil surface
$p_\infty, \rho_\infty, a_\infty$	= pressure, density, and velocity of sound, respectively, in undisturbed stream
Δp	= pressure on lower surface minus pressure at same point on upper surface
P, Q, R	= constants defined in Eq. (23) and Table 1
r_α	= ratio of radius of gyration in pitch to semichord $= (4I_\alpha/mc^2)^{1/2}$
$T_i (i = 1, 2, \ldots, 6)$	= constants defined in Eq. (23) and Table 1
t	= time
U	= velocity of undisturbed stream
U_f	= critical speed at flutter
$\bar{U}_f$	= $U_f/(c\omega_\alpha)$
w	= "effective piston velocity" $= (\partial Y/\partial t) + U(\partial Y/\partial x)$
w_a	= value of w resulting from α_0 and Y_a
w_i	= value of w resulting from Y_i
x	= coordinate parallel to airfoil chord
x_0	= distance of axis of pitching oscillations behind leading edge
x_α	= distance from axis of pitching oscillations (or elastic axis) to center of mass
y	= coordinate perpendicular to airfoil chord, measured *away* from airfoil on each side of it
$Y(x, t)$	= equation of airfoil surface (upper or lower) at time t
$Y_a(x) \pm Y_i(x, t)$	= equation of $\binom{\text{lower}}{\text{upper}}$ surface of symmetrical oscillating airfoil
Z	= normal force (positive downward) per unit span on airfoil
∞	= subscript for undisturbed stream
α_0	= initial angle of attack of airfoil
$\alpha(t)$	= variable angle of attack (in pitching oscillations)
$\bar{\alpha}$	= amplitude of airfoil pitching oscillations
β	= $(M^2 - 1)^{1/2}$
γ	= ratio of specific heats (assumed constant = 1.4)
δ	= larger of the two dimensionless quantities τ and ϵ
ϵ	= maximum displacement in oscillation divided by airfoil chord
ζ	= $\omega_h/\omega_f = \bar{\omega}_h/\bar{\omega}_f$
η	= ratio of wedge length to airfoil chord (see Fig. 3)
λ	= spanwise coordinate divided by wing semispan
μ	= wing density ratio $= m/(\rho c^2)$
ξ	= x/c
ξ_0	= x_0/c
ξ_α	= x_α/c
ρ	= density of air
σ	= ratio of density of air at altitude to that at sea level $= \rho_h/\rho_0$
σ_T	= density ratio at 35,330 ft. altitude
τ	= thickness-chord ratio of airfoil
$\phi_1(\lambda), \phi_2(\lambda)$	= bending and torsion mode shapes, respectively, of wing
$\omega/2\pi$	= frequency of wing oscillation
$\omega_f/2\pi$	= frequency of oscillation at flutter speed

Received April 26, 1957. Revised and received September 24, 1957.

† The author is grateful to the Hughes Aircraft Company for permission to publish this article and should like to express his appreciation to his colleagues, Drs. William M. Bleakney and Arthur F. Messiter, for helpful discussions. The work was done under contract to the USAF.

* Aerodynamics Department, Systems Development Laboratories.

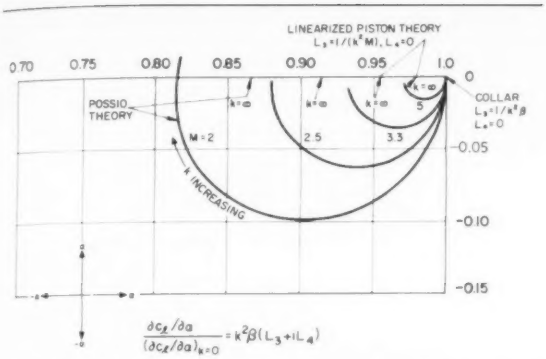

FIG. 1. Vectorial representation of two-dimensional dynamic lift curve slope with reference to steady-state value $4/\beta$ ($\tau = 0$, $\xi_0 = 0.5$).

$\omega_h/2\pi$ = natural frequency of wing in flexure $= (1/2\pi)(K_h/m)^{1/2}$

$\omega_\alpha/2\pi$ = natural frequency of wing in torsion $= (1/2\pi)(K_\alpha/I_\alpha)^{1/2}$

$\tilde{\omega}_f$ = ω_f/ω_α

$\tilde{\omega}_h$ = ω_h/ω_α

Γ = I_3^2/I_1I_2

$(\ )'$ = differentiation with respect to x

$(\ )\dot{}$ = differentiation with respect to time

(1) INTRODUCTION

FOLLOWING the original work of Hayes,[1] Goldsworthy,[2] and Lighthill,[3] the piston-theory concept, particularly as applied to problems in aeroelasticity, has been developed further by Ashley, Heller, Landahl, Mollo-Christensen, and Zartarian[4–7] at the Massachusetts Institute of Technology. Lighthill made use of a truncated binomial expansion of the "simple-wave" pressure relationship, Eq. (1), to derive aerodynamic coefficients for oscillating airfoils at high Mach Number.

$$p/p_\infty = [1 + (1/2)(\gamma - 1)(w/a_\infty)]^{2\gamma/(\gamma-1)} \quad (1)$$

An outstanding advantage of this approach is the simple manner in which the effect of airfoil thickness is taken into account. For a given profile at zero angle of attack this effect depends on the parameter $M\tau$. It can be shown that first-order piston theory (linear approximation for p/p_∞) gives results for the load distribution which are identical to those obtained by assuming $(1/M^2) \ll 1$ in the solution derived from linearized supersonic theory for a wing of infinite span. Inclusion of second-order terms in the pressure relation gives terms in the load distribution which are linear in thickness, and the third approximation gives terms quadratic in thickness. The magnitude of the parameter $M\tau$ offers an indication of the number of terms needed in the expansion of Eq. (1) for determining forces on oscillating airfoils at zero angle of attack.

It is interesting to note that the results of linearized piston theory are equivalent to the expressions given by Collar[8] if $M^2 \gg 1$. Collar attempted to derive the two-dimensional flutter derivatives for supersonic speeds from a rather intuitive approach by assuming that Ackeret's theory of steady flow might be applied, without modification, to the case of nonsteady flow. Temple and Jahn[9] provided a mathematical basis for Collar's work and showed that his results gave the correct (linearized) values for the limiting case of Mach Number approaching infinity, $M^2 \gg 1$.

Ashley, Heller, and Zartarian[6, 7] have given some applications of the piston-theory to problems in aeroelasticity such as the flutter of a rectangular wing, the flutter of a flat thin panel, and unsteady transients due to gusts. They have also done some elementary trend studies for preliminary design. In reference 7, in the section on three-dimensional flutter problems, they reported results obtained from strip theory and a standard Rayleigh-Ritz type of analysis making use of uncoupled modes. Their work is extended here to include a mode-shape parameter, and extensive parametric studies are carried out for preliminary design work, to aid in the estimation of the effect on flutter speed of the airfoil thickness and profile, initial angle of attack, and changes in elastic and inertial properties of the wing. Adding initial angle of attack to Lighthill's work, expressions containing elementary integrals are developed for the nondimensional flutter coefficients L_i and M_i ($i = 1, 2, 3, 4$) which are tabulated for five different profiles.

(2) LIMITATIONS OF THE PISTON THEORY

The inaccuracy and inadequacy of linearized theory of oscillating airfoils in supersonic flow, and the computational difficulties of existing nonlinear theories, led Lighthill to propose a simple nonlinear theory for high Mach Number, based on the piston concept. Since the publication of Lighthill's work, the Fluid Dynamics Research Group at the Massachusetts Institute of Technology have made extensive studies of the linear and nonlinear theories making use of this concept and have pointed to its usefulness for problems in aeroelasticity. It should be instructive to briefly review some of the salient features of these studies.

Landahl, Mollo-Christensen, and Ashley showed that linearized piston theory can be used for arbitrary small motions of thin two-dimensional airfoils whenever any one of the following conditions is met:

$$\text{(a)}\quad M^2 \gg 1, \qquad \text{(b)}\quad kM^2 \gg 1, \qquad \text{(c)}\quad (kM)^2 \gg 1 \quad (2)$$

In order to illustrate these requirements, a comparison is shown in Fig. 1, for rigid plunging and pitching oscillations, between the results of the linearized piston theory, the more exact Possio theory,[10] and the theory suggested by Collar. All these theories are applicable to a very thin airfoil of infinite aspect ratio, at a small angle of attack, and oscillating in a nonviscous, unseparated flow free from strong shocks.

Fig. 1 shows a vectorial representation of the dynamic two-dimensional lift curve slope at any frequency in terms of the steady state ($k = 0$) value of $4/\beta$. This ratio equals $k^2\beta(L_3 + iL_4)$. For the axis of pitch at

midchord, the limiting value of this ratio as $k \to \infty$, obtained from Possio theory, is β/M. Linearized piston theory gives the same value for $M^2 \gg 1$.

It is seen that for any value of the reduced frequency k the errors arising out of the simpler theories become progressively smaller with increasing Mach Number. If M is not large, the results of the linearized piston theory, namely, $L_1 = 0$, $L_2 = 1/(kM)$, etc., are correct only for $k \to \infty$, as predicted by the requirements of Eq. (2). Collar's results for L_1, L_2, etc., are identical to those of piston theory except that M is everywhere replaced by β; at moderate values of M his expressions are in error for all values of k. If, as indicated in reference 9, his formulas for L_1' and M_4' are multiplied by $[1 - (1/\beta^2)]$, they agree with the initial terms of the frequency expansions given by Possio, while the validity for large M and moderate k is not affected. Thus Collar's corrected results are valid for $k \to 0$, and linearized piston theory is valid for $k \to \infty$. For intermediate values of k, both theories are in error except for large values of M, say $M^2 \geqq 10$.

The authors of reference 4 also worked out a tip correction for a rectangular wing, disregarding the spanwise bending. The correction is based on an expansion in powers of k, given in reference 11, and can be utilized with advantage within the limitations mentioned above.

Landahl extended the above work by deriving corrections to the linear and nonlinear terms of Lighthill's piston theory. The corrections become important at lower Mach Numbers, say in the neighborhood of $M = 2$. The effect of δ/M^3 and δ/M^5 terms in the pressure coefficient is shown in reference 5. Landahl's solution is restricted to frequencies of oscillation for which $(k/M)^2 \ll 1$ and to thickness or amplitude of oscillations such that $(\delta M)^2 \ll 1$. He showed that the second-order terms in Lighthill's calculations are larger than the error in the linear term only when $\delta M^3 \gg 1$.

In the sections that follow, simplicity of Lighthill's approach is retained in order to make a detailed parametric variation and to study the effect of each parameter on flutter speed and frequency of oscillating airfoils at high Mach Number.

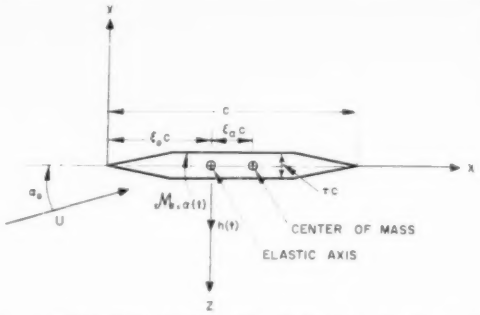

FIG. 2. Coordinate system and notations for an oscillating airfoil section.

(3) AERODYNAMIC FORCES ON OSCILLATING AIRFOILS

Consider a symmetrical airfoil at an angle of attack α_0 (see Fig. 2). Let the equation of both surfaces (with y measured away from the airfoil in each case) be $y = Y_s(x)$. Then the steady-state downwash is

$$w_s(x) = U[\mp \alpha_0 + Y_s'(x)] \tag{3}$$

The negative sign applies to the upper surface and the positive to the lower surface. Let the changes in y due to oscillations be $Y_t(x, t)$ and the corresponding downwash be $w_t(x, t)$. Then the total downwash is

$$w = UY_s'(x) \mp U\alpha_0 \mp w_t(x, t) \tag{4}$$

where $$w_t(x, t) = (\partial Y_t/\partial t) + U(\partial Y_t/\partial x) \tag{5}$$

Substituting Eq. (4) in the cubic expansion of Eq. (1), namely,

$$p/p_\infty = 1 + \gamma(w/a_\infty) + [\gamma(\gamma + 1)/4] \times (w/a_\infty)^2 + [\gamma(\gamma + 1)/12](w/a_\infty)^3 \tag{6}$$

and subtracting the pressure distribution on the upper surface from that on the lower surface, the load distribution on the airfoil is

$$\Delta p/p_\infty = 2\gamma \left\{ \left[M\alpha_0 + \frac{\gamma+1}{2}(M\alpha_0)\, MY_s'(x) + \frac{\gamma+1}{4}(M\alpha_0)\, M^2 Y_s'^2(x) + \frac{\gamma+1}{12}(M\alpha_0)^3 \right] + \left[1 + \frac{\gamma+1}{2} MY_s'(x) + \frac{\gamma+1}{4} M^2 Y_s'^2(x) + \frac{\gamma+1}{4}(M\alpha_0)^2 \right](w_t/a_\infty) + \left[\frac{\gamma+1}{4}(M\alpha_0) \right](w_t/a_\infty)^2 + \frac{\gamma+1}{12}(w_t/a_\infty)^3 \right\} \tag{7}$$

Eq. (7) is seen to have one part which is independent of the downwash due to oscillations. This is the steady-state loading on the airfoil due to angle of attack and profile and may be extracted to obtain the corresponding lift and pitching moment of the airfoil. Thus the two-dimensional lift is

$$L = \int_0^c \Delta p\, dx = 2\gamma p_\infty M\alpha_0 c \left[1 + \frac{\gamma+1}{12}(M\alpha_0)^2 + \frac{\gamma+1}{2} M \int_0^1 Y_s'(\xi)d\xi + \frac{\gamma+1}{4} M^2 \int_0^1 Y_s'^2(\xi)d\xi \right] \tag{8}$$

Defining $\partial C_L/\partial\alpha = (\partial L/\partial\alpha)/(1/2)\,\rho U^2 c$, the steady-state lift coefficient slope is

$$\left(\frac{\partial C_L}{\partial \alpha}\right)_{s.s.} = (4/M)\left[1 + \frac{\gamma+1}{4}(M\alpha_0)^2 + \frac{\gamma+1}{2} M \int_0^1 Y_s'(\xi)d\xi + \frac{\gamma+1}{4} M^2 \int^1 Y_s'^2(\xi)\, d\xi \right] \tag{9}$$

For an airfoil with sharp leading and trailing edges, $Y_s(0) = Y_s(1) = 0$, so that

$$\left(\frac{\partial C_L}{\partial \alpha}\right)_{s.s.} = (4/M)\left[1 + \frac{\gamma+1}{4}(M\alpha_0)^2 + \frac{\gamma+1}{4}M^2\int_0^1 Y_s'^2(\xi)\,d\xi\right] \tag{10}$$

Similarly, the pitching moment about an axis distant $x_0 = \xi_0 c$ from the leading edge is

$$\begin{aligned}-\mathfrak{M} &= \int_0^c \Delta p(x - x_0)dx \\ &= 2\gamma p_\infty M\alpha_0 c^2\left\{\left[1 + \frac{\gamma+1}{12}(M\alpha_0)^2\right]\left(\frac{1}{2} - \xi_0\right) + \left(\frac{\gamma+1}{2}\right)M\int_0^1 Y_s'(\xi)\,(\xi - \xi_0)d\xi + \right. \\ &\qquad \left.\left(\frac{\gamma+1}{4}\right)M^2\int_0^1 Y_s'^2(\xi)\,(\xi - \xi_0)d\xi\right\}\end{aligned} \tag{11}$$

Defining $(\partial C_m/\partial\alpha) = (\partial\mathfrak{M}/\partial\alpha)/(1/2)\,\rho U^2c^2$, the steady-state moment coefficient slope is

$$\begin{aligned}-\left(\frac{\partial C_m}{\partial\alpha}\right)_{s.s.} &= (4/M)\left\{\left[1 + \frac{\gamma+1}{4}(M\alpha_0)^2\right]\left(\frac{1}{2} - \xi_0\right) + \left(\frac{\gamma+1}{2}\right)M\int_0^1 Y_s'(\xi)\,(\xi - \xi_0)d\xi + \right. \\ &\qquad \left.\left(\frac{\gamma+1}{4}\right)M^2\int_0^1 Y_s'^2(\xi)\,(\xi - \xi_0)\,d\xi\right\}\end{aligned} \tag{12}$$

As to the time-dependent loading on the airfoil, it is now assumed that the downwash due to oscillations of the airfoil is small compared to the steady-state downwash due to initial angle of attack and profile—that is, (w_i/a_∞) is small compared to $M\alpha_0$ and $MY_s'(x)$, so that the last two terms of Eq. (7) may be neglected.

For an airfoil oscillating vertically and pitching about the axis $x = x_0 = \xi_0 c$, $y = 0$,

$$(w_i/a_\infty) = M\alpha(t) + (\dot{h}/a_\infty) + (\dot{\alpha}/a_\infty)(x - x_0)$$

hence the oscillatory loading on the airfoil is

$$\begin{aligned}(\Delta p/p_\infty) = 2\gamma\{&1 + [(\gamma+1)/4](M\alpha_0)^2 + \\ &[(\gamma+1)/2]MY_s'(x) + [(\gamma+1)/4]\times \\ &M^2Y_s'^2(x)\}[(\dot{h}/a_\infty) + M\alpha + (\dot{\alpha}/a_\infty)(x - x_0)]\end{aligned} \tag{13}$$

and the total load and pitching moment are

$$\left.\begin{aligned}-Z &= \int_0^c \Delta p\,dx \\ \text{and} \\ -\mathfrak{M} &= \int_0^c \Delta p(x - x_0)dx\end{aligned}\right\} \tag{14}$$

Following the lead of the National Advisory Committee for Aeronautics, it is standard American practice to express the section force and moment as

$$Z = -2\rho c U^2k^2\{(L_1 + iL_2)\times[h/(c/2)] + (L_3 + iL_4)\,\alpha\} \tag{15}$$

$$\mathfrak{M} = -\rho c^2U^2k^2\{(M_1 + iM_2)\times[h/(c/2)] + (M_3 + iM_4)\alpha\} \tag{16}$$

For a harmonic oscillation of the airfoil with $h = \bar{h}e^{i\omega t}$ and $\alpha = \bar{\alpha}e^{i\omega t}$, $\dot{h} = i\omega h$ and $\dot{\alpha} = i\omega\alpha$ can be substituted and the expressions for the sectional flutter coefficients become

$$\left.\begin{aligned}L_1 &= -(\partial Z/\partial h)\,(1/4\rho U^2k^2) \\ L_2 &= -(\partial Z/\partial\dot{h})\,(\omega/4\rho U^2k^2) \\ L_3 &= -(\partial Z/\partial\alpha)\,(1/2\rho c U^2k^2) \\ L_4 &= -(\partial Z/\partial\dot{\alpha})\,(\omega/2\rho c U^2k^2) \\ M_1 &= -(\partial M/\partial h)\,(1/2\rho c U^2k^2) \\ M_2 &= -(\partial M/\partial\dot{h})\,(\omega/2\rho c U^2k^2) \\ M_3 &= -(\partial M/\partial\alpha)\,(1/\rho c^2U^2k^2) \\ M_4 &= -(\partial M/\partial\dot{\alpha})\,(\omega/\rho c^2U^2k^2)\end{aligned}\right\} \tag{17}$$

Making use of Eqs. (13), (14), and (17), it can easily be shown that

$$\left.\begin{aligned}&L_1 = M_1 = 0, \quad M_2 = L_4 \\ &L_3 = (1/k)L_2, \quad M_3 = (1/k)M_2 = (1/k)L_4\end{aligned}\right\} \tag{18}$$

so that the flutter coefficients that need be evaluated are L_2, L_4, and M_4, which may be expressed as

$$L_2 = \frac{1}{Mk}\left\{\left[1 + \frac{\gamma+1}{4}(M\alpha_0)^2\right] + \frac{\gamma+1}{2}M\int_0^1 Y_s'(\xi)d\xi + \frac{\gamma+1}{4}M^2\int_0^1 Y_s'^2(\xi)\,d\xi\right\} \tag{19}$$

$$\begin{aligned}L_4 = \frac{1}{Mk}\left\{\left[1 + \frac{\gamma+1}{4}(M\alpha_0)^2\right](1 - 2\xi_0) + (\gamma+1)M\int_0^1 Y_s'(\xi)\,(\xi - \xi_0)\,d\xi + \right. \\ \left.\frac{\gamma+1}{2}M^2\int_0^1 Y_s'^2(\xi)\,(\xi - \xi_0)\,d\xi\right\}\end{aligned} \tag{20}$$

$$\begin{aligned}M_4 = \frac{1}{Mk}\left\{4\left(\frac{1}{3} - \xi_0 + \xi_0^2\right)\left[1 + \frac{\gamma+1}{4}(M\alpha_0)^2\right] + 2(\gamma+1)M\int_0^1 Y_s'(\xi)\,(\xi - \xi_0)^2\,d\xi + \right. \\ \left.(\gamma+1)M^2\int_0^1 Y_s'^2(\xi)\,(\xi - \xi_0)^2\,d\xi\right\}\end{aligned} \tag{21}$$

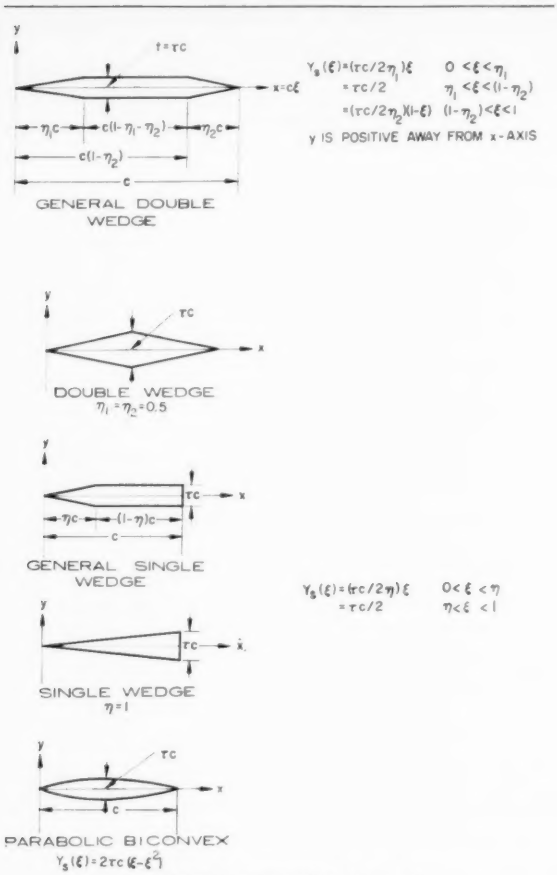

FIG. 3. Airfoil profiles and their equations.

Writing $\bar{L}_2 = (Mk)L_2$, $\bar{L}_4 = (Mk)L_4$, and $\bar{M}_4 = (Mk)M_4$, the flutter coefficients may be expressed in a matrix form:

$$\begin{bmatrix} \bar{L}_2 \\ \bar{L}_4 \\ \bar{M}_4 \end{bmatrix} = \begin{bmatrix} A_1 & T_1 & T_2 \\ A_2 & T_3 & T_4 \\ A_3 & T_5 & T_6 \end{bmatrix} \cdot \begin{bmatrix} P \\ Q \\ R \end{bmatrix} \tag{22}$$

where
$$A_1 = 1$$
$$A_2 = 1 - 2\xi_0$$
$$A_3 = 4[(1/3) - \xi_0 + \xi_0^2]$$
$$T_1 = (2/\tau)\int_0^1 Y_s'(\xi)d\xi$$
$$T_2 = (1/\tau^2)\int_0^1 Y_s'^2(\xi)d\xi$$
$$T_3 = (4/\tau)\int_0^1 Y_s'(\xi)\,(\xi - \xi_0)\,d\xi$$
$$T_4 = (2/\tau^2)\int_0^1 Y_s'^2(\xi)\,(\xi - \xi_0)\,d\xi$$
$$T_5 = (8/\tau)\int_0^1 Y_s'(\xi)\,(\xi - \xi_0)^2\,d\xi$$
$$T_6 = (4/\tau^2)\int_0^1 Y_s'^2(\xi)\,(\xi - \xi_0)^2\,d\xi$$

and
$$P = 1 + [(\gamma + 1)/4]\,(M\alpha_0)^2$$
$$Q = [(\gamma + 1)/4]\,(M\tau) \tag{23}$$
$$R = [(\gamma + 1)/4]\,(M\tau)^2$$

Note that A_2 and A_3 depend upon location of pitch axis, T_1 and T_2 on airfoil profile, and $T_i (i = 3, 4, 5, 6)$ upon airfoil profile as well as location of pitch axis. The coefficients $T_i (i = 1, 2, \ldots, 6)$ are tabulated in Table 1 for two general and three particular profiles of supersonic airfoils which are shown in Fig. 3.

TABLE I
Flutter Coefficients for Five Profiles

Coefficient	General Double Wedge	Double Wedge	General Single Wedge	Single Wedge	Parabolic Biconvex
T_1	0	0	1	1	0
T_2	$(\eta_1 + \eta_2)/(4\eta_1\eta_2)$	1	$1/(4\eta)$	$\frac{1}{4}$	$\frac{4}{3}$
T_3	$-\left[2 - (\eta_1 + \eta_2)\right]$	-1	$\eta - 2\xi_0$	$1 - 2\xi_0$	$-\frac{4}{3}$
T_4	$\left[\eta_1 - (\eta_1 + \eta_2)\xi_0\right]/(2\eta_1\eta_2)$	$1 - 2\xi_0$	$(\eta - 2\xi_0)/(4\eta)$	$(1 - 2\xi_0)/4$	$\frac{4}{3}(1 - 2\xi_0)$
T_5	$-4\left[1 - \eta_2 - \frac{1}{3}(\eta_1^2 - \eta_2^2) - \left[2 - (\eta_1 + \eta_2)\right]\xi_0\right]$	$-2(1 - 2\xi_0)$	$4\left[\frac{1}{3}\eta^2 - \eta\xi_0 + \xi_0^2\right]$	$4\left[\frac{1}{3} - \xi_0 + \xi_0^2\right]$	$-\frac{8}{3}(1 - 2\xi_0)$
T_6	$\left[\eta_1(1 - \eta_2) + \frac{1}{3}\eta_1\eta_2(\eta_1 + \eta_2) - 2\eta_1\xi_0 + (\eta_1 + \eta_2)\xi_0^2\right]/(\eta_1\eta_2)$	$4\left[\frac{1}{3} - \xi_0 + \xi_0^2\right]$	$\frac{1}{3}\eta - \xi_0 + \frac{1}{\eta}\xi_0^2$	$\frac{1}{3} - \xi_0 + \xi_0^2$	$\frac{16}{3}\left[\frac{2}{5} - \xi_0 + \xi_0^2\right]$

$A_1 = 1$ $\quad \bar{L}_2 = A_1P + T_1Q + T_2R$ $\quad P = 1 + \frac{\gamma + 1}{4}(M\alpha_0)^2$

$A_2 = 1 - 2\xi_0$ $\quad \bar{L}_4 = A_2P + T_3Q + T_4R$ $\quad Q = \frac{\gamma + 1}{4}(M\tau)$

$A_3 = 4\left[\frac{1}{3} - \xi_0 + \xi_0^2\right]$ $\quad \bar{M}_4 = A_3P + T_5Q + T_6R$ $\quad R = \frac{\gamma + 1}{4}(M\tau)^2$

(4) Solution of the Flutter Determinant

The critical speed and the corresponding frequency of vibration for aeroelastic instability of an airfoil section in two-dimensional flow and having freedom in vertical translation and pitch may be obtained by solving the following determinant [see reference 12, Eq. (27)]:

$$\begin{vmatrix} \mu(\zeta^2 - 1) + (L_1 + iL_2) & -2\mu\xi_\alpha + (L_3 + iL_4) \\ -2\mu\xi_\alpha + (M_1 + iM_2) & \mu r_\alpha{}^2[(1/\bar{\omega}_f{}^2) - 1] + (M_3 + iM_4) \end{vmatrix} = 0 \tag{24}$$

Making use of equalities (18) and separating the real and imaginary parts yields the following solutions for the critical speed and the corresponding frequency of vibration:

$$\frac{U_f}{c\omega_\alpha} = (1/2)\bar{\mu}\left[\frac{a_{11} + (1 - \bar{\omega}_f{}^2)\,(1 - \zeta^2)r_\alpha{}^2}{a_{21} + (a_3/\bar{\omega}_f{}^2)}\right]^{1/2} \tag{25}$$

$$\bar{\omega}_f{}^2 = \frac{1 + \bar{m}_4\bar{\omega}_h{}^2}{1 + \bar{m}_4 - 4\xi_\alpha\bar{I}_4} = (a_6/a_{41}) \tag{26}$$

where

$$\begin{aligned} \bar{\mu} &= \mu M/\bar{L}_2, \quad l_4 = \bar{L}_4/\bar{L}_2, \quad m_4 = \bar{M}_4/\bar{L}_2, \\ \bar{I}_4 &= I_4/r_\alpha{}^2, \quad \bar{m}_4 = m_4/r_\alpha{}^2, \quad a_{11} = 4\xi_\alpha{}^2\bar{\omega}_f{}^2, \\ a_{21} &= \bar{\mu}(2\xi_\alpha - l_4) - m_4 + l_4{}^2, \\ a_3 &= \bar{\mu}l_4\bar{\omega}_h{}^2, \quad a_{41} = 1 + \bar{m}_4 - 4\xi_\alpha l_4, \\ a_6 &= 1 + \bar{m}_4\bar{\omega}_h{}^2, \quad \bar{\omega}_h = \omega_h/\omega_\alpha, \\ \bar{\omega}_f &= \omega_f/\omega_\alpha, \quad \zeta = \omega_h/\omega_f = \bar{\omega}_h/\bar{\omega}_f \end{aligned} \tag{27}$$

(5) Aeroelastic Instability of a Uniform Cantilever Wing

Analysis of the Rayleigh type for a uniform cantilever wing involves the selection of a set of modal functions to approximate the mode of vibration at the critical speed. The uncoupled first bending and first torsion mode shapes are selected for this analysis and are represented as $\phi_1(\lambda)$ and $\phi_2(\lambda)$ where λ is the spanwise coordinate divided by the semispan of the wing. Using the two-dimensional air forces and moments, that is, neglecting the tip effect which is small for high Mach Number, the stability determinant of Eq. (24) is modified to the following form:

$$\begin{vmatrix} [\mu(\zeta^2 - 1) + (L_1 + iL_2)]\,I_1 & [-2\mu\xi_\alpha + (L_3 + iL_4)]I_3 \\ [-2\mu\xi_\alpha + (M_1 + iM_2)]I_3 & \{\mu r_\alpha{}^2[(1/\bar{\omega}_f{}^2) - 1] + (M_3 + iM_4)\}I_2 \end{vmatrix} = 0 \tag{28}$$

where

$$\begin{aligned} I_1 &= \int_0^1 \phi_1{}^2(\lambda)d\lambda \\ I_2 &= \int_0^1 \phi_2{}^2(\lambda)d\lambda \\ I_3 &= \int_0^1 \phi_1(\lambda)\phi_2(\lambda)d\lambda \end{aligned} \tag{29}$$

Separating the real and the imaginary parts as before and introducing a modal shape parameter $\Gamma = I_3{}^2/I_1I_2$ the following solution is obtained for the critical speed:

$$\frac{U_f}{c\omega_\alpha} = (1/2)\bar{\mu}\left[\frac{a_1 + (1 - \bar{\omega}_f{}^2)\,(1 - \zeta^2)r_\alpha{}^2}{a_2 + (a_3/\bar{\omega}_f{}^2)}\right]^{1/2} \tag{30}$$

where the corresponding frequency of vibration is obtained by solving the following quadratic in $\bar{\omega}_f{}^2$:

$$\begin{aligned} [a_5a_4 + a_5(1 - a_7)]\bar{\omega}_f{}^4 + \\ [a_3(a_4 - 1 + \Gamma) - a_5a_6 - a_5]\bar{\omega}_f{}^2 + \\ a_3(1 - \Gamma - a_6) = 0 \end{aligned} \tag{31}$$

The constants a_1 to a_7 are defined as

$$\begin{aligned} a_1 &= 4\Gamma\xi_\alpha{}^2\bar{\omega}_f{}^2 \\ a_2 &= \Gamma(2\bar{\mu}\xi_\alpha + l_4{}^2) - \bar{\mu}l_4 - m_4 \\ a_3 &= \bar{\mu}l_4\bar{\omega}_h{}^2 \\ a_4 &= 1 + \bar{m}_4 - 4\xi_\alpha l_4\Gamma \\ a_5 &= \bar{\mu}l_4(1 - \Gamma) \\ a_6 &= 1 + \bar{m}_4\bar{\omega}_h{}^2 \\ a_7 &= 4\Gamma(\xi_\alpha{}^2/r_\alpha{}^2) \end{aligned} \tag{32}$$

For $\Gamma = 1$, $a_5 = 0$, $a_1 = a_{11}$, $a_2 = a_{21}$, $a_4 = a_{41}$, and Eq. (31) yields two values for $\bar{\omega}_f{}^2$, namely, $\bar{\omega}_f{}^2 = a_6/a_{41}$ and $-a_3/a_{21}$. The first is the same as Eq. (26), while the second value is seen to be trivial as it leads to infinite critical speed by substitution in Eq. (25). Thus, the case $\Gamma = 1$ leads to the sectional solution of Eqs. (25) and (26) which may also be interpreted as $\phi_1(\lambda) = \phi_2(\lambda) = 1$.

(6) Parametric Studies

It is now evident that the solutions for the critical speed and the corresponding frequency of vibration given in Sections (4) and (5) lend themselves with ease to parametric studies for use in preliminary design.

First, the simple case of an airfoil in two-dimensional flow and free to pitch only is considered. The aerodynamic damping moment is given by the out of phase component from Eq. (16), namely,

$$\mathfrak{M}_4 = -\rho c^2U^2k^2M_4 = -\rho c^2a_\infty{}^2\,(kM)\bar{M}_4 \tag{33}$$

Substituting for $\bar{M}_4$ from Eq. (22),

$$\mathfrak{M}_4 = -\rho c^2a_\infty{}^2(kM)\,[A_3P + T_5Q + T_6R] \tag{24}$$

Considering the particular case of a double wedge profile and substituting the corresponding values of T_5 and T_6 from Table 1,

$$\begin{aligned} \mathfrak{M}_4 = -\rho c^2a_\infty{}^2(kM)\,\big(4[(1/3) - \xi_0 + \xi_0{}^2]\,\{1 + \\ [(\gamma + 1)/4]\,(M\alpha_0)^2 + [(\gamma + 1)/4]\,(M\tau)^2\} - \\ [(\gamma + 1)/2]\,(1 - 2\xi_0)\,(M\tau)\big) \end{aligned} \tag{35}$$

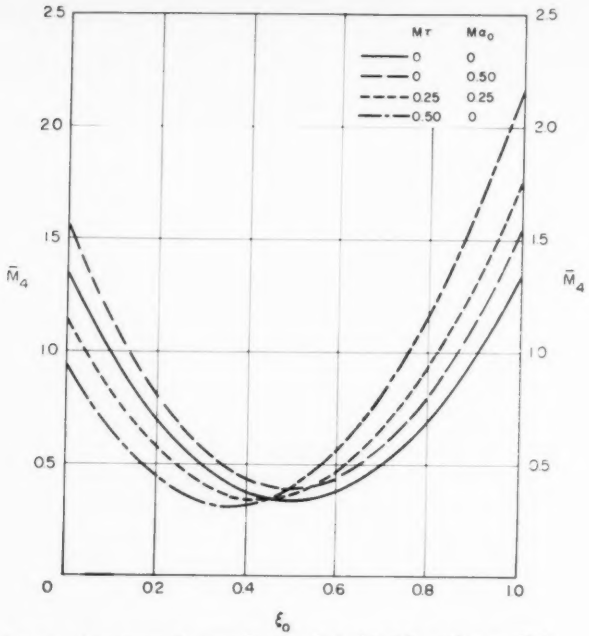

FIG. 4. Aerodynamic damping in pitch (double wedge profile).

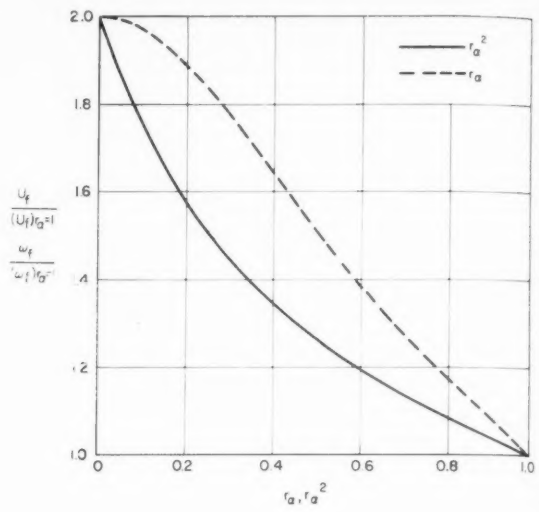

FIG. 5. Variation of flutter speed and frequency with moment of inertia in pitch. (Double wedge profile, constant wing stiffness in torsion; $\tau = \alpha_0 = \bar{\omega}_h = 0$, $\xi_0 = 0.5$, $\xi_\alpha = 0.1$.)

Fig. 4 shows the dependence of the aerodynamic damping in pitch on the location of the axis of pitch (ξ_0), the thickness parameter $M\tau$, and the initial angle of attack parameter $M\alpha_0$. For the zero thickness airfoil at zero angle of attack, the damping is maximum for $\xi_0 = 0$ and 1 and minimum for $\xi_0 = 1/2$. Angle of attack increases it for all values of ξ_0 by the factor $[1 + (\gamma + 1)(M\alpha_0)^2/4]$. The effect of thickness is to decrease the damping for locations of the pitch axis forward of the mid-chord and to increase it for $0.5 < \xi_0 < 1.0$. The curve for $M\tau$ and $M\alpha_0$ each equal to 0.25 shows a blending of the two effects. The outstanding feature is that the damping is always positive, thus eliminating the possibility of instability in pitch at high Mach Number.

It is seen from Eqs. (25), (26), and (27) that the following dimensionless parameters affect the critical speed and the corresponding frequency of vibration (independent of altitude) of the airfoil. In these, the frequencies have been normalized with respect to ω_α and the lengths, except the radius of gyration in pitch, with respect to the chord length c.

(1) r_α^2, or the moment of inertia of the airfoil about the axis of pitch
(2) ξ_0, chordwise location of the axis of pitch
(3) ξ_α, mass unbalance or distance between axis of pitch and axis through center of mass
(4) $\bar{\omega}_h = (\omega_h/\omega_\alpha)$, ratio of uncoupled flexural and torsional frequencies of the airfoil
(5) μM, altitude parameter
(6) τM, thickness parameter
(7) $\alpha_0 M$, angle of attack parameter
(8) Γ, modal shape parameter
(9) γ, ratio of specific heats (assumed constant = 1.4)

The effects of the first five parameters may be investigated for an airfoil of zero thickness at zero angle of attack. For this case, $P = 1$, $Q = R = 0$, so that $\bar{L}_2 = A_1 = 1$, $\bar{L}_4 = A_2 = 1 - 2\xi_0$, and $\bar{M}_4 = A_3 = 4[(1/3) - \xi_0 + \xi_0^2]$. Substitution in Eqs. (25), (26), and (27) gives

$$\frac{U_f}{c\omega_\alpha} = (1/2)\mu M \left\{ \frac{4\xi_\alpha^2\bar{\omega}_f^2 + r_\alpha^2(1 - \bar{\omega}_f^2)(1 - \zeta^2)}{\mu M[2\xi_\alpha - (1 - 2\xi_0)(1 - \zeta^2)] + (1 - 2\xi_0)^2 - 4[(1/3) - \xi_0 + \xi_0^2]} \right\}^{1/2} \tag{36}$$

$$\bar{\omega}_f^2 = \frac{1 + 4[(1/3) - \xi_0 + \xi_0^2](\bar{\omega}_h^2/r_\alpha^2)}{1 - [4\xi_\alpha(1 - 2\xi_0)/r_\alpha^2] + 4[(1/3) - \xi_0 + \xi_0^2]/r_\alpha^2} \tag{37}$$

The parameters will now be varied individually.

Moment of Inertia in Pitch

Let $\bar{\omega}_h = 0$ and $\xi_0 = 0.5$; then

$$\bar{\omega}_f^2 = r_\alpha^2/[r_\alpha^2 + (1/3)] \tag{38}$$

$$U_f/(c\omega_\alpha) = (1/2)\mu M\, r_\alpha^2 \times \left\{ \frac{4(\xi_\alpha^2/r_\alpha^2) + (1/3)/r_\alpha^2}{[r_\alpha^2 + (1/3)](2\mu M\, \xi_\alpha - (1/3)]} \right\}^{1/2} \tag{39}$$

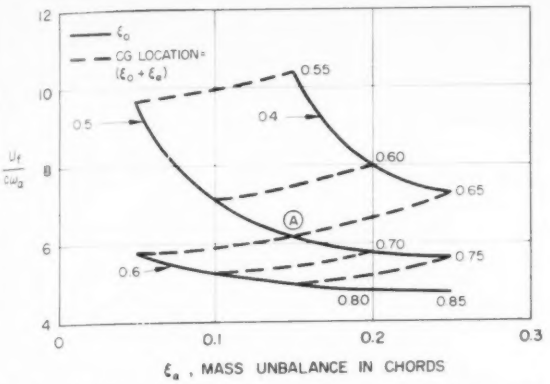

FIG. 6. Variation of flutter speed with mass unbalance and chordwise location of axis of pitch.

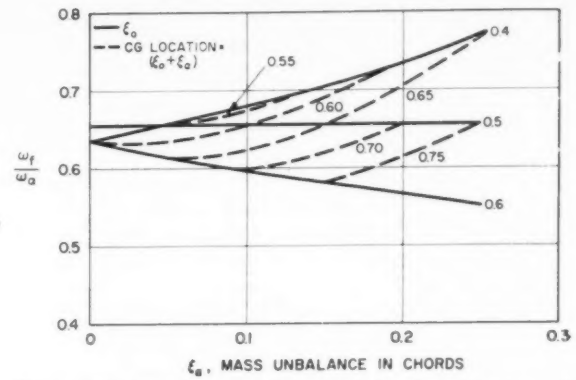

FIG. 7. Variation of flutter frequency with mass unbalance and chordwise location of axis of pitch.

Double wedge profile; $\tau = \alpha_0 = \bar{\omega}_h = 0$, $r_\alpha^2 = 0.25$, $\mu M = 250$

Since

$$\omega_\alpha = (K_\alpha/I_\alpha)^{1/2} = (K_\alpha/m)^{1/2}/(1/2)c\, r_\alpha$$

Eq. (39) becomes

$$U_f/(K_\alpha/m)^{1/2} = \mu M \left\{ \frac{4\xi_\alpha^2 + (1/3)}{[r_\alpha^2 + (1/3)]\,[2\mu M \xi_\alpha - (1/3)]} \right\}^{1/2} \quad (40)$$

and

$$\omega_f = [(2/c)\,(K_\alpha/m)^{1/2}]/[r_\alpha^2 + (1/3)]^{1/2} \quad (41)$$

For prescribed values of K_α, m, ξ_α, and μM, U_f and ω_f are seen to be proportional to $[r_\alpha^2 + (1/3)]^{-1/2}$. Normalizing Eqs. (40) and (41) with respect to their values for $r_\alpha^2 = 1$, the variation of flutter speed and frequency with radius of gyration and its square is shown in Fig. 5. Obviously r_α cannot be less than ξ_α; however, it is interesting to note that the critical speed and frequency can be doubled as the mass distribution of the airfoil is varied from concentrated masses at the leading and trailing edges inward to the center of mass, holding the torsional rigidity constant. Similar design charts may be prepared for other values of $\bar{\omega}_h$ and ξ_0.

In the past, the aeroelastician has been concerned more with the critical (flutter) speed than with the frequency of vibration of the airfoil at this speed. With the ever increasing use of servo and guidance systems in piloted and pilotless aircraft a knowledge of the frequency becomes imperative in order to avoid servoelastic instability.

Location of Pitch Axis and Mass Unbalance

It is evident from Eqs. (36) and (37) that the effects of the chordwise location of the axis of pitch and its distance from the center of mass (the mass unbalance) on the critical speed and frequency are interconnected

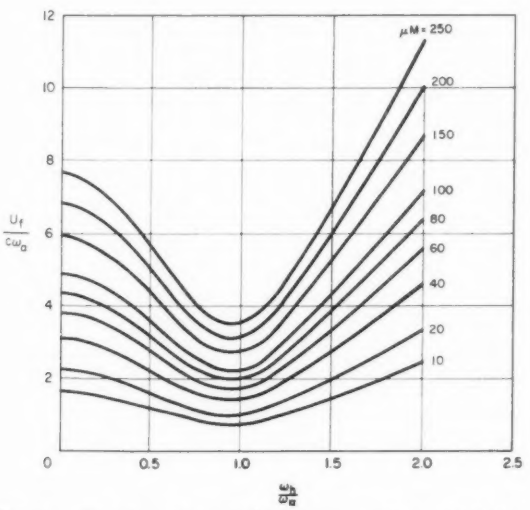

FIG. 8a. With flexural-torsional frequency ratio and altitude.

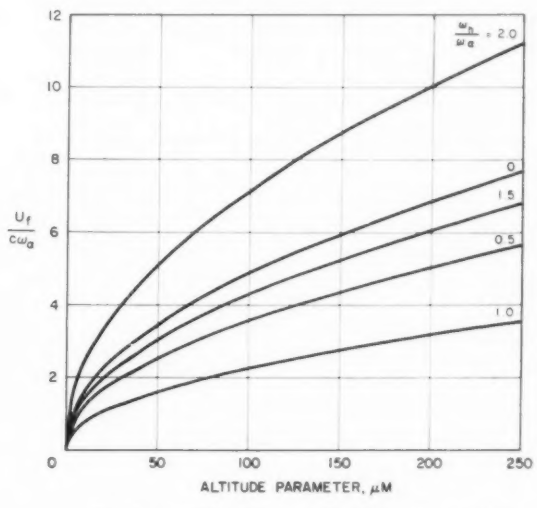

FIG. 8b. With altitude at fixed frequency ratios.

Variations of flutter speed. (Double wedge profile; $\tau = \alpha_0 = 0$, $\xi_0 = 0.5$, $\xi_\alpha = 0.1$, $r_\alpha^2 = 1/3$.)

with the frequency ratio $\bar{\omega}_h = (\omega_h/\omega_\alpha)$. However, it is well understood that, for a given mass unbalance, forward shift of the axis of pitch increases the flutter speed at all values of $\bar{\omega}_h$. For low values of $\bar{\omega}_h$ ($0 \leqq \bar{\omega}_h < 0.5$), the flutter speed generally decreases with increase in ξ_α, for practical values of the mass unbalance ($0 \leqq \xi_\alpha < 0.25$). For moderate values of $\bar{\omega}_h$($0.50 < \bar{\omega}_h < 0.70$), the flutter speed has a minimum approximately at $\xi_\alpha = 0.10$; further increase in mass unbalance becoming beneficial. For $\bar{\omega}_h = 1.0$, the mass unbalance is beneficial for all positive values of ξ_α.

Some typical curves for $\bar{\omega}_h = 0$ are shown in Fig. 6. It is instructive to examine the combined and the individual effects of ξ_0 and ξ_α on the critical speed and frequency.

The full lines show the variation of $U_f/(c\omega_\alpha)$ with ξ_α for a fixed location of the axis of pitch, and the dotted lines show the effect of moving the axis of pitch for a fixed location of the center of mass. A vertical intercept gives the effect of moving both axes forward keeping ξ_α constant. For example, start with point A with $\xi_0 = 0.5$, $\xi_\alpha = 0.15$ and $\bar{U}_f = U_f/(c\omega_\alpha) = 6.16$. Decreasing the mass unbalance by 10 per cent ($\xi_\alpha = 0.05$) raises $\bar{U}_f$ to 9.65, giving an increase of 57 per cent. Moving the pitch axis forward by 10 per cent ($\xi_0 = 0.4$), leaving the center of mass at 0.65 c raises $\bar{U}_f$ to 7.23 giving an increase of 17 per cent. Moving both axes forward by 10 per cent ($\xi_0 = 0.4$, $\xi_\alpha = 0.15$) raises $\bar{U}_f$ to 10.38, giving an increase of 68 per cent. The advantage of decreasing the mass unbalance is thus apparent, especially for midchord and forward locations of the axis of pitch.

Fig. 7 shows the corresponding variation of $\bar{\omega}_f = \omega_f/\omega_\alpha$ with ξ_0 and ξ_α. For small values of ξ_α the change in $\bar{\omega}_f$ with ξ_0 is small, but it becomes significant for larger values of ξ_α. In general, $\bar{\omega}_f$ increases as ξ_0 and $(\xi_0 + \xi_\alpha)$ are decreased. But for a mass-balanced airfoil ($\xi_\alpha = 0$), $\bar{\omega}_f$ decreases as the axis of pitch is moved away from the midchord location, the minimum value being for $\xi_0 = 0$ or 1 and equal to 0.3975 in this case of $\bar{\omega}_h = 0$ and $r_\alpha^2 = 1/4$.

Torsional Frequency and Its Ratio to Flexural Frequency

Eqs. (36) and (37) show that the critical speed U_f and the frequency ω_f increase linearly with torsional frequency ω_α if the flexural frequency is also raised proportionately leaving $\bar{\omega}_h$ unchanged. However, if ω_h is held constant, the effect on U_f of raising ω_α is different for $\omega_\alpha > \omega_h$ from that when $\omega_\alpha < \omega_h$. Some typical curves of U_f versus $\bar{\omega}_h$ for different values of μM are shown in Fig. 8a. For $\mu M = 250$, take the initial value of $\bar{\omega}_h = 0.8$ for which $U_f = 3.8$. Doubling the torsional frequency raises U_f by a factor of $2(6.3/3.8) = 3.32$. On the other hand, if the initial value of $\bar{\omega}_h$ were 1.6, doubling ω_α leaves U_f unchanged. Doubling the flexural frequency at $\bar{\omega}_h = 0.8$ gives $U_f = 7.65$, which, in this case, doubles U_f. Thus an obvious conclusion that may be drawn from these curves is that, for $0 < \bar{\omega}_h < 1.0$, the wing should be stiffened torsionally and, for $\bar{\omega}_h > 1.0$, it should be stiffened flexurally in order to raise its critical flutter speed.

TABLE 2
Effect on Flutter Frequency of Doubling Airfoil Torsional and Flexural Frequencies at Different Frequency Ratios.

	ω_f/ω_{f_1}	
$\bar{\omega}_h$	ω_α doubled	ω_h doubled
0.25	1.96	1.09
0.50	1.84	1.27
1.00	1.58	1.58
1.50	1.38	1.75
2.00	1.27	1.84

Fig. 8b shows a cross-plot of Fig. 8a. All curves are seen to be of a similar nature irrespective of the value of frequency ratio. Another common characteristic is the steep rise in U_f for values of μM less than 20—that is, for values of wing density ratio less than 8 or so.

As for $\bar{\omega}_f$, it is independent of μM and its variation with $\bar{\omega}_h$ is shown in Fig. 9. The effect on ω_f of doubling ω_α or ω_h at different values of $\bar{\omega}_h$ is shown in Table 2.

It may be well to point out that it is the square of the frequency ratio ($\bar{\omega}_h^2$) that appears in the expressions for U_f and $\bar{\omega}_f$. Since $\bar{\omega}_h^2 = (r_\alpha c/2)^2(K_h/K_\alpha)$ the parameter (K_h/K_α) could be used instead of (ω_h/ω_α) for these plots. A replot of Fig. 8a (for $\mu M = 250$ only) and of Fig. 9 is shown in Fig. 10 where the abscissa is $\bar{\omega}_h^2$ instead of $\bar{\omega}_h$.

Altitude Parameter μM

The variation of $U_f/(K_\alpha/m)^{1/2}$ and $U_f/(c\omega_\alpha)$ with μM for representative values of r_α^2 is shown in Figs. 11a and 11b, respectively. These curves as well as those of Fig. 8b indicate that U_f varies approximately as $(\mu M)^{1/2}$. This observation leads to rather simple results.

$$U_{f_2}/U_{f_1} = [(\mu M)_2/(\mu M)_1]^{1/2} \tag{42}$$

Squaring both sides and substituting $M = U/a$, and $\mu = \mu_0/\sigma$ gives

$$U_{f_2}/U_{f_1} = (a_1\sigma_1)/(a_2\sigma_2) \tag{43}$$

and

$$M_{f_2}/M_{f_1} = (a_1^2\sigma_1)/(a_2^2\sigma_2) = p_1/p_2 \tag{44}$$

Given the flutter speed U_{f_1} and the corresponding Mach Number M_{f_1} at one altitude, their values at another altitude may be obtained from the above relationships which are plotted in Fig. 12. Furthermore, for $35{,}330 < h < 105{,}000$ ft. where $(a_2/a_1) = 1.0$, U_f and M_f become inversely proportional to the density ratio. Fig. 12b shows a plot of (σ_r/σ) for $35{,}330 < h < 105{,}000$ ft. with $\sigma_r = \sigma$ at 35,330 ft. altitude.

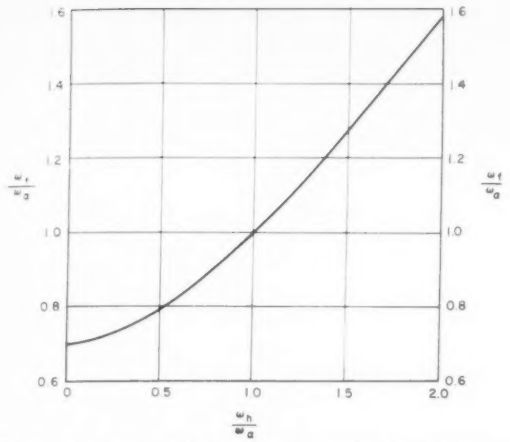

FIG. 9. Variation of flutter frequency with flexural-torsional frequency ratio. (Double wedge profile; $\tau = \alpha_0 = 0$, $\xi_0 = 0.5$, $\xi_\alpha = 0.1$, $r_\alpha^2 = 1/3$.)

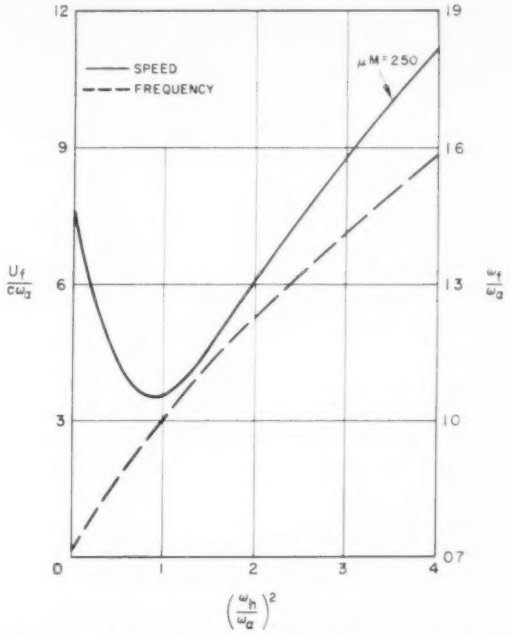

FIG. 10. Variation of flutter speed and frequency with flexural-torsional stiffness ratio. (Double wedge profile; $\tau = \alpha_0 = 0$, $\xi_0 = 0.5$, $\xi_\alpha = 0.1$, $r_\alpha^2 = 1/3$.)

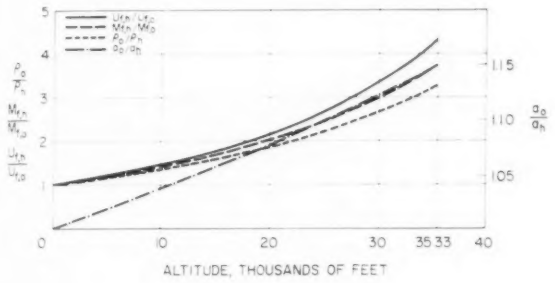

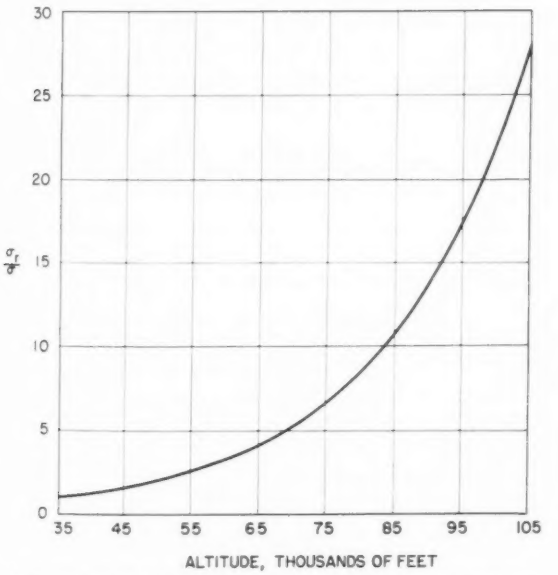

FIG. 12. Variation of flutter speed and Mach Number with altitude. FIG. 12a (*top*). $0 < h < 35{,}330$ ft. FIG. 12b (*bottom*). $35{,}330 < h < 105{,}000$ ft.

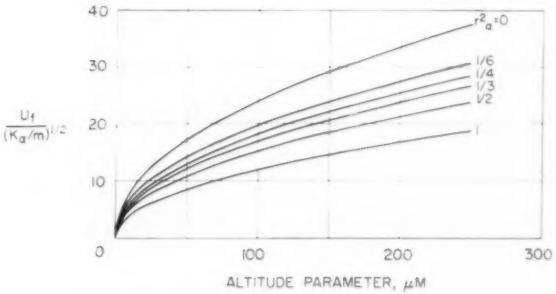

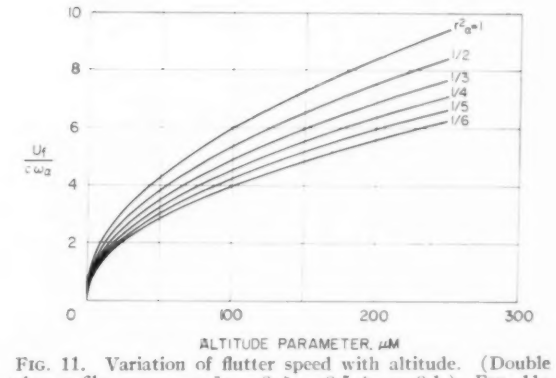

FIG. 11. Variation of flutter speed with altitude. (Double wedge profile; $\tau = \alpha_0 = \tilde{\omega}_h = 0$, $\xi_0 = 0.5$, $\xi_\alpha = 0.1$.) FIG. 11a (*top*). Constant wing stiffness in torsion. FIG. 11b (*bottom*). Constant wing torsional frequency.

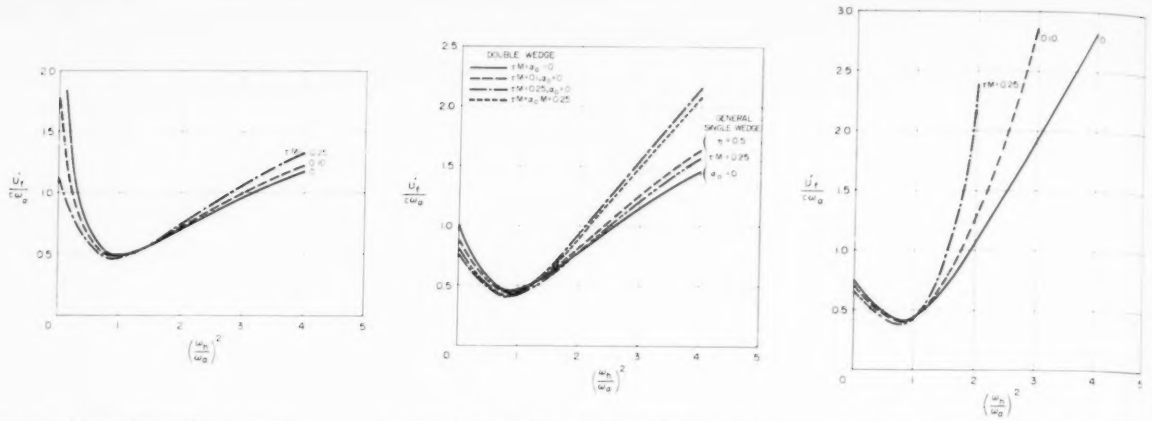

a. Double wedge profile, $\xi_0 = 0.4$. b. Double and single wedge profiles, $\xi_0 = 0.5$. c. Double wedge profile $\xi_0 = 0.6$.

FIG. 13. Effect of thickness on flutter speed. $\xi_\alpha = 0.1$, $r_\alpha^2 = 1/3$, $\mu M = 250$.

Alternate Approach

The flutter frequency is independent of altitude as seen from Eq. (26) or (37). Thus for given inertial and elastic properties of the airfoil and location of the axis of pitch, Eq. (36) may be written as

$$U_f = (1/2)\,(c\omega_\alpha)\bar{\omega}_f \mu M \left\{f_1/[(\mu M)f_2 + f_3]\right\}^{1/2} \quad (45)$$

where

$$\left.\begin{aligned} f_1 &= 4\xi_\alpha^2 + r_\alpha^2(1 - \bar{\omega}_f^2)\,(1 - \zeta^2)/\bar{\omega}_f^2 \\ f_2 &= 2\xi_\alpha - (1 - 2\xi_0)\,(1 - \zeta^2) \\ f_3 &= (1 - 2\xi_0)^2 - 4\,[(1/3) - \xi_0 + \xi_0^2] = -1/3 \end{aligned}\right\} \quad (46)$$

Squaring both sides of Eq. (45), substituting $U = aM$ and solving for M yields

$$\left.\begin{aligned} M_f &= (1/4)c^2\omega_\alpha^2\bar{\omega}_f^2(f_1/f_2)\,(\mu/a^2) - (f_3/f_2)(1/\mu) \\ &= [(1/2)c\omega_f]^2(f_1/f_2)(\mu_0/\sigma a^2) - (f_3/f_2)(\sigma/\mu_0) \\ &= [(1/2)\,(c\,\omega_f/a_0)]^2(f_1/f_2)[\mu_0/(p/p_0)] + (1/3f_2)(\sigma/\mu_0) \\ &= (kM)_0^2(f_1/f_2)[\mu_0/(p/p_0)] + (1/3f_2)(\sigma/\mu_0) \\ &= [\mu_0/f_2(p/p_0)]\,[f_1(kM)_0^2 + (1/3)\,(a/a_0)^2\,(\sigma/\mu_0)^2] \end{aligned}\right\} \quad (47)$$

The second term is much smaller than the first except when $(kM)_0$ and μ_0 are both small and of the same order of magnitude. Hence the *flutter Mach Number is inversely proportional to the pressure ratio*, the same relationship as derived in Eq. (44).

Since $(p/p_0) = (\sigma a^2)/a_0^2$, the flutter speed may be expressed as

$$U_f = aM_f = [a_0\mu_0/\sigma(a/a_0)f_2] \times [f_1(kM)_0^2 + (1/3)\,(a/a_0)^2\,(\sigma/\mu_0)^2] \quad (48)$$

By virtue of the aforesaid, *the flutter speed is inversely proportional to* $\sigma(a/a_0)$, the same relationship as shown in Eq. (43).

The dynamic pressure corresponding to the flutter speed is

$$\begin{aligned} q_f &= (1/2)\rho U_f^2 = (1/2)\rho_0\sigma[a_0^2\mu_0^2/\sigma^2(a/a_0)^2 f_2^2]\,[f_1(kM)_0^2 + (1/3)\,(a/a_0)^2\,(\sigma/\mu_0)^2]^2 \\ &\cong (1/2)\,[\rho_0(a_0\mu_0)^2/(p/p_0)]\,[f_1/f_2\,(kM)_0^2]^2 \end{aligned}$$

or

$$q_f \propto 1(p/p_0) \quad (49)$$

that is, *the dynamic pressure at flutter speed is inversely proportional to the pressure ratio*, or, *the product of the square of the indicated speed at flutter and the pressure ratio remains constant.*

It is evident from Eqs. (47), (48), and (49) that, between the altitudes of 35,330 and 105,000 ft., where the speed of sound in air is constant, the flutter speed, Mach Number, and dynamic pressure vary inversely as the density ratio.

Airfoil Thickness and Profile

In order to study the effects of airfoil thickness and profile, the airfoil is assumed to be at zero angle of attack. Two profiles are considered; the double wedge, and the general single wedge. The former is representative of the family of closed profiles for which $Y_s(0) = Y_s(1) = 0$, while the latter is representative of the family of profiles with blunt trailing edge, that is, $Y_s(1) \neq 0$.

Figs. 13a, 13b, and 13c show the effect of airfoil thickness on the reduced flutter speed $\bar{U}_f$ of a double wedge profile for three different locations of the axis of pitch, namely, $\xi_0 = 0.4$, 0.5, and 0.6 respectively, over a range of $(\omega_h/\omega_\alpha)^2$ from 0 to 4. $\bar{U}_f$ has been normalized with respect to its value, 7.67, for $\xi_0 = 0.5$ and $\tau = \bar{\omega}_h = 0$, and is denoted by $\bar{U}_f'$. It is to be noted

that for $0 < \bar{\omega}_h < 1.0$ airfoil thickness lowers the flutter speed, the severity of the effect decreasing as the axis of pitch is moved aft. However, $\bar{U}_f$ with $\xi_0 = 0.4$ and $M\tau = 0.25$ is higher than the $\bar{U}_f$ with $\xi_0 = 0.5$ and $M\tau = 0$; and the $\bar{U}_f$ with $\xi_0 = 0.5$ and $M\tau = 0.25$ is higher than that with $\xi_0 = 0.60$ and $M\tau = 0$. It is easy to show that for steady-state conditions the center of pressure is located at a distance $[\xi_0 + (1/2)(\bar{L}_4/\bar{L}_2)]c$ from the leading edge; that is, at about $0.43c$ for the double wedge profile at zero angle of attack. It would seem then that the location of pitch axis at $\xi_0 = 0.4$ should yield the double advantage of high flutter speed and low hinge moments for use as a control surface.

On the other hand, for $\bar{\omega}_h > 1.0$, the airfoil thickness raises the flutter speed and becomes increasingly beneficial with rearward movement of the axis of pitch. The dependence of thickness effects on frequency ratio was also shown by Garrick in the 1957 Minta Martin Lecture.[13]

The corresponding curves of airfoil frequency at flutter speed are shown in Figs. 14a, 14b, and 14c. Again, the flutter frequency ratio is normalized with respect to its value, 0.707, for $\xi_0 = 0.5$ and $\tau = \bar{\omega}_h = 0$, and is denoted by $\bar{\omega}_f'$. Thickness decreases the frequency and the effect decreases with aft position of the axis of pitch. However, since mass unbalance is kept constant in these curves, the frequency increases with forward shift of the axis of pitch, as already shown in Fig. 7 for $\bar{\omega}_h = 0$.

The effect of changing the profile shape is shown in Fig. 13b. For a general single wedge ($\eta = 0.5$, Fig. 3c) and $\tau = 0$ the curve is the same as for the double wedge. But for $\tau M > 0$ the flutter characteristics of this profile are different from those of the double wedge as shown. It is to be noted that, for the single wedge, the comparative thickness effects are smaller for $0 < \bar{\omega}_h^2 < 0.5$; they are slightly worse for $0.5 < \bar{\omega}_h^2 < 1.5$, and are substantially lower for $\bar{\omega}_h^2 > 1.5$, that is, less beneficial to flutter.

Decreasing η, that is, decreasing the length of the wedge, reduces the flutter speed for $0 < \bar{\omega}_h^2 < 1.0$ and increases it for $\bar{\omega}_h^2 > 1.0$. The effect, however, is rather small.

Initial Angle of Attack

For an airfoil of zero thickness, the initial angle of attack reduces the flutter speed by a constant factor. With the parameters of Fig. 13b and $M\alpha_0 = 0.25$, this multiplier is 0.982. For $\tau M = 0.25$, the effect of the initial angle of attack is almost negligible for $0 < \bar{\omega}_h < 1.0$; for $\bar{\omega}_h > 1.0$ it is shown in the Figure and is of the order of 2 to 3 per cent reduction in flutter speed.

Modal Shape

For a double wedge airfoil at zero angle of attack, the effect of the modal shape parameter Γ is shown in Fig. 15 for two values of τM, namely, zero and 0.25. Inclusion of mode shapes in the analysis is seen to increase the flutter speed. It is interesting to note that the initial angle of attack and the mode shape have opposite effects on flutter speed and, over a wide range of the frequency ratio $\bar{\omega}_h$, they are of the same order of magnitude. Hence it seems that, at least for small angles of attack, these two parameters may be disregarded in the preliminary calculations of flutter speed without much sacrifice of accuracy.

Conclusions

The results of this study may be summed up as follows.

Parametric studies of the type shown in Section (6) can be of invaluable help in preliminary design.

Flutter speed can be raised considerably by decreasing the moment of inertia in pitch while holding the torsional stiffness constant. For average values of the radius of gyration ($0.3 < r_\alpha < 0.6$) it varies almost linearly with r_α.

For midchord and forward locations of the axis of pitch, mass balancing can be used to great advantage.

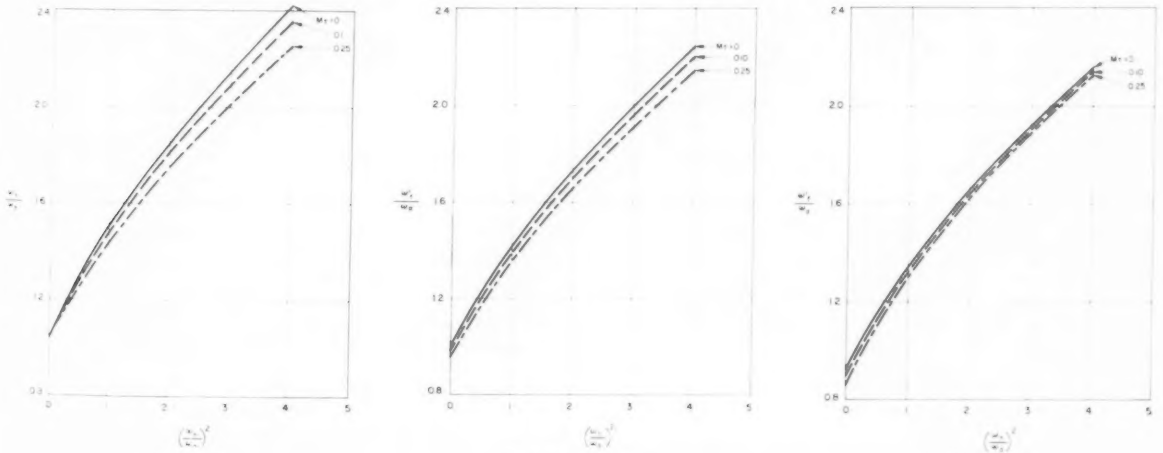

a. $\xi_0 = 0.4$ b. $\xi_0 = 0.5$ c. $\xi_0 = 0.6$

Fig. 14. Effect of thickness on flutter frequency at zero angle of attack. (Double wedge profile; $\xi_\alpha = 0.1$, $r_\alpha^2 = 1/3$).

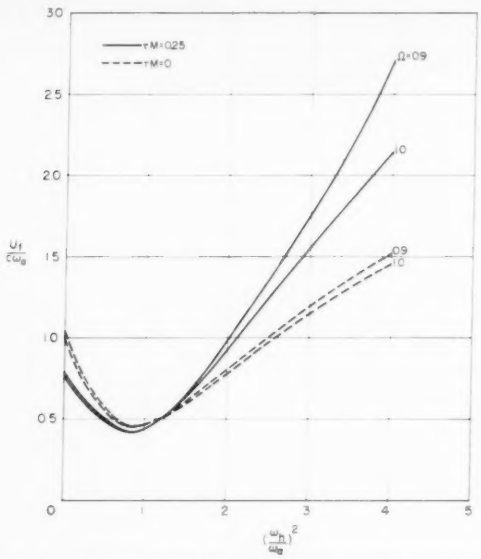

FIG. 15. Effect of mode shape on flutter speed of double wedge profile at zero angle of attack. $\xi_0 = 0.5$, $\xi_\alpha = 0.1$, $r_\alpha^2 = 1/3$, $\mu M = 250$.

For $0 < (\omega_h/\omega_\alpha) < 1.0$, a wing should be stiffened torsionally and, for $(\omega_h/\omega_\alpha) > 1.0$, it should be stiffened flexurally in order to raise its flutter speed.

At high Mach Number, the frequency at flutter is independent of altitude.

With changes in altitude, the flutter Mach Number and the dynamic pressure at flutter speed are inversely proportional to the pressure ratio, and the flutter speed is inversely proportional to the product of density ratio and speed of sound ratio, $\sigma(a/a_0)$.

Airfoil thickness lowers the flutter speed for $0 < (\omega_h/\omega_\alpha) < 1.0$. The effect increases with a forward shift in the axis of pitch. For $(\omega_h/\omega_\alpha) > 1$ these effects are reversed. These characteristics depend upon airfoil profile also.

Small angles of attack and spanwise mode shapes produce almost equal and opposite effects on flutter speed over a wide range of frequency ratio. Neglecting them in preliminary calculations should not result in a great loss of accuracy.

REFERENCES

[1] Hayes, W. D., *On Hypersonic Similitude*, Quarterly of Applied Mathematics, Vol. 5, No. 1, pp. 105–106, 1947.

[2] Goldsworthy, F. A., *Two-Dimensional Rotational Flow at High Mach Number Past Thin Aerofoils*, Quarterly Journal of Mechanics and Applied Mathematics, Vol. 5, pp. 54–63, 1952.

[3] Lighthill, M. J. *Oscillating Airfoils at High Mach Number*, Journal of the Aeronautical Sciences, Vol. 20, No. 6, pp. 402–406, June, 1953.

[4] Landahl, M., Mollo-Christensen, E. L., Ashley, H., *Parametric Studies of Viscous and Nonviscous Unsteady Flows*, USAF OSR, Technical Report No. 55-13, April, 1955.

[5] Landahl, M., *Unsteady Flow Around Thin Wings at High Mach Numbers*, Journal of the Aeronautical Sciences, Vol. 24, No. 1, pp. 33–38, January, 1957.

[6] Zartarian, G., Heller, A., and Ashley, H., *Application of Piston Theory to Certain Elementary Aeroelastic Problems*, Proceedings of the Fourth Midwestern Conference on Fluid Mechanics, Purdue University, Lafayette, Indiana, pp. 163–181, September, 1955.

[7] Ashley, H., and Zartarian, G., *Piston Theory—A New Aerodynamic Tool for the Aeroelastician*, Journal of the Aeronautical Sciences, Vol. 23, No. 12, pp. 1109–1118, December, 1956.

[8] Collar, A. R., *Resistance Derivatives of Flutter Theory, Part II: Results for Supersonic Speeds*, ARC R&M 2139, January, 1944.

[9] Temple, G., and Jahn, H. A., *Flutter at Supersonic Speeds: Derivative Coefficients for a Thin Aerofoil at Zero Incidence*, ARC R&M 2140, April, 1945.

[10] Possio, C., *The Aerodynamical Action on an Oscillating Aerofoil at Supersonic Speed, ARC 7668.* Translated from Italian, Acta, Pont. Academy Sci., Vol. I, No. 11, pp. 93–106, 1937.

[11] Nelson, H. C., Rainey, R. A., Watkins, C. E., *Lift and Moment Coefficients Expanded to the Seventh Power of Frequency for Oscillating Rectangular Wings in Supersonic Flow and Applied to a Specific Flutter Problem*, NACA TN 3076, April, 1954.

[12] Garrick, I. E., and Rubinow, S. I., *Flutter and Oscillating Air Force Calculations for an Airfoil in a Two-Dimensional Supersonic Flow*, NACA TR 846, May, 1946.

[13] Garrick, I. E., *Some Concepts and Problem Areas in Aircraft Flutter*, The Minta Martin Lecture, Institute of the Aeronautical Sciences, New York, 1957.

The Prospects for Magneto-Aerodynamics

(*Continued from page 245*)

[7] Elsasser, W. M., *Hydromagnetic Dynamo Theory*, Reviews of Modern Physics, Vol. 28, pp. 135–163, April, 1956.

[8] Rossow, V. J., *On Flow of Electrically Conducting Fluids over a Flat Plate in the Presence of a Transverse Magnetic Field*, NACA TN 3971, 1957.

[9] Shercliffe, J. A., *Steady Motion of Conducting Fluids in Pipes under Transverse Magnetic Fields*, Proc. Cambridge Phil. Soc., Vol. 49, pp. 166–168, 1953.

[10] Brogan, T. R., *The Conduction of Electric Current to Cold Electrodes in Shock Tubes*, Master of Aero. Engrg. Thesis, Cornell University Graduate School of Aero. Engrg., Ithaca, N.Y., 1956.

A Turbulent Analog of the Stewartson-Illingworth Transformation

FRED E. C. CULICK* AND JACQUES A. F. HILL**

Massachusetts Institute of Technology

SUMMARY

The Stewartson-Illingworth transformation is applied to the integral momentum equation for compressible boundary-layer flow, leaving the x-coordinate transformation unspecified, however. It is shown that the transformed equation is the integral momentum equation for incompressible flow if (a) the effect of compressibility on the boundary-layer shape parameter H can be represented by

$$H + 1 = (H_i + 1)\,(T_0/T_e)$$

and (b) the x-coordinate transformation is chosen to be suitably related to the ratio of skin-friction coefficients in compressible and incompressible flows.

Experimental evidence is presented which shows that condition (a) is satisfied for turbulent boundary layers up to $M = 5$. An x-transformation is chosen according to (b) and an equation is presented which gives the turbulent boundary-layer growth in compressible flow in terms of a simple quadrature. The predictions of this equation are then compared with some measurements on wind-tunnel nozzles.

SYMBOLS

a = speed of sound
c_f = local skin-friction coefficient $2\tau_w/\rho_e u_e^2$
C_F = average skin-friction coefficient
D = reference length
H = boundary-layer shape parameter δ^*/θ
M = Mach Number
N = exponent in empirical skin-friction equation (11)
Re_x = Reynolds Number based on distance from leading edge
Re_θ = Reynolds Number based on momentum thickness
T = temperature
u = velocity component parallel to wall
x = coordinate along wall
y = coordinate normal to wall
α = coefficient in empirical skin-friction equation (11)
γ = ratio of specific heats
δ^* = boundary-layer displacement thickness
η = variable scale factor in the transformation, defined by Eqs. (3)
θ = boundary-layer momentum thickness
μ = viscosity
ν = kinematic viscosity μ/ρ
ρ = density
τ = shear stress

Subscript and Superscripts

$()_e$ = evaluated in the free stream just outside the boundary layer
$()_i$ = corresponding quantities in the related incompressible flow
$()_w$ = evaluated at the wall
$()_0$ = evaluated at an isentropic stagnation point in the free stream
$()_1$ = evaluated at the initial point of the boundary-layer growth calculation
$()^*$ = evaluated at the reference temperature T^*

Received June 24, 1957. Revised and received December 27, 1957.

* Formerly, Aeronautical Engineer, Naval Supersonic Laboratory. Now, Fulbright Fellow, University of Glasgow, Scotland.

** Aeronautical Engineer, Naval Supersonic Laboratory.

DISCUSSION

THE PROBLEM of calculating the growth of the boundary layer on a body in an airstream, or on the internal walls of a duct through which air is flowing, has long been of interest to the aeronautical engineer. Methods for handling this problem are continually being developed and improved. In recent years there has been much interest in methods applicable to compressible flows. One approach, which has been very successful in the laminar case, is to seek a suitable transformation which will make applicable also to compressible flows the large body of results available for incompressible flows. It is the purpose of this paper to examine the relationship between turbulent boundary layers in compressible and incompressible flows and to show that a transformation developed for laminar flows is approximately valid, with a slight modification, for turbulent flows as well.

The specific problem which will be considered is that of the growth of the boundary layer in a two-dimensional accelerating flow with arbitrary pressure gradient. The restriction to accelerating flows avoids the difficult problem of predicting separation and yet is satisfied in many supersonic flows of practical interest. In incompressible flows of this kind the growth of the boundary layer may be calculated very conveniently by simple quadratures such as Thwaites' formula[1] for the laminar and Truckenbrodt's[2] for the turbulent case. If the flow is not too far from adiabatic, the laminar problem in compressible flow may be solved by applying the Stewartson-Illingworth transformation[3, 4] to Thwaites' formula, as suggested by Rott and Crabtree.[5] The question which will now be examined is whether this same transformation is also applicable to the turbulent problem, as suggested in references 6, 7, and 8.

Using the conventional symbols, the integral momentum equation for compressible boundary-layer flow may be written

$$(d\theta/dx) + \theta[(H + 2)\,(1/u_e)\,(du_e/dx) + (1/\rho_e)\,(d\rho_e/dx)] = \tau_w/\rho_e u_e^2 = c_f/2 \quad (1)$$

Stewartson originally transformed the boundary-layer differential equations using

TABLE 1
Values of H_i and of N and $\alpha(N)$ in Eq. (11) Appropriate to Various Ranges Re_θ for the Turbulent Boundary Layer in Incompressible Flow

$(Re_\theta)_i$	N	$\alpha(N)$	H_i
100–5,000	4	0.0123	1.4
500–50,000	5	0.0085	1.3
3,000–600,000	6	0.0062	1.25
10,000–10^7	7	0.0048	1.2

$$y' = \eta \int_0^y (\rho/\rho_e)dy, \quad u' = (a_0/a_e)u, \quad T' = T_0 \tag{2}$$

as well as transforms for x and v. Here

$$\eta = T_e/T_0^{(\gamma+1)/2(\gamma-1)} \; [= (T_e/T_0)^3 \text{ for } \gamma = 1.4] \tag{3}$$

and the subscript $(\,)_0$ refers to stagnation conditions in the external stream. The transformed integral equation obtained by using Eq. (2) and leaving the x-transformation undefined is

$$(d\theta'/dx') + \theta'[\tfrac{1}{2}(H+1)(T_e/T_0) + 1\tfrac{1}{2} \times (1/u_e')(du_e'/dx')] = (dx/dx')\eta(c_f/2) \tag{4}$$

with

$$\theta' = \eta\theta \tag{5}$$

This result may now be compared with the integral momentum equation for an incompressible flow;

$$(d\theta_i/dx_i) + \theta_i(H_i + 2)(1/u_{ei})(du_{ei}/dx_i) = c_{fi}/2 \tag{6}$$

with fluid properties ρ_0 and μ_0 evaluated at T_0. If the conditions

$$(H+1)(T_e/T_0) = H_i + 1 \tag{7}$$

$$dx'/dx = \eta(c_f/c_{fi}) \tag{8}$$

are satisfied, the transformed flow may be considered incompressible and may be represented by the solution

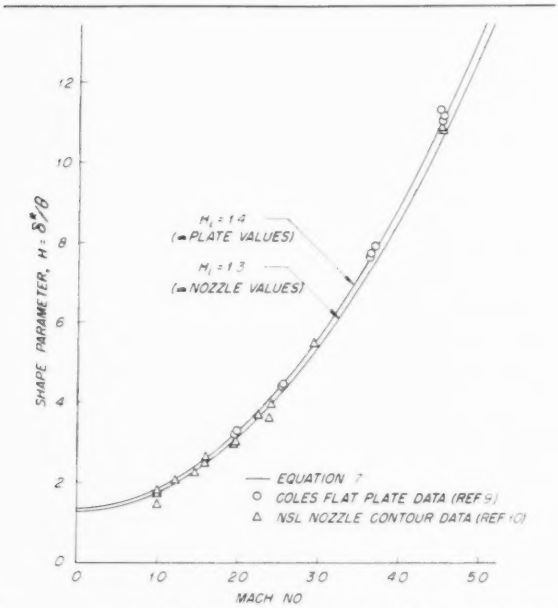
SHAPE PARAMETER, H = δ*/θ
MACH NO
H_i = 1.4 (≈ PLATE VALUES)
H_i = 1.3 (≈ NOZZLE VALUES)
EQUATION 7
COLES FLAT PLATE DATA (REF 9)
NSL NOZZLE CONTOUR DATA (REF 10)

FIG. 1. Variation of shape parameter, H, with Mach Number for turbulent boundary layers.

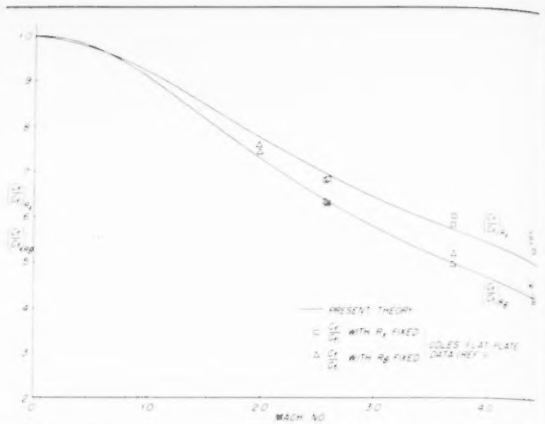

FIG. 2. Present theory for variation of C_F/C_{F_i} and C_f/C_{f_i} with Mach Number ($T^* = T_0$).

of Eq. (6) with

$$\theta' = \theta_i, \qquad u_e' = u_{ei} \tag{9}$$

The first condition is clearly one which must be checked by examining experimental results or otherwise; whereas the second may simply be used to define the required x-transformation.

Both H and c_f depend on Reynolds Number and pressure gradient as well as on Mach Number. The pressure-gradient effects in supersonic flow are not known well enough to be considered here; it seems that they are small in any case for accelerated flows. The Reynolds Number dependence, however, must be taken into account, and it is necessary first of all to note that the values of momentum-thickness Reynolds Number in the two flows represented by Eq. (1) and Eq. (6) are different; in fact,

$$(Re_\theta)_i = \rho_0 u_e \theta_i/\mu_0 = \rho_0 u_e' \theta'/\mu_0 = (\mu_e/\mu_0)(\rho_e u_e \theta/\mu_e) = (\mu_e/\mu_0)Re_\theta \tag{10}$$

The variation of c_{fi} and H_i with $(Re_\theta)_i$ in incompressible flows is well known. It is convenient in this case (and consistent with the approximations inherent in use of integral methods) to use the approximate formula

$$c_{fi}/2 = \alpha(N)/(Re_\theta)_i^{1/N} = \tau_w/\rho_0 u_{ei}^2 \tag{11}$$

Very good agreement with the Kármán-Schoenherr formula over wide ranges of $(Re_\theta)_i$ may be obtained by choosing appropriate values of N and $\alpha(N)$, as given in Table 1. Also given are appropriate values of H_i corresponding to each choice of N. If the values of θ in any compressible flow are known to fall in a certain range, it is a simple matter to calculate the corresponding range of values of $(Re_\theta)_i$ from Eq. (10) and hence to obtain suitable values of N and H_i.

Now that H_i has been defined, condition (7) may be checked experimentally for flows in which θ and H have been measured. Fig. 1 shows the observed variation of H with Mach Number for supersonic flows on a flat plate and on a set of wind-tunnel nozzles. Also shown is the variation predicted by Eq. (7) for the two

values of H_i corresponding to the two sets of measurements. For flows with zero heat transfer at any rate, condition (7) seems to be satisfied if $M < 5$.

The required x-transformation defined by Eq. (8) can only be evaluated in terms of the ratio of the skin-friction coefficients in compressible and incompressible flows. This ratio may be conveniently evaluated if the effects of compressibility are expressed in terms of the concept of an effective temperature T^* as used, for instance, in reference 11. The formula for compressible flow is written

$$\tau_w / \rho^* u_e^2 = \alpha(N)\,(\rho^* u_e \theta / \mu^*)^{-(1/N)} = (\rho_e / \rho^*)\,(c_f/2) \quad (12)$$

with the same value of $\alpha(N)$ as in Eq. (11). Various expressions for the ratio c_f/c_{fi} may be written on this basis, each corresponding to a particular relation between the Reynolds Numbers of the two flows. For comparison with experiments, it is convenient to use

$$[c_f/c_{fi}]_{Re_\theta \text{ fixed}} = (\mu^*/\mu_e)^{1/N}\,(T_e/T^*)^{(N-1)/N} \quad (13)$$

and the value of T^*, which is purely empirical concept will here be chosen by fitting this expression to the measurements of Coles.[9] The choice of N, like that of H_i will be based on Table 1 and the transformed Reynolds Number $(Re_\theta)_i$ given by Eq. (10); the value of $N = 4$ is appropriate in this case. Fig. 2 shows a comparison of the experimental results with the expression (13) evaluated for

$$T^* = T_0 \quad (14)$$

This choice seems good for flows with zero heat transfer and $0 < M < 5$. The discrepancy with various other expressions for T^* given in the literature is only apparent because the latter have been chosen to represent the effects of compressibility with Re_x, rather than Re_θ, fixed.

The ratio c_f/c_{fi} corresponding to the relation (10) between the Reynolds Number in the two flows may now be obtained by multiplying Eq. (13) by

$$[(Re_\theta)_i / Re_\theta]^{1/N} = (\mu_e/\mu_0)^{1/N} \quad (15)$$

and may be written

$$c_f/c_{fi} = (\mu_0/\mu_e)^{1/N}\,(T_e/T_0)^{(N-1)/N}\,(\mu_e/\mu_0)^{1/N} = (T_e/T_0)^{(N-1)/N} \quad (16)$$

The x-transformation (8) for turbulent flow now becomes

$$dx'/dx = (T_e/T_0)^{[(\gamma+1)/2(\gamma-1)]+[(N-1)/N]} \quad (17)$$

or

$$dx'/dx = (T_e/T_0)^{4-(1/N)} \quad \text{for } \gamma = 1.4 \quad (18)$$

The relation completes the definition of a transformation which (at least for small heat-transfer rates) relates the integral properties of a turbulent boundary layer in compressible flow to those in a related incompressible flow. The transformation is completely defined, for $\gamma = 1.4$, by the three relations

$$u_{ei} = a_0 M_e \quad (19)$$

$$\theta_i = (T_e/T_0)^3\,\theta \quad (20)$$

$$x_i = \int (T_e/T_0)^{4-(1/N)}\,dx \quad (21)$$

The only difference between this and Stewartson's transformation appears in Eq. (21).

Application of this transformation to Truckenbrodt's simple formula[2] for the growth of momentum thickness in incompressible flow,

$$(\theta_i/D)^{(N+1)/N}\,(u_{ei}D/\nu_0)^{1/N} = [(N+1)/N]\,\alpha(N) u_{ei}^{-[3+(2/N)]} \int_{x_1/D}^{x/D} u_{ei}^{3+(2/N)} d(x/D) + (\theta_i/D)_1^{(N+1)/N}\,(u_{ei}D/\nu_0)_1^{1/N}\,(u_{ei_1}/u_{ei})^{3+(2/N)} \quad (22)$$

yields the result

$$[(\theta/D)\,(T_e/T_0)^3]^{(N+1)/N} = [(N+1)/N]\,\alpha(N)(a_0 D/\nu_0)^{-(1/N)}\,M_e^{-[3+(3/N)]} \times \int_{x_1/D}^{x/D} M_e^{3+(2/N)}\,(T_e/T_0)^{4-(1/N)}\,d(x/D) + [(\theta/D)\,(T_e/T_0)^3]_1^{(N+1)/N}\,(M_{e_1}/M_e)^{3+(3/N)} \quad (23)$$

where D is a suitable reference length. The similar result obtained by applying Stewartson's transformation is

$$[(\theta/D)\,(T_e/T_0)^3]^{(N+1)/N} = [(N+1)/N]\,\alpha(N)\,(a_0 D/\nu_0)^{-(1/N)}\,M_e^{-[3+(3/N)]} \times \int_{x_1/D}^{x/D} M_e^{3+(2/N)}\,(T_e/T_0)^4\,d(x/D) + [(\theta/D)\,(T_e/T_0)^3]_1^{(N+1)/N}\,(M_{e_1}/M_e)^{3+(3/N)} \quad (24)$$

These equations may be used, in particular, to predict the growth of momentum thickness on a flat plate in compressible flow, where M_e and T_e/T_0 are independent of x. The result obtained from Eq. (23) is

$$\theta/x = C_F/2 = \tfrac{1}{2}[(N+1)/N]\alpha(N)\}^{N/(N+1)}\,(\rho_e u_e x/\mu_e)^{-[1/(N+1)]}\,(\mu_0/\mu_e)^{1/(N+1)}\,(T_e/T_0)^{(N-1)/(N+1)} \quad (25)$$

where C_F is the average skin-friction coefficient. This expression may be compared with the corresponding one for incompressible flow to obtain the effect of compressibility on average skin friction in the form

$$[C_F/C_{Fi}]_{Re_x \text{ fixed}} = (\mu_0/\mu_{ei})^{1/(N+1)} \times (T_e/T_0)^{(N-1)/(N+1)} \quad (26)$$

for equal values of Re_x in the two flows. The agree-

ment with Coles' measurements, shown in Fig. 2, is quite satisfactory.

Finally, Eq. (23) has been checked by comparisons of its predictions with measurements made on the surfaces of $M = 2.5$ and $M = 3.5$ nozzles of the Naval Supersonic Laboratory's wind tunnel. In each case the momentum thickness was measured both at the throat and in the nozzle exit plane; the measured values at the throat were used as initial values in the calculations. The measurements were also used to compute values of $(Re_\theta)_t$, on the basis of which a value of $N = 5$ was chosen. The results are given in Table 2, together with percentage errors based on the measured values; the predictions of Eq. (24) are also tabulated. In each case the new transformation gives a satisfactory result, closer to the experimental value than the result of applying Stewartson's transformation.

TABLE 2

Boundary-Layer Momentum Thicknesses in the Exit Planes of $M = 2.5$ and $M = 3.5$ Wind-Tunnel Nozzles—Comparison of Theory and Experiment

	θ (in.)	% Error
	$M = 2.5$ nozzle	
Measured	0.061	0
Eq. (23)	0.056	− 8%
Eq. (24)	0.051	−16%
	$M = 3.5$ nozzle	
Measured	0.046	0
Eq. (23)	0.047	+ 2%
Eq. (24)	0.040	−13%

References

[1] Thwaites, B., *Approximate Calculation of the Laminar Boundary Layer*, Aeronautical Quarterly, Vol. 1, pp. 245–280, 1949.

[2] Truckenbrodt, E., *A Method of Quadrature for Calculation of the Laminar and Turbulent Boundary Layer in Case of Plane and Rotationally Symmetrical Flow*, NACA TM 1379, 1955.

[3] Stewartson, K., *Correlated Incompressible and Compressible Boundary Layers*, Proc. Roy. Soc., Series A, Vol. 200, p. 84, 1949.

[4] Illingworth, I. R., *Steady Flow in the Laminar Boundary Layer of a Gas*, Proc. Roy. Soc., Series A, Vol. 199, p. 533, 1949.

[5] Rott, N., and Crabtree, L. F., *Simplified Laminar Boundary Layer Calculations for Bodies of Revolution and for Yawed Wings*, Journal of the Aeronautical Sciences, Vol. 19, No. 8, pp. 553–565, August, 1952.

[6] Crocco, L., and Lees, L., *A Mixing Theory for the Interaction Between Dissipative Flows and Nearly Isentropic Streams*, Journal of the Aeronautical Sciences, Vol. 19, No. 10, pp. 649–676, October, 1952.

[7] Mager, A., *Prediction of Shock-Induced Turbulent Boundary-Layer Separation*, Journal of the Aeronautical Sciences, Readers' Forum, Vol. 22, No. 3, pp. 201–202, March, 1955.

[8] Meyer, R. E., *Turbulent Boundary Layers on Nozzle Liners*, Journal of the Aeronautical Sciences, Readers' Forum, Vol. 22, No. 8, pp. 572–573, August, 1955.

[9] Coles, D., *Measurements in the Boundary Layer on a Smooth Flat Plate in Supersonic Flow III—Measurements in a Flat Plate Boundary Layer at the Jet Propulsion Laboratory*, California Institute of Technology, Jet Propulsion Laboratory, Report No. 20-71, 1953.

[10] Baron, Judson R., *Analytic Design of a Family of Supersonic Nozzles by the Friedrichs Method (Including Computation Tables and a Summary of Calibration Data)*, Massachusetts Institute of Technology, Naval Supersonic Laboratory, TR 66, July 1954, WADC TR 54-279, 1954.

[11] Monaghan, R. J., *On the Behavior of Boundary Layers at Supersonic Speeds*, published in *Proceedings, Fifth International Aeronautical Conference*, Los Angeles, Calif., June, 1955.

Discussion of the Lecture

(*Continued from page 229*)

on spheres at Mach 10 in the hypersonic wind tunnel and fired them at 10,000 ft./sec. in the range to measure the drag and real gas effects, it was considered to be of only academic interest to a few research people who were not really interested in hardware since everybody knew, at that time, that hypersonic vehicles must have sharp-pointed noses to reduce the drag. Mr. Allen's dissertation shows how fast and unexpectedly such results of systematic research can advance the solution of apparently insurmountable problems. His charts show in a few simple revealing curves the principal characteristics of long-range vehicles including those of their re-entry process. It is, for example, a startling fact that the maximum deceleration of spherical bodies with weights varying within eight orders of magnitude, and entering with the same speed, does not vary at all. Only the altitude changes where the peak occurs.

Once such general principles are demonstrated, detailed calculations can immediately be pointed toward the missing links in the final solution. For example, in finding within the indicated limits the correct shape of the body, the dependency of aerodynamicists, ballisticians, and materials and structures people on each other shows up as never before. Their arguments about the fraction of kinetic energy which is converted in heat and how much of it enters the vehicle are considerably simplified by having such charts as we have just seen.

I wish for the sake of our future work that we had more of this kind of communication which puts in a nutshell clear and precise information.

Mr. Allen, I enjoyed your lecture.

Readers' Forum

BRIEF REPORTS of investigations in the aeronautical sciences and discussions of papers published in the JOURNAL are presented in this special department. Entries must be restricted to a maximum of 1,300 words or the equivalent of one JOURNAL page including formulas and illustrations. Publication is completed as soon as possible after receipt of the material. The Editorial Committee does not hold itself responsible for the opinions expressed by the correspondents.

Contents

On Optimum Nose Curves for Superaerodynamic Missiles ..... H. S. TAN 263

Blocking in the Supersonic Wind Tunnel ..... BAIN DAYMAN, JR. 264

Transient Temperature Distribution in Aircraft Structures ..... IRVING FRANK 265

An Iteration Method for Solving Linear Problems in the Theory of Shallow Shells ..... WILLIAM A. NASH AND P. L. SHENG 267

A Note on the Optimum Distribution of Material in a Beam for Stiffness ..... B. SAELMAN 268

Note on Hydrogen as a Real-Gas Driver For Shock Tubes ..... PAUL W. HUBER 269

Calculation of Supersonic Flow Past an Axially Symmetric Cylinder ..... MARTHA W. EVANS AND FRANCIS H. HARLOW 269

Combustion in the Laminar Boundary Layer of Chemically Active Sublimating Surfaces ..... M. R. DENISON AND D. A. DOOLEY 271

Effect of Loads on the Spring Constant of a Particular Type of Flexure ..... FREDERICK G. BLOTTNER 272

Hypersonic Heat Transfer to Catalytic Surfaces ..... SINCLAIRE M. SCALA 273

A Comment on the Methods of Calculating Natural Modes and Frequencies of Vibration ..... SAMUEL SILVERBERG 275

The Effect of External Sound on the Vortex Shedding From Cylinders ..... DONALD I. GARBER 275

Remarks on Systematizing the Calculations of the Natural Modes of a Free Structure ..... R. KAPPUS AND D. CLERC 276

A Note on Isentropic Compressible Flow of Air With Variable Specific Heats ..... K. E. TEMPELMEYER AND L. SELF 278

Propagation of Weak Waves in a Dissociated Gas ..... F. K. MOORE 279

On Optimum Nose Curves for Superaerodynamic Missiles

H. S. Tan

Consultant, Therm-Electric Meters Co., Ithaca, N.Y.

November 27, 1957

IN A RECENT NOTE,[1] Dennis has pointed out that the optimum missile-nose curve for superaerodynamic regime obtained under the assumption of regular molecule reflection[2] is precisely that for the hypersonic regime derived according to Newtonian slip flow.[3]

While the above-observed coincidence between superaerodynamic and hypersonic missile-nose shape is obviously of important significance, there is no such coincidence for the case of random molecular re-emission, which, to certain extent, is actually a more realistic model. Thus, it seems that a more thorough statistical investigation of the actual manner of free-molecular reflection should be conducted next. On the other hand, it seems not without interest at this stage to compare the two curves corresponding to these two different assumptions. The integrations are briefly indicated in what follows, together with tabulated results and curves drawn to scale. As already noted,[4] the fairing of nose tip beyond $y' = \sqrt{k}$ does not merit discussion because this point can always be brought as close to the axis as we like by a simple change of scale.

The differential equation for the missile-nose curve is given by

$$y'' = -(y'^2/y)\,(1 + y'^2)/(k - y'^2) \tag{1}$$

Its first integral with respect to y is obtained by noting $y'' = y'dy'/dy$, and is given by:

$$y = C_1(1 + y'^2)^{(k+1)/2}/y'^k \tag{2}$$

Its first integral with respect to x is obtained by noting that $y'' = dy'/dx$ and that y is given by Eq. (2). Indeed Eq. (1) then gives, upon integration,

Contributors Please Note

Readers' Forum items must be confined to the equivalent of one page in the *Journal*. Contributions that exceed this limit will be returned to the authors for condensation and rewrite. To avoid inconvenience and delay, please adhere to the following specifications:

(1) Five, double-spaced, typewritten, manuscript pages (8½ by 11 in.), including wide margins, formulas, and headings equal one printed page.

(2) For every illustration, deduct at least one-half or as much as one manuscript page, depending on the size of the illustration.

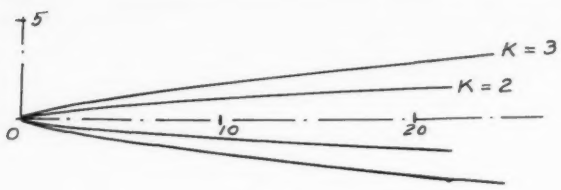

FIG. 1.

TABLE 1
($x_0 = 0$, $y_0 = 0.010$)

	$k = 3$				$k = 2$	
	$y_0' = \sqrt{3}$		$y_0' = \sqrt{2}$		$y_0' = \sqrt{2}$	
y'	x	y	x	y	x	y
$\sqrt{3}$	0	0.010				
$\sqrt{2}$			0	0.010	0	0.010
1	0.00255	0.0130			0.0008	0.0109
0.50	0.0466	0.0406				
0.25	0.668	0.235				
0.20	1.519	0.440				
0.15	4.956	1.005	4.822	0.973	0.759	0.177
0.12	11.97	1.935	11.63	1.881	1.480	0.273
0.10	24.69	3.315	24.00	3.220	2.560	0.391
0.075					5.940	0.693
0.05	391.3	26.10	380.5	25.39	20.55	1.540
0.01	243,600	3,256	237,000	3,166	2,567	38.50
	C_1 0.00325		C_1 0.00316		C_1 0.00385	
	C_2 −0.00314		C_2 −0.00327		C_2 −0.00441	

$$x = -C_1 \int [(1 + y'^2)^{(k-1)/2} (k - y'^2)/y'^{(k+2)}] dy' + C_2 \quad (3)$$

The resulting curves for these two respective cases are easily obtained by quadrature as follows:
Regular molecular reflection, $k = 3$

$$\left.\begin{aligned} y &= C_1 [y' + (2/y') + (1/y'^3)] \\ x &= C_1 [\ln y' + (1/y'^2) + (3/4y'^4)] + C_2 \end{aligned}\right\} \quad (4)$$

Random molecular re-emission, $k = 2$

$$\left.\begin{aligned} y &= C_1(1 + y'^2)^{3/2}/y'^2 \\ x &= (C_1/3)\{[2(1 + y'^2)^{1/2}/y'^2] - \\ &\quad [(1 + y'^2)^{1/2}/y'] + 3 \ln (y' + \sqrt{1 + y'^2})\} + C_2 \end{aligned}\right\} \quad (5)$$

It can readily be shown that the asymptotic behavior of Eqs. (4) and (5) are indeed given by Eqs. (9) and (11) of the previous note.[4] It is also interesting to note that the optimum nose corresponding to random molecular re-emission is substantially more slender than that corresponding to regular molecular reflection.

REFERENCES

[1] Dennis, D. H., *On Optimum Nose Shapes for Missiles in the Superaerodynamic Region*, Journal of the Aeronautical Sciences, Readers' Forum, Vol. 25, No. 3, p. 216, March, 1958.

[2] Carter, W. J., *Optimum Nose Shapes for Missiles in the Superaerodynamic Region*, Journal of the Aeronautical Sciences, Vol. 24, No. 7, pp. 527–532, July, 1957.

[3] Eggers, A. E., Jr., Resnikoff, M. M., Dennis, D. H., *Bodies of Revolution Having Minimum Drag at High Supersonic Airspeeds*, NACA TN 3666, February, 1956.

[4] Tan, H. S., *On Optimum Nose Curves for Missiles in the Superaerodynamic Regime*, Journal of the Aeronautical Sciences, Readers' Forum, Vol. 25, No. 1, pp. 56, 57, January, 1958.

Blocking in the Supersonic Wind Tunnel*

Bain Dayman, Jr.
Jet Propulsion Laboratory, California Institute of Technology, Pasadena, Calif.

November 27, 1957

AN IMPORTANT PROBLEM in the use of supersonic wind tunnels for research and development work is to determine, for a given model configuration, wind tunnel, and Mach Number, the maximum permissible model size. Tests were run in the Jet Propulsion Laboratory (JPL) 12-in. supersonic wind tunnel in order to obtain a reliable method of predicting the blocking characteristics of models during an attempted start—i.e., if supersonic flow could be established in the test section for a particular model (size and shape) at a given Mach Number. Fig. 1

* This paper presents the results of one phase of research carried out at the Jet Propulsion Laboratory, California Institute of Technology, under Contract No. DA-04-495-Ord 18, sponsored by the Department of the Army, Ordnance Corps.

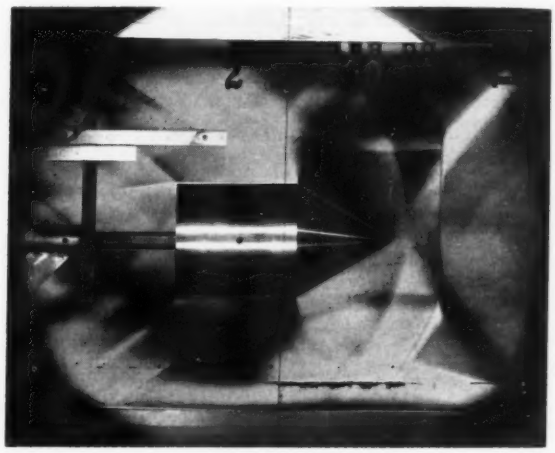

FIG. 1. Cone-cylinder model in a 12-in. supersonic wind tunnel showing barely blocked flow.

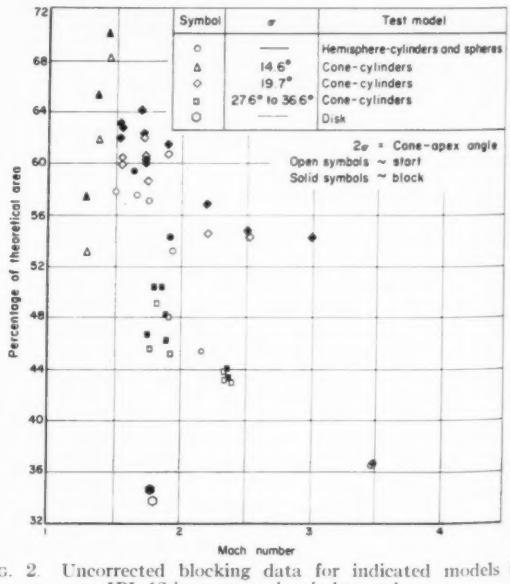

FIG. 2. Uncorrected blocking data for indicated models in JPL 12-in. supersonic wind tunnel.

TABLE 1

Mach Number	Area Ratio
1.5	0.0854
2.0	0.1782
3.0	0.2808
4.0	0.3276
∞	0.4000

presents, for one model, an example of barely blocked flow (M = 1.9). Four classes of models were used: spheres, hemisphere cylinders (3 to 4 in. diameter), cone cylinders (2 to 4.5 in. diameter, 30° to 73° cone apex angle), and a disk (3 in. diameter).

Previously, a rule-of-thumb value was used to determine the maximum size of a model that could be run at a chosen Mach Number. The value used was 60 per cent of the maximum one-dimensional theoretical area (based upon a normal shock wave across the test section upstream of the model and sonic flow about the model). The ratio of the model frontal area to the test-section area from this simplified theory can be expressed by the following equation:

$$\frac{\text{Model frontal area}}{\text{Test-section area}} = 1 - \frac{p_{t_1}/p_{t_2}}{A/A^*}$$

where

A/A^* = ratio of local cross-sectional area of an isentropic stream tube to cross-sectional area at the point where the Mach Number is unity (one-dimensional theory)

p_{t_1}/p_{t_2} = total pressure ratio (upstream to downstream) across a normal shock wave

Table 1 gives several values of this theoretical area ratio (from the equation for $\gamma = 1.400$).

Although the 60 per cent value of the theoretical model area is generally adequate for models having slender pointed noses, it is unconservative for blunter models. Fig. 2 presents the data from these blocking studies in the manner normally used in wind-tunnel operation. The start and block conditions are normally separated by 0.02 in Mach Number. The ordinate represents the frontal areas of the tested models as percentages of the theoretical model areas. It is readily apparent, for the data as a group, that this method of presenting the data is of little or no use insofar as the prediction of blocking during an attempted start is concerned.

Fig. 3 presents the data of Fig. 2 with the bow-shock-wave strength instead of the Mach Number as the abscissa. The shock-wave strength is defined as the perimeter average of the ratio of the static pressure increase across the shock wave to the free-stream static pressure upstream of the shock wave. The perimeter average is taken along the intersection of the bow shock wave with the test section walls, using the shock-wave shape which would have existed had there been no wall interference. The test section wall is taken to be at the displacement boundary layer on the physical wall. Hence, the test section area is less than the physical area by the area of the displacement boundary layer. It is this smaller area upon which the data are based. An arbitrary straight line was drawn in an attempt to separate the starts (open symbols) from the blocks (solid symbols). Except for the disk model, the data correlate to about 2 per cent in model diameter or in Mach Number (whichever gives the greater latitude from this blocking correlation line). At this time, no final conclusions have been reached on a correlation method which will include disk models.

The ability to start the tunnel with a particular model does not guarantee a successful test. The wake shape may be deformed, or the bow shock wave may reflect back onto the model.

Although this correlation pertains specifically to the JPL 12-in. supersonic wind tunnel and to the types of models tested, similar correlations probably exist for other supersonic wind tunnels and other types of models. The closer the operating conditions of the various tunnels (such as supply pressure, diffuser efficiency, compression ratio), the closer the correlations may be. Preliminary checks in the JPL 20-in. supersonic wind tunnel support the possibility of extending the correlation to other similar wind tunnels.

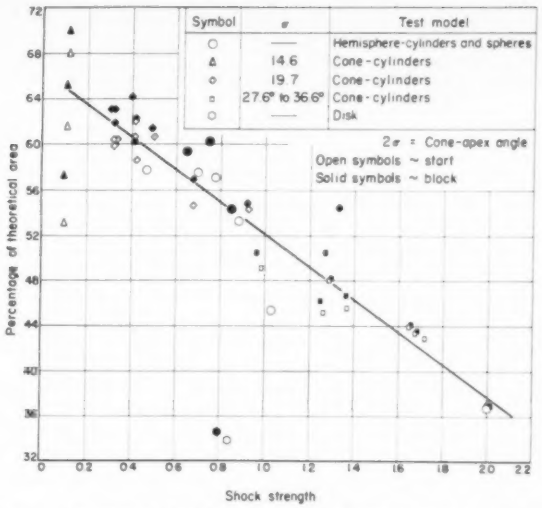

FIG. 3. Corrected blocking data for indicated models in JPL 12-in. supersonic wind tunnel.

REFERENCE

[1] Dayman, B., Jr., *Prediction of Blocking in the Supersonic Wind Tunnel During an Attempted Start*, Report No. 20-109, Jet Prop. Lab., Pasadena, Calif., June 28, 1957.

Transient Temperature Distribution in Aircraft Structures*

Irving Frank
Staff Mathematician, Allied Research Associates, Inc., Boston, Mass.
November 25, 1957

INTRODUCTION

VARIOUS APPROXIMATE numerical methods are available for calculating temperature distributions in aircraft sections exposed to high heat inputs.[1-4] Such numerical procedures are used because of the complex geometry and boundary conditions which apply to the ordinary aircraft section. These methods, however, usually require the use of computing equipment, and furthermore, lack the generality of analytic solutions. It is, therefore, frequently advantageous to determine the temperature distribution analytically by making appropriate simplifying assumptions. The accuracy of the solutions will in these cases depend on the validity of the simplifying assumptions.

ANALYSIS

Consider an aircraft cross section (Fig. 1) exposed to a heat input on one surface or to a symmetrical heat input on both surfaces. It is assumed that: the structural members are thermally thin so that the one-dimensional heat conduction equation is valid in each, the mechanism of joint heat conductance can be represented analytically by convective heat relations,

* This research was performed for the Structures Branch, Aircraft Laboratory, Wright Air Development Center, under Contract No. AF 33(616)-5001.

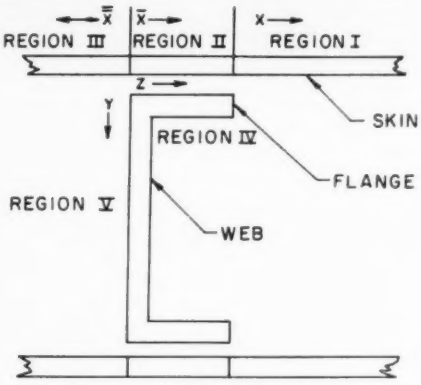

FIG. 1. Aircraft cross section.

the increase in temperature of the internal structure due to irradiation from the skin is negligible, and the heat transport properties including the joint conductivity are independent of temperature.

In addition, it is assumed that the heat flux to the web is independent of the existence of the flange—i.e., the heat capacity of the flange is negligible. Thus, the temperature distribution in the web can be determined by considering the temperature distribution in the "T" section. The heat balance equations for this section are

$$\partial^2 u/\partial x^2 = (1/\alpha)\,(\partial u/\partial t) - [F(t)/aK] \tag{1}$$

$$\partial^2 v/\partial y^2 = (1/\alpha)\,(\partial v/\partial t) \tag{2}$$

where u and v are the skin and web temperature, respectively, x is the distance from the web on the skin, y is the distance from the skin on the web, a is the skin thickness, α is the skin diffusivity, K is the aircraft material conductivity, t is the time, and $F(t)$ is the heat input to the skin.

The boundary and initial conditions are:

(a) at $t = 0$: $u = v = 0$
(b) at $x = 0$, $y = 0$: $-2aK\,(\partial u/\partial x) = -hb\,[u - v]$, $-bK(\partial v/\partial y) = hb\,[u - v]$
(c) at $x = \infty$, $y = \infty$: u is finite, v is finite

where b is the web thickness and h is the joint conductivity.

Taking the Laplace Transform of Eqs. (1) and (2) yields

$$d^2u^*/dx^2 = (p/\alpha)u^* - [F(p)/aK] \tag{3}$$

$$d^2v^*/dy^2 = (p/\alpha)v^* \tag{4}$$

where $F(p)$ is the transform of $F(t)$, and u^* and v^* are the transforms of u and v. Solving Eqs. (3) and (4) and applying boundary and initial conditions (a)–(c) gives

$$u^* = [-hb\alpha F(p)/2a^2K^2(q + \gamma)]e^{-qx} + [\alpha F(p)/aKp] \tag{5}$$

$$v^* = [h\alpha F(p)/aK^2p(q + \gamma)]\,e^{-qy} \tag{6}$$

where $\gamma = h(b + 2a)/2aK$ and $q = \sqrt{p/\alpha}$

Returning to the channel section, and assuming the temperature of the flange at the junction of the flange and the web is given by Eq. (6) with $y = 0$, the temperature distribution in the remainder of the section can now be determined.

The heat-balance equations for the four regions (Fig. 1) become

$$\partial^2 u/\partial x^2 = (1/\alpha)\,(\partial u/\partial t) - [F(t)/aK] \quad \text{Region I} \tag{7}$$

$$\partial^2 \bar{u}/\partial \bar{x}^2 = (1/\alpha)\,(\partial \bar{u}/\partial t) - [F(t)/aK] + [G(t)/aK] \quad \text{Region II} \tag{8}$$

$$\partial^2 \bar{\bar{u}}/\partial \bar{\bar{x}}^2 = (1/\alpha)\,(\partial \bar{\bar{u}}/\partial t) - [F(t)/aK] \quad \text{Region III} \tag{9}$$

$$\partial^2 w/\partial z^2 = (1/\alpha)\,(\partial w/\partial t) - [G(t)/bK] \quad \text{Region IV} \tag{10}$$

where $G(t)$ is the heat flux from the skin to the flange and will be determined by solving the above equations.

The initial and boundary conditions are

(d) at $t = 0$: $u = \bar{u} = \bar{\bar{u}} = w = 0$
(e) at $x = 0$, $\bar{x} = l$: $u = \bar{u}$, $\partial u/\partial x = \partial \bar{u}/\partial \bar{x}$
(f) at $\bar{x} = 0$, $\bar{\bar{x}} = 0$: $\bar{u} = \bar{\bar{u}}$, $\partial \bar{u}/\partial \bar{x} = -\partial \bar{\bar{u}}/\partial \bar{\bar{x}}$
(g) at $x = \infty$, $\bar{\bar{x}} = \infty$: u is finite, $\bar{\bar{u}}$ is finite
(h) at $z = 0$: $w = v = L^{-1}[h\alpha F(p)/aK^2\,p(q + \gamma)]$, $(\partial w/\partial z) = -(\partial v/\partial y) = L^{-1}[qh\alpha F(p)/aK^2p(q + \gamma)]$
(i) at $z = l$: $(\partial w/\partial z) = 0$

where L^{-1} is the inverse Laplace Transform and u is the temperature in Region I, $\bar{u}$ is the temperature in Region II, $\bar{\bar{u}}$ is the temperature in Region III, and w is the temperature in Region IV. The coordinates for the various regions are shown in Fig. 1.

Taking the Laplace Transform of Eqs. (7)–(10) yields

$$d^2u^*/dx^2 = (p/\alpha)u^* - [F(p)/aK] \quad \text{Region I} \tag{11}$$

$$d^2\bar{u}^*/d\bar{x}^2 = (p/\alpha)\bar{u}^* - [F(p)/aK] + [G(p)/aK] \quad \text{Region II} \tag{12}$$

$$d^2\bar{\bar{u}}^*/d\bar{\bar{x}}^2 = (p/\alpha)\bar{\bar{u}}^* - [F(p)/aK] \quad \text{Region III} \tag{13}$$

$$d^2w^*/dz^2 = (p/\alpha)w^* - [G(p)/bK] \quad \text{Region IV} \tag{14}$$

Solving Eqs. (11) to (14) with the boundary conditions (d)–(i) yields

$$u^* = \Gamma(e^{-ql} - 1)e^{-qx} + [\alpha F(p)/aKp] \quad \text{Region I} \tag{15}$$

$$\bar{u}^* = \Gamma e^{-q\bar{x}} + e^{-q(l-\bar{x})} + [\alpha F(p)/aKp] - 2\Gamma \quad \text{Region II} \tag{16}$$

$$\bar{\bar{u}}^* = \Gamma(e^{-ql} - 1)e^{-q\bar{\bar{x}}} + [\alpha F(p)/aKp] \quad \text{Region III} \tag{17}$$

$$w^* = (-b\Gamma/a)e^{-qz} + e^{-q(2l-z)} + (2q\Gamma/b) \quad \text{Region IV} \tag{18}$$

where $\Gamma = [h\alpha bF(p)/a^2K^2p(q + \gamma)\,(1 - e^{-2ql})]$

Upon setting $[1/(1 - e^{-2ql})] = 1 + e^{-2ql} + e^{-4ql} + \ldots$

it is found that the solutions for the temperature distributions are all of the form

$$\sum_{i=1}^{\infty} A_i \frac{e^{-qx_i}}{q^2(q + \gamma)}\,F(p) + [\alpha F(p)/aKp]\epsilon \tag{19}$$

where $\epsilon = 1$ in the skin and is zero in the web and flange, and the A_i are independent of p and x_i.

From reference 5

$$L^{-1}[e^{-qx}/q^{n+1}(q + \gamma)] = [\alpha/(-\gamma)^n\,\left\{e^{\gamma x + \alpha t\gamma^2}\,\text{erfc}\,\left[(x/2\sqrt{\alpha t}) + \gamma\sqrt{\alpha t}\right] - \sum_{r=0}^{n-1}\left[-2\gamma\sqrt{\alpha t}\right]^r i^r\,\text{erfc}\,(x/2\sqrt{\alpha t})\right\} \tag{20}$$

Hence, by the convolution theorem

$$\sum_{i=1}^{\infty} A_i[e^{-qx_i}/q^{n+1}(q + \gamma)]\,F(p) = [\alpha/(-\gamma)^n]\int_0^t \sum_{i=1}^{\infty} A_i\left\{e^{\gamma x_i + \alpha\tau\gamma^2}\,\text{erfc}\,\left[(x_i/2\sqrt{\alpha\tau}) + \gamma\sqrt{\alpha\tau}\right] - \sum_{r=0}^{n-1}\left[-2\gamma\sqrt{\alpha\tau}\right]^r i^r\,\text{erfc}\,(x/2\sqrt{\alpha\tau})\right\}\{F(t - \tau)\}\,d\tau \tag{21}$$

If $F(t)$ is any polynomial in t, then Eq. (19) can be inverted directly. For let $F(t) = a_0 + a_1t + a_2t^2 + \ldots$ then $F(p) = (a_0/p) + (a_1/p^2) + (2a_2/p^3) + \ldots = (a_0/\alpha q^2) + (a_1/\alpha^2q^4) + (2a_2/\alpha^3q^6) + \ldots$ and Eq. (19) can be inverted by using the inversion formula in Eq. (20).

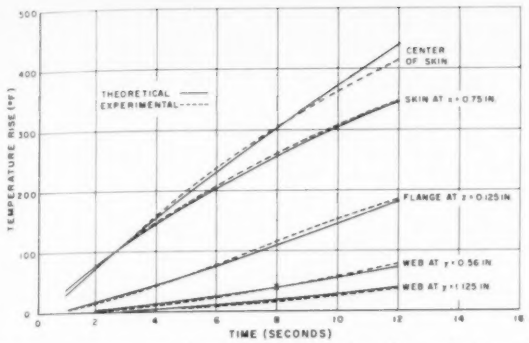

FIG. 2. Temperature distribution correlation of a typical panel.

The functions appearing in Eq. (20) are tabulated in reference 5 and 7.

EXPERIMENTAL CORRELATION

The preceding analysis has been employed to correlate temperature distribution data obtained in experimental tests held at the U.C.L.A. thermal facility, reference 6. Fig. 2 compares the experimental and calculated temperatures for one of the test panels. The joint conductivity for this panel was found by matching the experimental and calculated temperatures at one point. This point is indicated by an "X" in Fig. 2. As may be seen from the figure, the agreement between the calculated and experimental results is quite good. A full discussion of the procedure followed in performing the temperature calculations and additional experimental correlations are contained in reference 8.

REFERENCES

[1] Ambrosio, A., and Ishimoto, T., *Analytical Studies of Aircraft Structures Exposed to Transient External Heating.* Vol. III; *Thermal Response of Skin and Support Flange of a Structural Joint.* WADC TR 54–579.

[2] Quinville, J. A., and Sneyd, J. M., *Methods of Calculating Heat Conduction for Transient Aerodynamic Heating of Supersonic Wing Structures.* Northrop Aircraft, Inc. NAI–54–452. June 30, 1954.

[3] Schmit, L. A., *The Influence of Aerodynamic Heating on the Structural Design of High-Speed Aircraft.* Part II, "The Temperature Distribution Problem," Bureau of Aeronautics, Department of the Navy. TR 55–2, August, 1955. (Confidential).

[4] Jakob, Max, *Heat Transfer*, Vol. I; John Wiley & Sons, New York, 1953.

[5] Carlslaw, H. S., and Jaeger, J. C., *Conduction of Heat in Solids.* First Ed.; Oxford University Press, London, 1947.

[6] Gray, E. I., and Franklin, D., *Experimental Response of B-47E Elevator Panels to High Intensity Thermal Inputs.* WADC TR 56–191. April, 1956. (Confidential).

[7] Kaye, Joseph, *A Table of the First Eleven Repeated Integrals of the Error Function.* J. Math. & Phys., Vol. XXXIV, No. 2, July, 1955.

[8] Gray, E. I., Frank, I., and Atamian, L. J., *Thermoelastic Studies on Heated Aircraft Sections with Correlation of Experimental Data.* WADC TR 57–184. May, 1957.

An Iteration Method for Solving Linear Problems in the Theory of Shallow Shells*

William A. Nash and P. L. Sheng
Professor and Research Assistant, Respectively, Department of Engineering Mechanics, University of Florida, Gainesville, Fla.
December 2, 1957

THE BEHAVIOR of a thin elastic shallow shell is described by two simultaneous differential equations for the deflection w and the Airy function F of the membrane stresses. These equations, due to Marguerre[1] and Reissner[2] are

$$\nabla^2\nabla^2 F = Eh\{2(\partial^2 z/\partial x\partial y)\cdot(\partial^2 w/\partial x\partial y) - (\partial^2 z/\partial x^2)\cdot(\partial^2 w/\partial y^2) - (\partial^2 z/\partial y^2)\cdot(\partial^2 w/\partial x^2)\} \quad (1)$$

$$D\nabla^2\nabla^2 w = (\partial^2 z/\partial x^2)\cdot(\partial^2 F/\partial y^2) + (\partial^2 z/\partial y^2)\cdot(\partial^2 F/\partial x^2) - 2(\partial^2 z/\partial x\partial y)\cdot(\partial^2 F/\partial x\partial y) + p \quad (2)$$

where ∇^2 denotes the Laplacian operator.

Here x, y are Cartesian coordinates, $z = z(x, y)$ denotes the equation of the middle surface of the shell, h the shell thickness, and $D = Eh^3/12(1 - \nu^2)$ where E is Young's modulus and ν represents Poisson's ratio. The applied load, of intensity p, acts in a direction normal to the x-y plane. A shell is considered to be shallow if the ratio of its height to a representative base dimension is less than approximately 1/8.

An iteration-type solution of Eqs. (1) and (2) is possible if the equation of the middle surface of the shell can be written in the form

$$(z/b) = \lambda\cdot f(x, y) \quad (3)$$

where $f(x, y)$ denotes a dimensionless function, and λ represents a dimensionless shallowness parameter. Also, b denotes some representative base dimension of the shell. If the characterization of the shell is such that the maximum value of $f(x,y)$ is unity, then $\lambda \leq 1/8$ for shallow shells. This representation of the shell was first introduced by Nazarov.[3]

To perform the iteration, we expand the desired unknowns w and F in terms of powers of the small dimensionless parameter λ, namely,

$$w = w_1 + \lambda w_2 + \lambda^2 w_3 + \ldots \quad (4)$$

$$F = F_1 + \lambda F_2 + \lambda^2 F_3 + \ldots \quad (5)$$

where w_1, w_2, F_1, F_2, etc. are functions of x,y but are independent of λ. Substituting these values into Eqs. (1) and (2) and equating terms containing like powers of λ, we obtain the set of equations

$$\nabla^2\nabla^2 F_1 = 0 \quad (6)$$

$$D\nabla^2\nabla^2 w_1 = p \quad (7)$$

$$\lambda\nabla^2\nabla^2 F_2 = Eh\{2(\partial^2 z/\partial x\partial y)\cdot(\partial^2 w_1/\partial x\partial y) - (\partial^2 z/\partial x^2)\cdot(\partial^2 w_1/\partial y^2) - (\partial^2 z/\partial y^2)\cdot(\partial^2 w_1/\partial x^2)\} \quad (8)$$

$$D\lambda\nabla^2\nabla^2 w_2 = (\partial^2 z/\partial x^2)\cdot(\partial^2 F_1/\partial y^2) + (\partial^2 z/\partial y^2)\cdot(\partial^2 F_1/\partial x^2) - 2(\partial^2 z/\partial x\partial y)\cdot(\partial^2 F_1/\partial x\partial y) \quad (9)$$

etc.

Additional equations may be added by equating the squares and higher powers of λ, and, in each, the right-hand sides will be functions of previously determined expressions in the series, Eqs. (4) and (5). Thus at every step it is only necessary to solve a pair of uncoupled equations for F_i and w_i with respect to boundary conditions. In this manner the solution to Eqs. (1) and (2) may be obtained to any desired degree of accuracy. Although the linear theory of shallow shells is derived on the basis of neglecting, in comparison with unity, terms involving squares and higher powers of λ, there is no justification for discarding such terms in Eqs. (4) and (5).

Further it is of interest to note that in certain cases the boundary conditions may also be treated independently. This is true, for example, if the edge deflection and the edge bending and twisting moments together with the normal and shear forces along the boundary are prescribed. In this case, the boundary conditions regarding deflection and moment may be expressed in terms of w only while those regarding normal and shear forces may be formulated in terms of F only.

REFERENCES

[1] Marguerre, K., *Zur Theorie der gekrummten Platte grosser Formanderung*, Proceedings 5th International Congress of Appl. Mech., pp. 93–101, Cambridge, Mass., 1938.

[2] Reissner, E., *On Some Aspects of the Theory of Thin Elastic Shells*, J. Boston Society of Civil Engineers, Vol. XLII, No. 2, pp. 100–133, 1955.

[3] Nazarov, A. A., *On the Theory of Thin Shallow Shells*, NACA TM 1426, 1956. (Translated from Prik. Mat. i. Mekh., Vol. 13, pp. 547–550, 1949.)

* These results were obtained in the course of research conducted under Grant G-1652 from the National Science Foundation.

A Note on the Optimum Distribution of Material in a Beam for Stiffness

B. Saelman
Design-Weight Engineer, Lockheed Aircraft Corp., Burbank, Calif.
December 2, 1957

SYMBOLS

J = torsion constant
θ = angular rotation
T = applied torque
G = modulus of rigidity
A = enclosed area
t = wall thickness
W = total weight
ρ = material density
s = perimeter
l = length of beam
λ = Lagrangian multiplier
f = shear stress
V = volume of material

IT HAS BEEN STATED by some authors[1] that the maximum stiffness of a beam for a given weight is attained when the strain energy is a minimum or when the stress is constant. It can be shown that this condition does not, generally, result in maximum stiffness; however, it closely approximates the optimum condition in some cases.

The optimum distribution of material for torsional stiffness of tubular beams is such that the thickness is constant around any cross section, and, for positions along the axis of the tube, the wall thickness should be proportional to the square root of the torsional moment and inversely proportional to the enclosed area. For maximum bending stiffness, the effective flange thickness should be proportional to the square root of the bending moment or the square root of the product of the moment and the axial length on the beam, depending on whether angular or linear deflections are being considered.

For the case of torsion, stiffness is measured by the amount of angular rotation, and, if t is independent of s, is given by:

$$\theta = (1/G)\int_0^l (T/J)dx = (1/4G)\int_0^l (Ts/A^2t)dx \qquad (1)$$

where T, s, A and t are functions of x.

The weight of the tube can be expressed by

$$W = \rho\int_0^l ts\,dx \qquad (2)$$

Considering the weight fixed, the minimizing condition for θ is found by application of The Calculus of Variations:

$$(\partial/\partial t)\,[(Ts/A^2t) + \lambda ts] = 0 \qquad (3)$$

Performing the operations in Eq. (3), solving for t, and eliminating by Eq. (1),

$$t = (1/A)\sqrt{T/\lambda} = (W/A\rho)\left[\sqrt{T}\Big/\int_0^l (\sqrt{T}s/A)dx\right] \qquad (4)$$

and

$$\theta_1 = (\rho/4GW)\left[\int_0^l (\sqrt{T}s/A)dx\right]^2 \qquad (5)$$

The strain energy due to twist can be written

$$U = (1/G)\int_0^l (T/J)dx = (1/2G)\int_0^l f^2 t ds = (1/2G)\int_0^l f^2\,dV \qquad (6)$$

The minimizing condition for U with W fixed is

$$(\partial/\partial t)\,[f^2ts - \lambda ts] = 0 \qquad (7)$$

This leads to the conclusion that the stress, f, is constant

$$f = \sqrt{\lambda} \qquad (8)$$

and that the strain energy per unit volume is constant

$$dU/dV = f^2/2G \qquad (9)$$

With the aid of Eq. (2) we can write

$$t = T/2Af = T/2A\sqrt{\lambda} = (W/A\rho)\left[T\Big/\int_0^l (Ts/A)dx\right] \qquad (10)$$

Substituting Eq. (10) into Eq. (1) we find

$$\theta_2 = (\rho/4GW)\int_0^l (Ts/A)dx\int_0^l (s/A)dx \qquad (11)$$

It is observed from Eq. (4) and Eq. (10) that the wall thickness, t, is proportional to $\sqrt{T}$ for maximum stiffness and proportional to T for minimum strain energy.

Comparing Eq. (5) and Eq. (11) it will be found that, in general, $\theta_1 \leq \theta_2$ except $\theta_1 = \theta_2$ when the torque is constant.

Fig. 1 illustrates the case for

$$A_x = A_R(x^2/L^2), \quad s = S_R(x/L), \quad T = T_R(x/L)$$

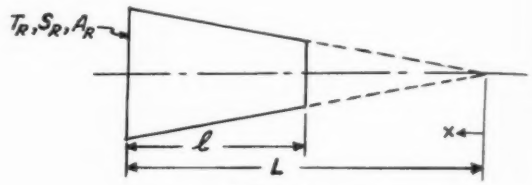

SKETCH 1.

We have

$$\theta_1 = BM, \quad M = 4l[R^{1/2} - (R-1)^{1/2}]$$

and

$$\theta_2 = BN, \quad N = l\log[R/(R-1)]$$

where

$$B = \rho T_R S_R^2 L/4GWA_R^2 \text{ and } R = L/l$$

Factors M and N in Fig. 1 are measures of the relative stiffness for the two cases. The limits of integration for the integrals become a and L.

If t_1 is a specified strength level and t is the unknown value to be determined for stiffness requirements, then if $t - t_1 = \tau$ and $\tau > 0$, τ is obviously a minimum when t is a minimum, and the latter value is determined by Eq. (4).

REFERENCE

[1] Cox, H. Roxbee, *Stiffness of Thin Shells*, Aircraft Eng., p. 245, September, 1936.

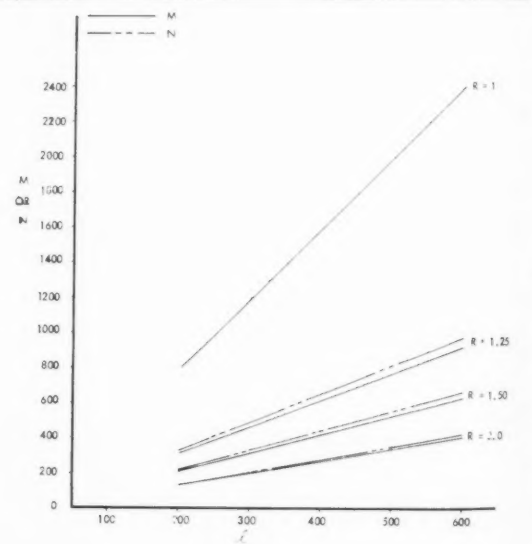

FIG. 1.

Note on Hydrogen as a Real-Gas Driver For Shock Tubes

Paul W. Huber
Head, Aero-Thermodynamics Section, Langley Aeronautical Laboratory, NACA, Langley Field, Va.
December 4, 1957

RECENTLY there has been renewed emphasis on the use of noncombustion shock-tube drivers of low molecular weight[1] because of the lower shock attenuation observed than with the theoretically more desirable combustion drivers. Nearly as high shock Mach Numbers are obtained when attenuation is accounted for and more uniform test conditions result from using the noncombustion drivers.

In reference 2 the maximum shock velocities observed along a shock tube were compared with the theoretically computed shock velocities for two pure gas drivers other than air—namely, helium and hydrogen. The computed velocities were based on real air as the driven gas and on ideal gas drivers. The helium-driven velocities were significantly higher than theory, while the hydrogen-driven case resulted in values about equal to, or slightly higher than, theoretical shock velocities.

It would be expected, intuitively, that these two drivers would exhibit more similarity since the velocity of sound in either gas is much greater than in air, and also in view of the similar shock attenuation characteristics found in reference 1 and the similar driver transport characteristics noted in reference 3 for these gases, as compared with other gas drivers.

One important difference between helium and hydrogen, however, may be found in the validity of the ideal-gas assumption. Helium is very close to a truly ideal gas both as to low compressibility and constancy of specific heat, while hydrogen is far from an ideal gas in both of these respects in the temperature and pressure range of interest for shock-tube drivers.

A computation of real-gas hydrogen driving real-gas air has been made, and the resulting diaphragm pressure ratio versus shock Mach Number is plotted in Fig. 1 for two cases of driver pressure, p_4. The curve labeled $p_4 = 0$ is shown to illustrate the large departure from an ideal gas due to the variation of specific heat with temperature. The other real-gas curve bearing the three driver-pressure labels is computed for about the driver-pressure range used in reference 2. The latter curve was actually obtained by first plotting three real-gas curves (p_4 = 50, 100, and 125 atmospheres), and judiciously fairing through these three curves to represent an approximate theoretical case for the driver conditions of reference 2. The computation was made using Riemann's unsteady-flow characteristics relation where the quantity conserved (see reference 4) in the driver gas is $\sigma + u$, where

$$\sigma = \int (a/\rho)d\rho$$

and this quantity is evaluated along an isentrope for each driver pressure using real-gas values for velocity of sound and density of hydrogen from reference 5. The corresponding pressure and fluid velocity are then matched across the discontinuity to the real-air shock values, as in reference 2, to obtain diaphragm pressure ratio.

It is also seen from Fig. 1 that a pronounced effect of pressure (compressibility) results when comparing the $p_4 = 0$ curve with the points indicated for finite driver pressure.

An interesting observation is that the effect of compressibility is to partially compensate for the effect of variable specific heat. The net result of the computations, however, is to show that hydrogen is not so unlike helium as a driver gas with respect to the shock Mach Numbers obtained in comparison with theory, when a real gas is assumed. The reasons why both gases yield significantly higher than theoretical shock velocities is still unexplained.

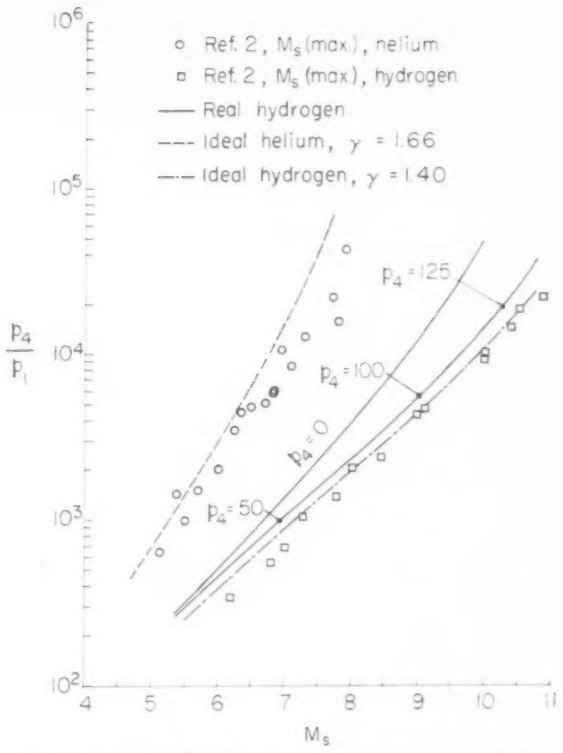

FIG. 1. Real hydrogen as a shock-tube driver. Driver pressure is indicated in atmospheres. Real air as the driven gas; $T_1 = T_4 = 540°$ R.

REFERENCES

[1] Hertzberg, A., *The Shock Tunnel and Its Applications to Hypersonic Flight*, Cornell Aeronautical Lab Report AD-1052-A-5, June, 1957.

[2] Jones, Jim J., *Experimental Investigation of Attenuation of Strong Shock Waves in a Shock Tube With Hydrogen and Helium as Driver Gases*, NACA TN 4072, July, 1957.

[3] Trimpi, Robert L., and Cohen, Nathaniel B., *An Integral Solution to the Flat-Plate Laminar Boundary-Layer Flow Existing Inside and After Expansion Waves and After Shock Waves Moving Into Quiescent Fluid With Particular Application to the Complete Shock-Tube Flow*, NACA TN 3944, June, 1957.

[4] Hirschfelder, J. O., Curtiss, C. F., and Bird, R. B., *Molecular Theory of Gases and Liquids*, pp. 560, 736; John Wiley and Sons, New York, 1954.

[5] Hilsenrath, J., et al., *Tables of Thermal Properties of Gases*, National Bureau of Standards Circular 564, Govt. Printing Office, Washington, D.C., 1955.

Calculation of Supersonic Flow Past an Axially Symmetric Cylinder*

Martha W. Evans and Francis H. Harlow
University of California, Los Alamos Scientific Laboratory, Los Alamos, N.M.
December 9, 1957

WE HAVE USED a numerical calculation method[1] to determine the axially symmetric flow pattern about a flat-nosed cylinder moving parallel to its axis at Mach Number $M_\infty = 1.58$ along the axis of a rigid cylindrical chamber. The approach to steady state was studied in detail for the case in which the cylinder, starting from rest, instantaneously attained its fixed speed. The air was represented by a nonviscous polytropic gas with specific heat ratio $\gamma = 1.4$. The calculations were performed on an IBM Electronic Data Processing Machine, type 704.

An extensive discussion of the general computation technique has been given by the authors in reference 2. The gas is repre-

* This work was performed under the auspices of the United States Atomic Energy Commission.

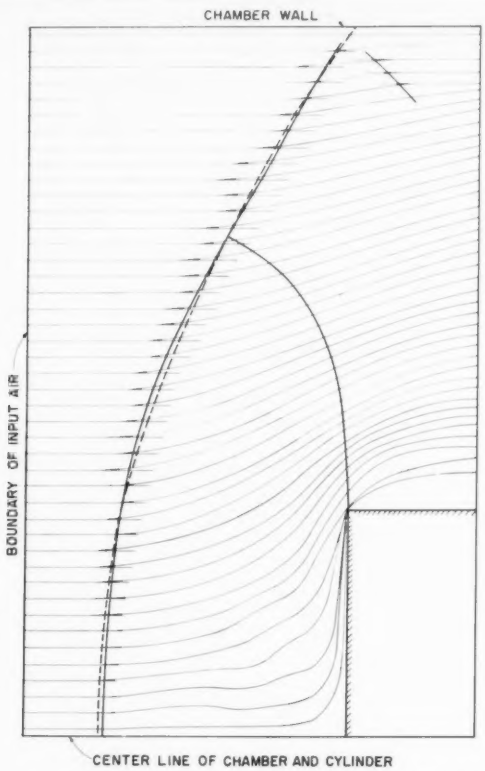

FIG. 1. Air configuration at steady state, showing streamlines, detached-shock position, and sonic line. Dashed line is experimental shock position measured by Marschner.[3] Horizontal projections were added to streamlines to show points of departure for determining shock position. Position of shock reflected from chamber wall is indicated by flow line deflections.

sented by Lagrangian mass points, called "particles," moving through an Eulerian computational mesh. The flow region studied is adjacent to the front of the cylinder, as shown in Fig. 1. For the computation, this region was divided into a mesh of 14×22 toroidal cells of square cross section. The coordinate system was at rest relative to the moving cylinder. The particles representing the air were arranged initially with four per cell. As the air compressed against the cylinder face, the particle-number average rose, reaching about six per cell at steady state. In order to achieve an incoming uniform density, the particles were given masses proportional to their radii. The left boundary was far enough upstream that the flow across it was unperturbed.

The only novel procedure not discussed in previous reports was the technique for stabilizing the finite difference equations in the stagnation region. It is assumed that every velocity vector should point to the right and outward, and whenever any component violated this assumption, it was set to zero, and a corresponding change made in internal energy to preserve total energy.

The configuration at steady state is shown in Fig. 1. The flow lines are drawn from particle positions. The calculated position of the detached shock is determined by observing where each flow line departs from horizontal. Toward the axis, this becomes difficult to observe, and the shock position is determined by the point, along a horizontal line, at which M^2 has dropped to $(1/2)\ (M_\infty{}^2 + M_a{}^2)$, where M_a is the Mach Number just behind the shock at the axis, as calculated from normal-shock relations.

Close to the cylinder face, the flow lines are poorly represented, and their positions are drawn only approximately. The central five flow lines tended to coalesce at the cylinder shoulder and thereafter to follow a single flow line.

The sonic line position was determined as the locus of points at which the interpolated cell-wise Mach Numbers were 1. Its intersection with the shock wave was placed at the point where the latter makes an angle of 61.7° with the cylinder axis (as predicted by conical shock theory).

There is some indication of a reflected shock from the chamber wall. Its position was determined by the flow-line deflections indicated.

The drag coefficient for the front face of the cylinder was also calculated. As the flow approached steady state, the drag coefficient approached, asymptotically (except for small oscillations), the value C_D (nose) = 1.48. This value is about 8 per cent higher than the mean value given by Hoerner.[4]

The same calculations have been performed with several other Mach Numbers. To compare with the work of Oliver,[5] one study was made at $M_\infty = 5.8$. While the nose drag agreed closely with his, the calculated detached-shock position stood outside of his by an average distance which was about 5 per cent of the cylinder diameter. The discrepancy could easily be attributed to the mesh coarseness, since the actual shock should stand less than four cells away from the cylinder face.

The calculations indicate that the time required for the local flow pattern to reach steady state is given roughly by $t = d \div C_\infty \sqrt{M_\infty}$ where d is the cylinder diameter, C_∞ is the free-stream sound speed, and M_∞ is the flow Mach Number.

The experience gained in these calculations shows that a number of improvements could be made.

(1) The calculation mesh could be made finer. This would be at the expense of additional calculation time, but would increase the accuracy and fineness of detail. Approximately two calculation hours were required to reach steady state in the problem reported here, and this increases approximately as the inverse cube of the length of a cell side.

(2) The incoming air density and velocity could be varied as a function of time to represent passage of the cylinder through a variable atmosphere and its slowing due to drag.

(3) The equation of state of the air could be changed to include various real gas effects which occur at high Mach Numbers.

(4) The cylinder could be terminated with a generalized nose shape.

The first of these improvements is of considerable importance, especially with regard to definition of the shock. The criteria used to determine shock position are reasonable and yield good results, but the shock line as drawn really represents the center of a band of rapid variation which is spread over a thickness of several cells. Likewise, lines of constant Mach Number are impossible to locate accurately near the shock, and their points of intersection with the shock must be determined by other means. As discussed by the authors in reference 2, it would seem necessary to require the computational cells to be much smaller than any significant dimensions in the problem. It is, therefore, remarkable that many average functionals calculated in this and various other test problems agree as well as they do with known results.

Calculations are now being prepared to include several of the above features. In particular, the generalization to more complicated shapes is being undertaken, and the calculation mesh is being made finer.

REFERENCES

[1] Harlow, F. H., *Hydrodynamic Problems Involving Large Fluid Distortions*, Journal of the Association for Computing Machinery, Vol. 4, p. 137, April, 1957.

[2] Evans, M. W., and Harlow, F. H., Los Alamos Scientific Laboratory Report Number LA-2139, November, 1957.

[3] Marschner, B. W., A.E. Thesis, California Institute of Technology, 1948.

[4] Hoerner, S. F., *Aerodynamic Drag*, p. 222, 1951.

[5] Oliver, R. E., *An Experimental Investigation of Flow Over Simple Blunt Bodies at a Nominal Mach Number of 5.8*, GALCIT Memorandum No. 26, Guggenheim Aeronautical Laboratory, California Institute of Technology, June, 1955.

Combustion in the Laminar Boundary Layer of Chemically Active Sublimating Surfaces*

M. R. Denison and D. A. Dooley
Aeronutronic Systems, Inc., Glendale, Calif.
December 13, 1957

A DETAILED ANALYSIS has been carried out in reference 1 for the heat and mass transfer from sublimating surfaces where the sublimated material subsequently reacts with the atmosphere. The boundary-layer equations were transformed in the conventional manner and the effects of streamwise pressure gradients neglected in accordance with the argument of Lees, reference 2. If the diffusion coefficients of all species present are equal, if $P_r = Le = 1$, and if $\rho\mu$ = constant, then the heat and mass transfer can be estimated with very little detailed knowledge of the chemical reactions in the boundary layer. Under these conditions the mass fractions Γ_m of atomic species m, irrespective of molecular configuration, and the total enthalpy h_s, including the chemical enthalpy, can be expressed as linear functions of the velocity ratio u/u_e where u_e is the velocity at the outer edge of the boundary layer.

Fast combustion reactions of the type

$$\nu_f' f + \nu_0' O \rightarrow \nu_{P_1}'' P_1 + \nu_{P_2}'' P_2 \qquad (1)$$

are well approximated by a thin reaction surface or flame front where both oxygen, O, and fuel, f, are completely consumed by combustion to form products, P_1 and P_2. On one side, cf. Fig. 1, oxygen is mixed with products and inerts, while on the other side, fuel is mixed with products and inerts. The combustion surface may be located either within the boundary layer or at the solid surface. Dissociation and recombination reactions for oxygen and nitrogen are also included.

The heat flux, q_a, conducted into or radiated from the body at the surface is found to be given by

$$q_a = (\rho_e \mu_e C_{fe}/2)(h_{se} + \Gamma_{oe} Q_{pow} - B\lambda_{fw} - h_{ew}) \qquad (2)$$

where Γ_{oe} is the mass fraction of oxygen at the edge of the boundary layer, Q_{pow} is the heat of combustion at wall conditions per unit mass of oxygen, λ_{fw} is the heat of sublimation, and h_{ew} is the enthalpy per unit mass of air evaluated at the wall condition of temperature and degree of dissociation. It should be noted that although the form of Eq. (2) is invariant with the physical model assumed, the numerical values of the last three terms are somewhat model dependent. The quantity B represents a ratio of mass transfer to skin friction or heat transfer:

* The authors wish to express their appreciation to Dr. F. E. Marble, Professor, California Institute of Technology, and Consultant, Aeronutronic Systems, Inc., who has followed the development of the analysis closely and contributed many valuable suggestions.

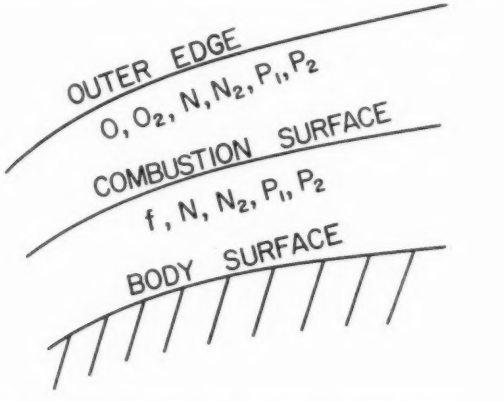

FIG. 1. Model of combustion process in boundary layer.

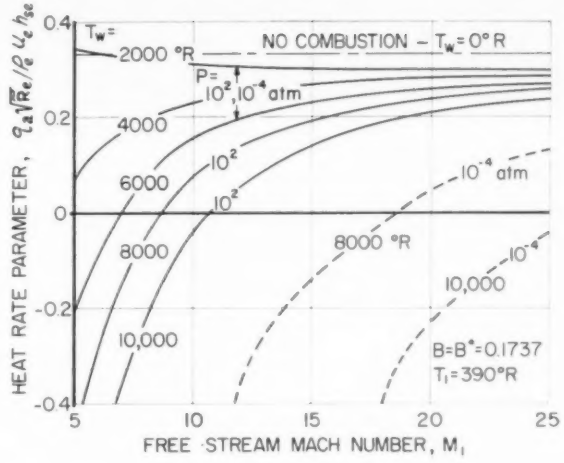

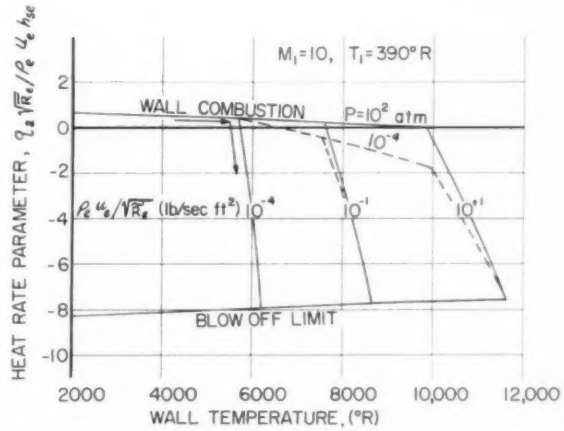

FIG. 2 (*top*). Effect of wall temperature, pressure, and Mach Number on heat transfer for surface combustion.
FIG. 3 (*bottom*). Effect of wall temperature, pressure, and flow parameter on heat transfer at free-stream Mach Number $M_1 = 10$ (for burning rate assumptions of reference 1).

$$B = (2\dot{m}_w/\rho_e u_e C_{fe}) \qquad (3)$$

where $\dot{m}_w$ is the mass rate at which the surface material enters the boundary layer. When combustion takes place at the body surface, $B = B^* = \Gamma_{oe}\nu_f' M_f/\nu_0' M_0$.

For a given value of the wall temperature the combustion reaction will remain at the surface so long as the oxygen is able to diffuse to the wall at a rate in excess of that required to oxidize all of the surface material sublimed. If the wall temperature becomes sufficiently high, however, the surface material will sublime at such a large rate that the combustion zone will leave the surface and both oxygen and fuel will diffuse toward that zone. If $\dot{m}_{w_s}$ is the sublimation rate at a given surface temperature, then the reaction remains at the wall if $\dot{m}_{w_s} < \dot{m}_w$, while the combustion zone is somewhere in the boundary layer away from the wall if $\dot{m}_{w_s} = \dot{m}_w$.

The skin friction can be related to B through the boundary-layer solutions of Emmons and Leigh.[3] Their results can be fitted empirically by the expression

$$C_{fe}\sqrt{\tilde{R}_e} = 0.664 - 1.388\left[(\dot{m}_w/\rho_e u_e)\sqrt{\tilde{R}_e}\right] + 0.824\left[(\dot{m}_w/\rho_e u_e)\sqrt{\tilde{R}_e}\right]^3 \qquad (4)$$

where the effective Reynolds Number for blunt bodies is given by

$$\tilde{R}_e = \left(\int_0^s \rho_e \mu_e u_e r_0^{2k} ds/\mu_e^2 r_c^{2k}\right)$$

The quantity k is unity for bodies of revolution and zero for two-dimensional cylindrical bodies.

As an example, the analysis has been applied to the sublimation and combustion of graphite surfaces inasmuch as the physical and chemical data required for numerical calculation are readily available for graphite. These data are summarized in reference 1. In the case of a high temperature environment such as that generated by hypersonic flight, the graphite oxidizes principally to carbon monoxide:

$$C + O \rightarrow CO$$

The manner in which the free-stream Mach Number, wall temperature, and static pressure affect the heat-transfer rate is indicated in Fig. 2 for the case of wall combustion. It is to be noted that over most of the temperature range considered, the heat-transfer parameter is actually less than it would be for an ordinary boundary layer at zero wall temperature. Evidently, the negative potential due to the combination of wall enthalpy, h_{ew}, and heat of vaporization, $B\lambda_{fw}$, more than offsets the increase in positive potential due to combustion, $\Gamma_{oe}Q_{pow}$. The value of B^* in the case of graphite is so small, $B^* = 0.17$, that the decrease in skin friction and in heat transfer due to the effect of mass transfer on the velocity profile is rather negligible for surface combustion. Incidentally, q_a would rarely be negative.

Plots similar to Fig. 2 could be constructed for larger values of B, corresponding to gas phase combustion. As B increases, the whole level of heat-transfer rates shifts downward until finally the entire plot is in the negative region. A graph showing the complete range of operation at a free-stream Mach Number of 10 is presented in Fig. 3.

References

[1] Denison, M. R., and Dooley, D. A., *Combustion in the Laminar Boundary Layer of Chemically Active Sublimators*, Technical Report U-110, Aeronutronic Systems, Inc., Glendale, Calif., September 23, 1957.

[2] Lees, L., *Laminar Heat Transfer over Blunt-Nosed Bodies at Hypersonic Flight Speed*, Jet Prop., Vol. 26, No. 4, pp. 259–269, April, 1956.

[3] Emmons, H. W., and Leigh, D., *Tabulation of the Blasius Function with Blowing and Suction*, Div. of Appl. Sci., Combustion Aero. Lab., Interim Technical Report No. 9, Harvard Univ., November, 1953.

Effect of Loads on the Spring Constant of a Particular Type of Flexure

Frederick G. Blottner

Staff Member, Sandia Corporation, Albuquerque, N.M.

December 16, 1957

Introduction

Flexural pivots are frequently used in wind-tunnel instrumentation. One special use is to support models in wind tunnels when static and dynamic stability coefficients are being determined. In order to determine the static stability coefficient, it is necessary to know the spring constant of the flexure when the wind tunnel is at the desired air speed. Sometimes it is assumed that the flexure spring constant is independent of the air speed or normal and axial forces; therefore, the spring constant at zero air speed (normal and axial forces equal zero) is used. However, the spring constant can change appreciably with normal and axial forces and serious errors in the static stability coefficient can occur.

The effect of loads on the spring constant of one type of flexure has been considered by Wittrick,[1] but another type as shown in Fig. 1 was not considered. This type of flexure has been used by several organizations doing dynamic testing. Therefore, for this type of flexure, the analysis of Wittrick is extended, and corroborating experimental data are presented in this paper.

Analysis

Wittrick has written the relation between torque and rotation as

$$T = EI/L\,(K\theta + b\theta^2 + \dots) \qquad (1)$$

where

T = applied torque about the point at which the undeflected strips cross, in.-lbs.
θ = angle of rotation of the moving end of the pivot, rad.
E = Young's modulus of the material, lb./in.^{2}
I = moment of inertia of the cross section of the strips, in.^{4}
L = length of each flexure strip, in.
K, b = dimensionless coefficients

In reference 2, it was shown that for the typical flexure of the type considered in this paper, the coefficient b is very small and can be neglected (see Fig. 2 which is from reference 2). Then the spring constant in in.lb./rad. is

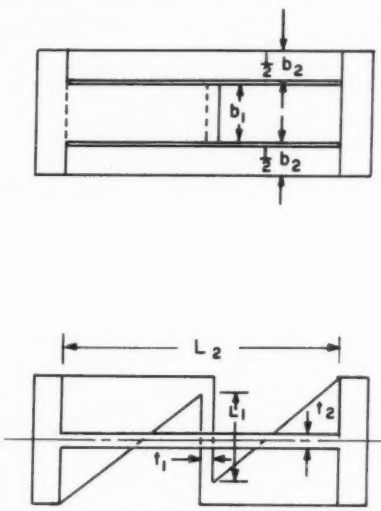

Fig. 1. Typical crossed flexure pivot.

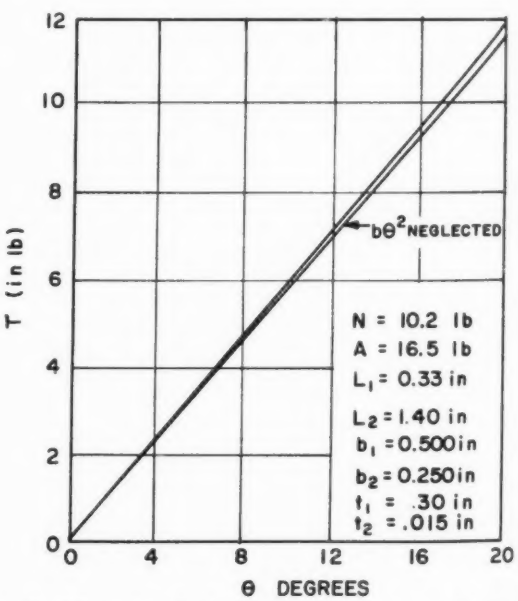

Fig. 2. Effect of neglecting second-order term on relation between torque and rotation.

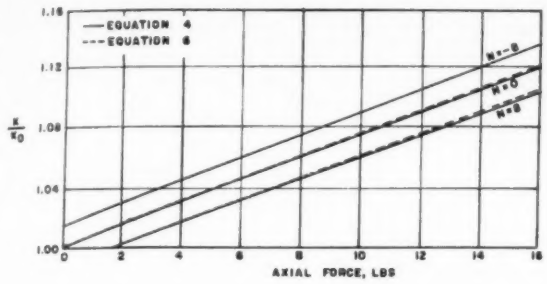

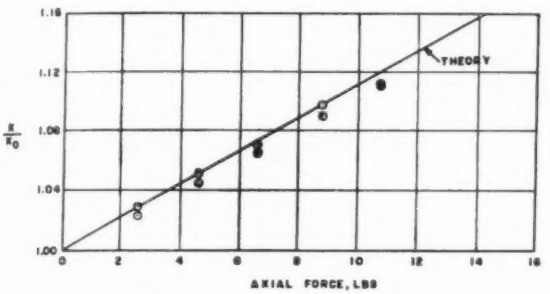

FIG. 3 (*top*). Effect of neglecting higher order terms on Eq. 4.
FIG. 4 (*bottom*). Effect of axial force on spring constant.

$$k = EIK/L \tag{2}$$

The value of K as given by Wittrick is

$$K = \beta_1 (\coth \beta_1 - \beta_1) + \beta_2 (\coth \beta_2 - \beta_2) \tag{3}$$

where for this flexure

$$\beta_1^2 = NL_1^2/4E_1I_1, \quad \beta_2^2 = -(AL_2^2/4E_2I_2)$$

and A is axial force, N is normal force, and subscripts 1 and 2 refer to vertical and horizontal strips respectively. Using $\beta_2 = i\gamma_2$ and substituting Eq. 3 in Eq. 2, the following is obtained for the spring constant:

$$k = (E_1I_1\beta_1/L_1)(\coth \beta_1 - \beta_1) + (E_2I_2\gamma_2/L_2)(\cot \gamma_2 + \gamma_2) \tag{4}$$

Two points should be noticed about this equation. Since the normal force N can be either positive or negative, the first part of Eq. 4 can change from hyperbolic to trigonometric. The second point of interest is the value of the spring constant when N and A are zero. This is

$$k_0 = (E_1I_1/L_1) + (E_2I_2/L_2) \tag{5}$$

A more useful relation than Eq. 4 can be derived if the cot and coth are expanded in a series and terms of order β_1^4, γ_2^4, and greater are neglected. The result of the above procedure is

$$k = k_0 + (1/6)(AL_2 - NL_1) \tag{6}$$

In order to see the effect of neglecting higher-order terms, see Fig. 3 where both Eqs. 4 and 6 are plotted for the typical flexure (see Fig. 2 for dimensions of flexure).

Comparison of Theory With Experiment

The change in spring constant was determined experimentally for a flexure of the following dimensions:

$b_1 = 0.250$ in.	$b_2 = 0.500$ in.
$L_1 = 0.233$ in.	$L_2 = 1.234$ in.
$t_1 = 0.015$ in.	$t_2 = 0.025$ in.
$E_1 = 30 \times 10^6$ psi	$E_2 = 17 \times 10^4$ psi

In the experiment, several bodies of different weights, but of the same moment of inertia, were placed on the flexure to simulate axial loads. Then the periods of oscillation of the different bodies were determined, and, from this, the change in spring constant was calculated. A plot of the theoretical curve (Eq. 6) and experimental points is shown in Fig. 4. From this figure, one can see that there are large changes in the spring constant as predicted by the theory.

References

[1] Wittrick, W. H., *The Properties of Crossed Flexure Pivots and the Influence of the Point at Which the Strips Cross*, Aero. Quart., Vol. II, February, 1951.

[2] Blottner, F. G., *Effect of Drag and Lift on the Relation Between Torque and Rotation of a Crossed-Flexure Pivot*, Sandia Corp. Research Report, SC-4036, December, 1956.

Hypersonic Heat Transfer to Catalytic Surfaces*

Sinclaire M. Scala
Research Engineer, Missile and Ordnance Systems Dept., General Electric Co., Philadelphia, Pa.
December 17, 1957

Introduction

THE DETERMINATION of hypersonic heat transfer to fully catalytic and noncatalytic surfaces has been considered previously by Lees[1] and by Fay and Riddell.[2] This note will clarify these limiting cases and will also present some results of a recently declassified study.[3] In Fig. 1 are indicated the various physicochemical phenomena which occur in a dissociated gas in the mean free path (shown to exaggerated scale) near a surface. Since atom recombination is only one of several simultaneous processes, the catalytic efficiency, defined by

$$\gamma_A = \frac{\text{atomic collisions effective in recombination}}{\text{total number of atomic collisions}} \tag{1}$$

is a gross quantity which includes the effects of the intermediate steps. Thus, a treatment is required which reconciles a continuum and a molecular approach.

Symbols

c_A = mass fraction of atoms
c_p = specific heat
f = similarity stream function
h = enthalpy, including chemical
Le = Lewis Number
Le^T = thermal Lewis Number
l = normalized product of density and viscosity

* Presented at The Ramo-Wooldridge Second Symposium on Ballistic Missiles, Los Angeles, Calif., June, 1957.

The author would like to acknowledge the assistance of Leon Gilbert in numerical computations and in drawing the Figures.

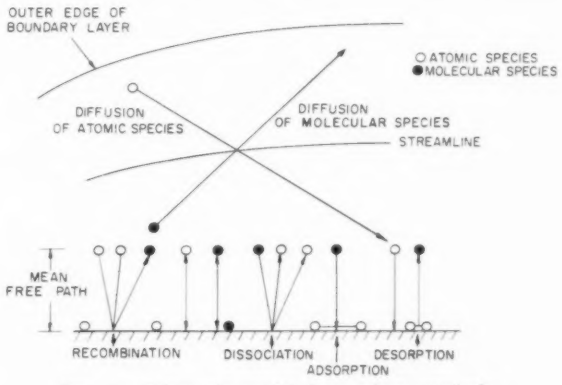

FIG. 1. Schematic model for surface catalysis.

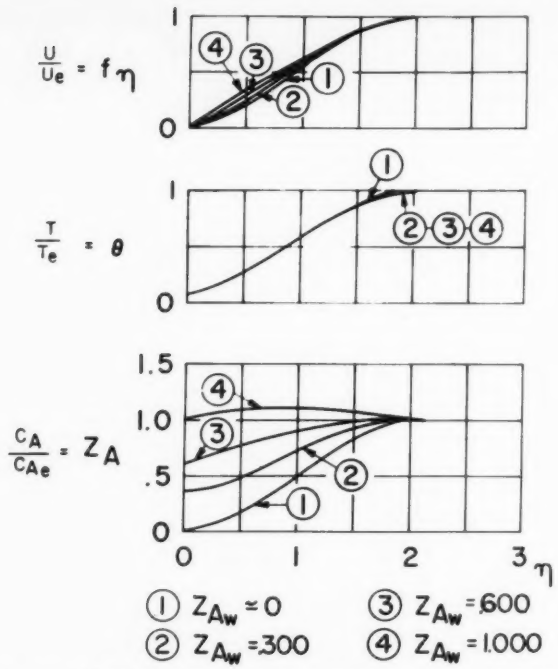

FIG. 2. Nondimensional velocity, temperature, and concentration profiles (altitude = 120,000 ft., Mach Number = 20).

M_i = molecular weight of the ith species
N = Avogadro's Number
p = static pressure
Pr = Prandtl Number
Q = energy flux
R = universal gas constant
T = temperature
u = x component of velocity, parallel to surface
$\dot{w}_A$ = net mass rate of production of atomic species per unit volume by chemical reaction
$\dot{W}_A$ = net mass collision flux of atoms per unit area
Z_A = (c_A/c_{Ae}) referred atom mass fraction
γ_A = catalytic efficiency
η = similarity variable
θ = T/T_e dimensionless temperature
ρ = density
μ = viscosity

Subscripts

A = atom
e = edge of boundary layer
$eq.$ = equilibrium
M = molecule
w = wall
η = differentiation with respect to η

ANALYSIS

When dissociated air is treated as a binary mixture of atoms and molecules, the stagnation point boundary-layer equations become,[3] for steady laminar flow,

$$\{(1/Pr)\,[Le\,c_{Ae}Z_{A\eta} + Le^T(\theta_\eta/\theta)]\}_\eta + f\,c_{Ae}Z_A + [\dot{w}_A/2\rho(du_e/dx)] = 0 \quad (2)$$

$$(lf_{\eta\eta})_\eta + ff_{\eta\eta} + (1/2)\,[(\rho_e/\rho) - f_\eta^2] = 0 \quad (3)$$

$$[(\bar{c}_p l/Pr)\theta_\eta]_\eta + \bar{c}_p f\theta_\eta + (l/Pr)\theta_\eta(c_{pA} - c_{pM})\,[Le\,c_{Ae}Z_{A\eta} + Le^T(\theta_\eta/\theta)] - [\dot{w}_A(h_A - h_M)/2\rho T_e(du_e/dx)] = 0 \quad (4)$$

which are, respectively, the conservation of atoms, momentum, and energy. These equations were programed for digital computation on an IBM 704 computer by Paul Gordon, and a considerable number of exact solutions have been obtained utilizing variable Prandtl and Lewis Numbers and including the effects of thermal diffusion. We will restrict our discussion here to atom recombination on catalytic surfaces when gas phase reactions are frozen.

It has been previously assumed[1, 2] that a fully catalytic wall corresponds to a zero atom concentration at the wall—i.e., $c_{A_w} = 0$. This surface boundary condition yields the maximum atom diffusion flux to the surface and simultaneously the largest counterdiffusion flux of molecules. However, this is not entirely satisfactory because a microscopic condition is being violated. Surface recombination of atoms which occurs ultimately by means of collision processes cannot occur if no atoms are present. A more realistic interpretation requires that the surface atom concentration be small (to ensure maximum diffusion flux) but finite (to satisfy microscopic conditions). Indeed, it is found on equating the diffusion flux, obtained from the simultaneous solution of Eqs. (2), (3), and (4) above,

$$\dot{W}_{A_w} = \sqrt{2\rho_w\mu_w(du_e/dx)}\,[(Le/Pr)\,c_{Ae}Z_{A\eta} + (Le^T/Pr)\,(\theta_\eta/\theta)]_w \quad (5)$$

to the collision flux obtained from kinetic theory

$$\dot{W}_{A_w} = (\gamma_A\,M_A/\sqrt{2\pi M_A R T_w})\,[p_A - (p_{A_{eq.}}/p_{M_{eq.}})\,p_M]_w \quad (6)$$

and taking $\gamma_A = 1.0$ as the definition of a fully catalytic wall, compatibility between the boundary-layer solution and kinetic theory can usually be achieved when c_{A_w} is on the order of 10^{-4}. Thus for computation purposes, one may still take $c_{A_w} = 0$ as being synonymous with a fully catalytic wall, if one holds out the mental reservation that the precise surface concentration of atoms can only be obtained a posteriori by satisfying Eqs. (5) and (6).

With regard to noncatalytic walls, it has been assumed[2] that the atom concentration is a constant across the boundary layer—i.e., $c_{A_w} = c_{Ae}$ is synonymous with $Z_{A\eta_w} = 0$. Actually, if one includes the effects of thermal diffusion, the net diffusion flux of atoms vanishes ($\gamma_A = 0$) for a surface that can maintain a wall concentration equal to $0.8\,c_{Ae}$. The physical explanation for this is that the thermal diffusion coefficient is negative and atoms tend to diffuse thermally from a cold region to a hot region. This means that for a cool wall, thermal diffusion opposes concentration diffusion and for a sufficiently large value of $c_{A_w} < c_{Ae}$ (i.e, $c_{A_w} \cong 0.8\,c_{Ae}$) the two fluxes balance each other completely. For larger values of c_{A_w}, the net atom flux is away from the surface, which implies a net surface dissociation of molecules. In any case, when $c_{A_w} = c_{Ae}$, the atom concentration is not constant. See curve 4 of Fig. 2.

Having disposed of the two limiting cases, it is clear that surfaces having finite catalytic efficiency must maintain a surface atom concentration which lies between the limits $0 \leq c_{A_w} \leq 0.8\,c_{Ae}$.

A typical calculation for the full range of catalytic efficiency is shown is Fig. 3. The variation of surface energy transfer and the net collision flux of atoms corresponds to the boundary-layer solutions of Fig. 2.

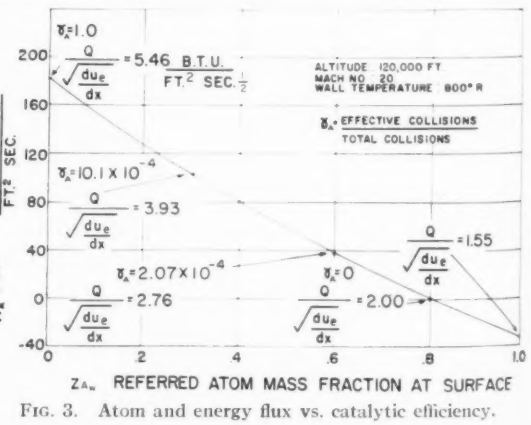

FIG. 3. Atom and energy flux vs. catalytic efficiency.

Conclusions

With the exception of pyrex, ($\gamma_A \simeq 1.2 \times 10^{-4}$), most common materials have a catalytic efficiency for oxygen atom recombination[4] that exceeds 50×10^{-4}, which means that they are virtually perfect catalysts at least at low wall temperature (see Fig. 3). Further experimental effort seems warranted if one wishes to minimize the heat release due to catalytic recombination of atomic species.

References

[1] Lees, Lester, *Laminar Heat Transfer Over Blunt Bodies at Hypersonic Flight Speeds*, Jet Propulsion, Vol. 26, No. 4, pp. 259–269, April, 1956.

[2] Fay, James, and Riddell, Frederick R., *Theory of Stagnation Point Heat Transfer in Dissociated Air*, Avco Research Laboratory, Research Note 18, June, 1956. Also published in the Journal of the Aeronautical Sciences, Vol. 25, No. 2, pp. 73–85, February, 1958.

[3] Scala, Sinclaire M., *Hypersonic Heat Transfer to Surfaces Having Finite Catalytic Efficiency*, General Electric Co., Aerophysics Laboratory Research Memorandum 4, June, 1957.

[4] Linnett, J. W., private communication.

A Comment on the Methods of Calculating Natural Modes and Frequencies of Vibration

Samuel Silverberg
Mechanical Engineer, Flutter and Vibration Group, Douglas Aircraft Company, Inc., El Segundo, Calif.

December 24, 1957

The procedure outlined by N. O. Myklestad,[1] and that suggested by W. T. Thomson,[2] for the determination of natural modes of vibration, contain expressions for certain elastic coefficients, which might be modified to generalize and simplify the calculations. It is noted that in the evaluation of these coefficients, $\bar{v}_M$, $\bar{d}_M$, $\bar{v}_F$, and $\bar{d}_F$, the solutions become indeterminate for the case of beams of uniform sections. Each of the expressions for these quantities contain a term of the form

$$(1/b^p)\cdot[f(a, b)]$$

such that

$$\lim_{b \to 0} (1/b^p)\cdot[f(a, b)] = 0/0 \quad \text{(indeterminate)}$$

In the above expression, a represents the bending stiffness (EI) of station n and b represents the difference between the stiffness at station n and that at station $(n + 1)$.

In the derivation of these expressions the graph of bending stiffness (EI) of the beam plotted against the beam span was approximated by a series of straight lines. The purpose of this note is to suggest that this approximation be replaced by one in which the bending flexibility ($1/EI$) graph, again plotted versus the beam span, is approximated by the series of straight lines.

It is seen from Fig. 1 that, for the section of the beam between stations n and $(n + 1)$,

$$1/EI = [A - (A - C)(\xi/L)]$$

$$\bar{v}_M = \int_0^L [A - (\xi/L)(A - C)]d\xi = (L/2)(A + C)$$

$$\bar{d}_M = \bar{v}_F = \int_0^L [A\xi - (\xi^2/L)(A - C)]d\xi = (L^2/3)[(A/2) + C]$$

$$\bar{d}_F = \int_0^L [A\xi^2 - (\xi^3/L)(A - C)]d\xi = (L^3/4)[(A/3) + C]$$

where A represents the flexibility ($1/EI$) at station n, C represents the flexibility ($1/EI$) at station $(n + 1)$, and the quantities $\bar{v}_M$, $\bar{v}_F$, $\bar{d}_M$, and $\bar{d}_F$ represent the elastic coefficients of the Myklestad method. A similar procedure can be used to determine the coefficients of Thomson's method.

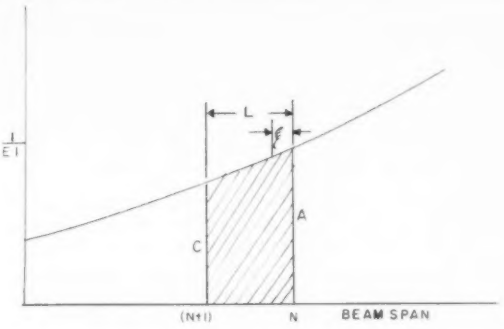

Fig. 1.

It might be noted that there exists an error in the relationship between the two sets of coefficients as given by Thomson. The relationships should read

$$\alpha_{Mi} = \bar{\alpha}_{Mi}, \qquad \alpha_{Si} = \bar{\alpha}_{Si} = \bar{d}_{Mi},$$
$$d_{Mi} = l_i\,\bar{\alpha}_{Mi} - \bar{d}_{Mi}, \quad d_{Si} = l_i d_{Mi} - \bar{d}_{Si}$$

It is seen that these new expressions for the elastic coefficients are continuous for all finite values of A and C. Further, when A equals C (uniform section of beam) the expressions yield the exact solutions for uniform beams. In addition to this, the above expressions greatly simplify the calculations by eliminating the logarithmic terms and certain products of terms which appear in the Myklestad expressions.

This approximation is in every respect as valid as that presented by Myklestad, since the error introduced by one approximation is within a small percentage of the error due to the other. The method which will produce the better accuracy is dependent on the shape of the original curve. Further, the continuity and simplicity of the new expressions should aid greatly in the programing of the general problem of beam vibrations for automatic computers.

References

[1] Myklestad, N. O., *A New Method of Calculating Natural Modes of Uncoupled Bending Vibrations of Airplane Wings and Other Types of Beams*, Journal of Aeronautical Sciences, Vol. 11, No. 2, pp. 153–162, April, 1944.

[2] Thomson, W. T., *A Note on Tabular Methods for Flexural Vibrations*, Journal of Aeronautical Sciences, Vol. 20, No. 1, pp. 62–64, January, 1953.

The Effect of External Sound on the Vortex Shedding From Cylinders

Donald I. Garber*
Lewis Flight Propulsion Laboratory, NACA, Cleveland, Ohio

December 30, 1958

The investigation reported herein was a part of the development of an instrument utilizing the vortex-shedding technique[1] for stream-velocity measurement. The possibility of resonant modes of acoustic oscillation excited by the vortex shedding suggested a study of the effect of sound waves on the vortex-shedding frequency.

The apparatus is shown in Fig. 1. Sound was introduced laterally into the vicinity of the vortices. To eliminate any standing wave reinforcement, the apparatus had only two possible resonant dimensions: 3/8 in. and 50 ft. Since the wavelength of the imposed sound was 2.5 in. to 2 ft., no reinforced resonance existed in the range studied.

* Undergraduate Student, Carnegie Institute of Technology.

It is notable that the test apparatus gives Strouhal Numbers which are higher than those obtained by Roshko,[1] as shown in Fig. 2. Roshko, however, used a large duct, so that the cylinder aspect ratio was very high. The low aspect ratio data show Strouhal Number decreasing with Reynolds Number,[2] while the high aspect ratio data have Strouhal Number increasing with Reynolds Number. This suggests the possibility that an intermediate aspect ratio exists where the Strouhal Number might be constant.

Fig. 3 illustrates the variation of vortex-shedding frequency with the introduction of sound frequencies for a constant Reynolds Number. At the bottom of Fig. 3, the approximate intensity of sound at the point of entry into the duct is given as a function of frequency. Reflection from the opposite wall could possibly add 6 db to the values shown. When the frequency of the introduced sound is sufficiently lower than the vortex-shedding frequency without sound input point (A), there is no effect on the shedding frequency. However, as the frequency of the introduced sound is raised, the vortex frequency soon becomes "unstabilized" and begins to oscillate (B). Gradually as the input frequency is increased, the vortex-shedding frequency is decreased until it is "locked-in" and the two frequencies are identical and constant (C). Over a limited range the vortex-shedding frequency follows the frequency of the introduced signal until a frequency is reached that is higher than the original vortex frequency (D). Raising of the input frequency results in an extreme "unstabilized" region where the vortex frequency oscillates over a considerable range (E). At still higher input frequencies,

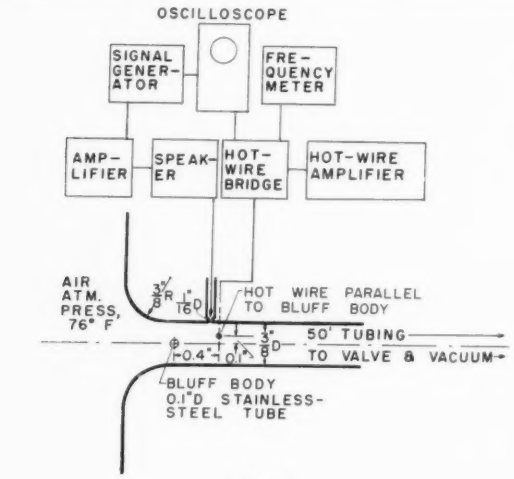

FIG. 1.

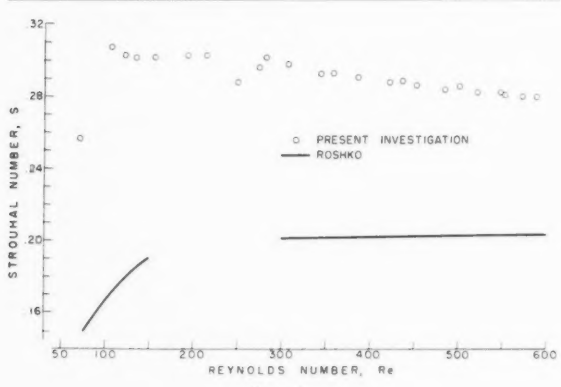

FIG. 2.

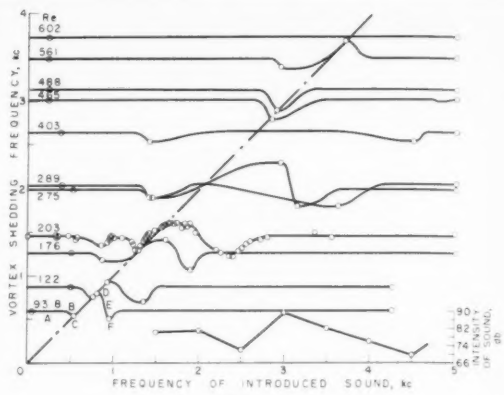

FIG. 3.

the vortex-shedding frequency can be decreased to a value that is lower than the vortex-shedding frequency with no sound introduction (F).

As the Reynolds Number is increased, the vortex signal becomes less regular, and the vortex-shedding frequency is less subject to interference. Whether this is due to the irregularity of the vortex signal at the higher Reynolds Numbers or to the increase in the kinetic energy of the system is not known.

The results of the investigation indicate that ducting resonance or external sound sources may affect the frequency of vortex shedding from cylinders.

REFERENCES

[1] Roshko, Anatol, *On the Development of Turbulent Wakes from Vortex Streets*, NACA TN 2913, 1953.

[2] Goldstein, S., (Ed.), *Modern Developments in Fluid Dynamics*, Oxford, The Clarendon Press, 1938.

Remarks on Systematizing the Calculations of the Natural Modes of a Free Structure

R. Kappus and D. Clerc
Office National d'Etudes et de Recherches Aéronautiques, Chatillon-sous-Bagneux (Seine), France

December 31, 1957

DISCUSSION

IT IS WELL KNOWN that the calculation of the natural modes of a structure with a finite but rather high number of vibrating masses usually requires iterative methods. In addition, when the vibrating body is free in space, *free-body equilibrium* must be taken into account.

This free-body equilibrium can be dealt with once and for all in an absolutely sure and systematic fashion with the aid of a geometric matrix T, as the authors pointed out in detail in 1955.[1] This general scheme, which leads in a very simple manner to the classical matrix relation for a characteristic-value problem, requires only the a priori establishment of certain matrices of geometric, mass, and elastic information. Thus the engineer need not enter explicitly into the numerical details of the free-body equilibrium relations. The method also avoids reintroducing these relations at each iteration step as is sometimes done (see, for example, references 2 and 3).

In reference 1 we treated a more general case (the vibrating structure being additionally tied to a jig by means of certain springs), and details for handling the flexibility matrices relative to the various structural parts were given (see chapter III). In this reference two different calculation routes were outlined.

Of the two, that which consists in undertaking the mode and characteristic-value calculation in terms of the *relative* displacements (columns $r^{(i)}$) proved to be much superior to that using directly the *absolute* mode displacements (columns $p^{(i)}$), which are the ones ultimately sought.† We have therefore considered it worthwhile here to extract from reference 1, for the most commonly encountered case of a completely free structure, the essential relations entering into the calculation of the relative modes $r^{(i)}$ through presentation of an outline of the calculation scheme together with a simplified example. In addition, we supply certain new details.

It might further be remarked that a somewhat similar procedure based on tensor notation has been developed by C. E. Mack.[4]

Outline of the Calculation Scheme

(1) Define the column p^* consisting of the m^* (≤ 6) absolute (linear and angular) displacements (with respect to its own rest position) of a conveniently chosen *reference system* adhering to the structure; define the column p consisting of the m *absolute* displacements of the vibrating masses of the rest of the structure. In the simplified example of Fig. 1 we choose the reference system as the trihedron defined by the xyz-axis system with origin at the arbitrary point 0, and we endow it with certain mass properties (see below). Assuming, as usual, that the only important displacements are those perpendicular to the xy-plane, we shall take into account (a) as p^*-displacements, translation w_0 parallel to the z-axis and the two rotations θ_{x0} and θ_{y0}; and (b) as p-displacements, linear displacements w parallel to the z-axis of all the other points (i.e., points 1 to 6) and, in addition, the rotations θ_z of the "points" 7 and 8 (which do not necessarily coincide with the points 3 and 4 endowed with point masses M_3 and M_4). Thus, in the example chosen here, if it be temporarily assumed, in order to cover the most general case, that the structure has no symmetry,

$$p^* = \begin{bmatrix} p_1{}^* \\ p_2{}^* \\ p_3{}^* \end{bmatrix} = \begin{bmatrix} w_0 \\ \theta_{x0} \\ \theta_{y0} \end{bmatrix} \quad \text{and} \quad p = \begin{bmatrix} p_1 \\ p_2 \\ \cdot \\ \cdot \\ \cdot \\ p_6 \\ p_7 \\ p_8 \end{bmatrix} = \begin{bmatrix} w_1 \\ w_2 \\ \cdot \\ \cdot \\ \cdot \\ w_6 \\ \theta_{z7} \\ \theta_{z8} \end{bmatrix}$$

Naturally, in the case of a real airplane the number m of elements in the column p will be much greater than 8.

(2) Set up the *geometric matrix* T (consisting of m rows and m^* columns) so that the column $T\,p^*$ represents the *rigid-body displacements* relative to the rest position of the reference system. Thus, in the example chosen (where $m = 8$, $m^* = 3$),

$$T = \begin{bmatrix} (w_0) & (\theta_{x0}) & (\theta_{y0}) \\ 1 & y_1 & -x_1 \\ 1 & y_2 & -x_2 \\ 1 & y_3 & -x_3 \\ 1 & y_4 & -x_4 \\ 1 & y_5 & -x_5 \\ 1 & y_6 & -x_6 \\ 0 & 1 & 0 \\ 0 & 1 & 0 \end{bmatrix} \quad (\text{where } y_3 = y_4 = 0)$$

(3) Set up the symmetric square matrices M^*, M, and D, defined for all cases by the relations

$$f^* = \omega^2 \cdot M^* p^* \tag{1}$$

$$f = \omega^2 \cdot M p \tag{2}$$

$$r = Df \tag{3}$$

where f^* and f (referring respectively to the reference system and the rest of the structure) are the columns of inertia forces, and r is the column of the mass displacements *relative to the reference system* chosen. The *flexibility matrix* D (matrix of influence coefficients) is obtained by means of an elastic analysis which may often be rather complicated. It should be noted that D (like r) is specified always with respect to the reference system (chosen more or less arbitrarily), which is therefore assumed to furnish the "support" reactions. In what follows D is supposed known, its calculation not being an object of the present note (see, however, reference 1, chapter III). The matrix D always has order m, and is symmetric and regular. The same holds for the *inertia matrix* M (which is even very often diagonal). As for the *reference system inertia matrix* M^* it has only order m^* (≤ 6) and can even be singular as is the case in our example where we assume that the reference system possesses no pitching moment of inertia: $\Theta_{y0} = 0$. Thus, in this example,

$$M^* = \begin{bmatrix} (w_0) & (\theta_{x0}) & (\theta_{y0}) \\ M_0 & & \\ & \Theta_{x0} & \\ & & 0 \end{bmatrix}, \quad M = \begin{bmatrix} (w_1)\ (w_2)\ \ldots\ (w_6)\ (\theta_{z7})\ (\theta_{z8}) \\ M_1 & & & & & & \\ & M_2 & & & & & \\ & & \ddots & & & & \\ & & & M_6 & & & \\ & & & & \Theta_{z7} & & \\ & & & & & \Theta_{z8} & \end{bmatrix}$$

Note further that point 0 of the reference system may be any point whatever.

(4) Carry out in successive steps the following matrix operations:‡

$$MT, \quad \bar{T}(MT), \quad M^* + (\bar{T}MT), \quad (M^* + \bar{T}MT)^{-1}$$

$$H = (M^* + \bar{T}MT)^{-1}(\bar{T}M) \tag{4}$$

$$S = (MT)H \tag{5}$$

$$\tilde{M} = M - S \tag{6}$$

The matrix S is evidently symmetric and, moreover, always singular. The *modified inertia matrix* $\tilde{M}$ is therefore also symmetric; it is generally regular.

(5) Solve, for the lowest modes desired, the classical characteristic-value problem**

$$D\tilde{M}r^{(i)} = (1/\omega_i{}^2) \cdot r^{(i)}, \quad i = 1, 2, 3, \ldots \tag{7}$$

$r^{(i)}$ being the column representing the ith *relative natural mode*.

(6) For each of the modes thus obtained, calculate the column

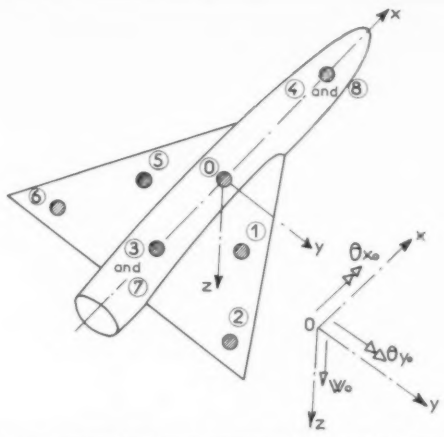

FIG. 1. Perspective figure representing a stylized version of an airplane having 7 mass points (M_0, M_1, . . . , M_6) and 3 moments of inertia in roll (Θ_{x0}, Θ_{z7}, Θ_{z8}).

† In reference 1 p is called q; some other notations have also been changed in the present note.

‡ A bar over a letter indicates transposition of the corresponding matrix; we recall that $AB = BA$.

** For iterations concerning modes higher than the first, see for example reference 5. The procedure of this reference, called the method of "augmented matrices" (matrices allongées), has recently been programed by Clerc for the IBM 704 calculator.

$$p^{*(i)} = -Hr^{(i)} \tag{8}$$

and finally the column

$$p^{(i)} = Tp^{*(i)} + r^{(i)} \tag{9}$$

$p^{*(i)}$ and $p^{(i)}$ constituting the ith *absolute natural mode*.

In the example considered in Fig. 1 the matrices D and $\tilde{M}$ are of order $m = 8$. There exist, however, only $8 - 1 = 7$ modes and characteristic frequencies; for it is clear that M^* is here simply degenerate, and it can be shown that this is also true for $\tilde{M}$ and hence for $D\tilde{M}$ (see Addendum I of reference 6).

Of course, in practical cases the structural symmetry is always taken into account; as a consequence, the symmetric and antisymmetric vibrations are uncoupled. In this case the following columns and matrices will be separately defined (see reference 6):

$$p_S{}^*,\ p_S,\ T_S,\ M_S{}^*,\ M_S,\ D_S$$

and

$$p_A{}^*,\ p_A,\ T_A,\ M_A{}^*,\ M_A,\ D_A$$

It should also be mentioned that it is always possible to choose apother reference system constituted, for example, by three points located in a plane (see reference 6).

Note finally that the generalized masses can be calculated in two different ways (see Addendum II of reference 6):

$$\mu_i = \overline{p^{(i)}}Mp^{(i)} + \overline{p^{*(i)}}M^*p^{*(i)} = \overline{r^{(i)}}\tilde{M}r^{(i)}, \quad i = 1, 2, 3, \ldots$$

References

[1] Clerc, D., and Kappus, R., *Systématisation du Calcul des Vibrations Propres d'une Structure Quelconque Libre ou Partiellement Maintenue par un Bâti Fixe à Partir de Coefficients d'Influence*, La Recherche Aéronautique, No. 46, 1955.

[2] Levy, S., *Computation of Influence Coefficients for Aircraft Structures with Discontinuities and Sweepback*, (Appendix III), Journal of the Aeronautical Sciences, Vol. 14, No. 10, pp. 547–560, October, 1947.

[3] Cahill, W. F., and Levy, S., *Computation of Vibration Modes and Frequencies on SEAC*, Journal of the Aeronautical Sciences, Vol. 22, No. 12, pp. 837–843, December, 1955.

[4] Mack, C. E., *Tensor Analysis of Aircraft Structural Vibration*, Presented at the Sixteenth Annual Meeting, IAS, New York, January 26–29, 1948 (IAS Preprint No. 104).

[5] Clerc, D., *Sur le Calcul par Itération des Modes Propres d'Ordre Supérieur*, La Recherche Aéronautique, No. 54, 1956, and No. 56, 1957.

[6] Kappus, R., and Clerc, D., *Notice sur la Systématisation du Calcul des Vibrations d'une Structure Libre*, ONERA Mémo Technique No. 2, 1958.

A Note on Isentropic Compressible Flow of Air With Variable Specific Heats

K. E. Tempelmeyer and L. Self

ARO, Inc., Arnold Engineering Development Center, Tullahoma, Tenn.

January 2, 1958

Symbols

a, b, c = coefficients
c_p = specific heat at constant pressure, B.t.u./lb.m-°R.
J = mechanical equivalent of heat, 778, ft.-lb. f/B.t.u.
M = free-stream Mach Number
p = absolute pressure, lb.f/ft.²
R = gas constant for air, 53.35, ft.-lb.f/lb.m-°R.
T = absolute temperature, °R.
V = velocity, ft./sec.
γ = ratio of specific heats
ρ = density, lb.m/ft.³
λ = ratio of value for variable specific heat to value for constant specific heat

Subscripts

c_p = constant c_p
p = pressure ratio
T = temperature ratio
t = stagnation condition
ρ = density ratio

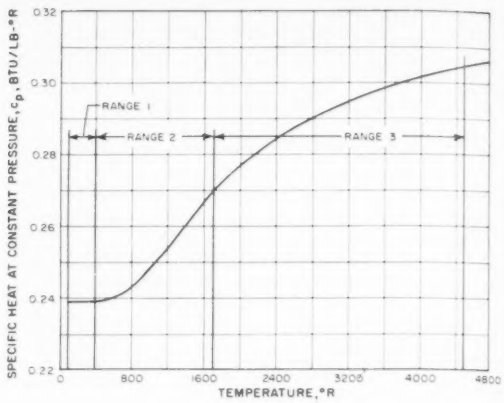

FIG. 1.

Discussion

COMPRESSIBLE FLOW RELATIONSHIPS are usually derived for a gas medium which has constant specific heats and an equation of state given by the perfect gas law.[1, 2] Since air satisfies these conditions accurately over only a limited range of pressure and temperature, use of the usual tabulated compressible relationships for air flows at high Mach Numbers can produce significant errors. However, compressible flow equations which are valid over considerably wider pressure and temperature ranges may be derived for air from the perfect gas equation of state if the variation of specific heat with temperature is considered (see Fig. 1). Equations derived with variable specific heats provide relatively accurate values when

$$0 < p < 3 \text{ atmos.}; \quad 300°\text{R.} < T < 4{,}500°\text{R.}$$

and in this range the additional complication arising from the use of a more complex equation of state (such as the Beattie-Bridgeman[3]) may be avoided.

Compressible flow relationships have been derived in reference 1 for a perfect gas with variable specific heats as well as with constant specific heats; however, because of the complex c_p-T relationship employed, the variable specific heat equations are somewhat difficult to use. Simpler relationships for compressible isentropic flow of air have been derived by using the perfect gas equation of state and relatively simple but accurate expressions for the c_p-T relationship.

The c_p-T curve has been separated into three ranges, as shown in Fig. 1, and empirical equations accurately fitted to each section of the curve with a mean c_p deviation of 0.2 per cent from the values of reference 4. The resulting equations are of the form

$$c_p = a + bT + cT^2 \tag{1}$$

The coefficients a, b, and c for each range are listed in Table 1.

Euler's equation for isentropic flow may be written as

$$\int V\,dV + \int c_p\,dT = 0 \tag{2}$$

If Eq. (1) is utilized in the integration of Eq. (2),

$$(V^2/2) + aT + (b/2)T^2 + (c/3)T^3 = \text{const.} \tag{3}$$

TABLE 1

Range	Temperature Range, °R.	Coefficients a	b	c
1	100–400	0.2393	0	0
2	400–1,700	0.2318	0.1040×10^{-4}	0.7166×10^{-8}
3	1,700–4,500	0.2214	0.3521×10^{-4}	-0.3776×10^{-8}

Then, if a stagnation condition is assumed at one point in the flow, Eq. (3) may be simplified to express the following relationship between static and stagnation temperature and stream Mach Number for isentropic flow of air with variable specific heats:

$$[(c/3)T_t^3 + (b/2)T_t^2 + aT_t] - [(c/3)T^3 + (b/2)T^2 + aT] = (\gamma RT/2J)M^2 \quad (4)$$

Since c_p is given by Eq. (1), γ may be determined from

$$\gamma = c_p/[c_p - (R/J)] \quad (5)$$

Eq. (4) may be written when T and T_t lie within a single temperature range or any combination of ranges by using the coefficients (a, b, and c) which correspond to the range of their particular temperature (see Table 1).

Static to stagnation pressure and density ratios may be obtained by evaluating the following form of the general energy equation for isentropic flow:

$$\int (dp/\rho) = \int c_p dT \quad (6)$$

If Eq. (6) is combined with the perfect gas law and Eq. (1) and the resulting expression divided by T, then Eq. (6) becomes

$$R\int (dp/p) = a\int (dT/T) + b\int dT + c\int TdT \quad (7)$$

Then, integrating and simplifying within a given single temperature range produces a relationship between pressure and temperature ratios for an isentropic process for air with variable specific heats, which may be written for a flow process as

$$p/p_t = (T/T_t)^{aJ/R} \cdot e^{J/R[b(T-T_t)+(c/2)(T^2-T_t^2)]} \quad (8)$$

If the substitution into Eq. (6) is accomplished in a slightly different manner, the expression for density ratio is obtained as

$$\rho/\rho_t = (T/T_t)^{(aJ/R)-1} \cdot e^{J/R[b(T-T_t)+(c/2)(T^2-T_t^2)]} \quad (9)$$

Eqs. (8) and (9) are valid when T and T_t are both within the same temperature range. Additional equations may be derived when the temperatures lie in any combination of ranges by writing an equation for each range at their common point—i.e., T = 400°R. for ranges 1 and 2 and T = 1,700°R. for ranges 2 and 3—and then equating the two equations. For illustrative purposes, the pressure ratio equation, when T and T_t are in ranges 1 and 3, respectively, is given below. All coefficients and constants have been inserted and simplified.

$$p/p_t = (1{,}700/T_t)^{3.229} \cdot (T/400)^{3.491} \cdot (0.00535) \times e^{[(2.753\times10^{-8})T_t^2 - (5.134\times10^{-4})T_t + 0.7932]} \quad (10)$$

These equations produce results which are in excellent agreement with results obtained from other equations based on variable specific heats, as in reference 1. The equations here, however, are easier to apply than those of reference 1. Additional comparisons with results produced by equations based on the Beattie-Bridgeman equation of state with variable specific heats[3] are also favorable. For example, at M = 3.5 and T_t = 1,100°R. the Beattie-Bridgeman based equations[3] gave T = 326°R., whereas the equations derived here yield T = 325.5°R., and those based on constant specific heat[1] indicate T = 322.6°R.

The errors associated with the use of the usual compressible flow relationship may be indicated by considering a typical flight condition of M = 5.0 at an altitude of 140,000 ft. The altitude defines the static conditions as p = 4.3 lb.f/ft.^{2} and T = 485°R., and if compressible flow relationships with constant specific heats are used, the stagnation conditions may be computed as

$$p_t)_{cp} = 2{,}275 \text{ lb.f/ft.}^2 \quad \text{and} \quad T_t)_{cp} = 2{,}909°\text{R.}$$

If the stagnation conditions are computed with variable specific heats, Eq. (4) may be used to determine the temperature; and, since T is in range 1 and T_t is probably in range 3, Eq. (10) may be used to compute the pressure. Thus, for variable specific heats,

$$p_t = 2{,}643 \text{ lb.f/ft.}^2 \quad \text{and} \quad T_t = 2{,}684°\text{R.}$$

It is apparent that the magnitude of the error associated with use of equations based on constant c_p is quite significant at high temperatures. Consequently, if the pressure and temperature are within the previously specified limits, the use of any equations based on variable specific heats is dictated by the magnitude of the stagnation temperature as illustrated below:

M	T_t, °R.	λp	λT	$\lambda \rho$
5.0	1,000	0.996	1.007	0.990
5.0	3,000	0.826	1.100	0.753

Thus, in general when the stagnation temperature is greater than 1000°R., the use of equations based on variable specific heat is indicated.

It is also possible to extend the method outlined here to develop flow equations for use across normal and oblique shocks. Also, by modifying the c_p-T relationship, equations may be derived for other gases which could be used for engine nozzle flow if the pressure level is within the prescribed limits.

References

[1] *Equations, Tables, and Charts for Compressible Flow*, NACA Report 1135, 1953.

[2] *Tables of Various Mach Number Functions for Specific-Heat Ratios from 1.28 to 1.39*, NACA TN 3981, 1957.

[3] Randall, G. E., *Thermodynamic Properties of Gases: Equations Derived from the Beattie-Bridgeman Equation of State Assuming Variable Specific Heats*, AEDC-TR-10, 1957.

[4] Kennan, J. H., and Kaye, J., *Gas Tables*; John Wiley & Sons, Inc., New York, 1945.

Propagation of Weak Waves in a Dissociated Gas*

F. K. Moore

Head, Aerodynamic Research Department,
Cornell Aeronautical Laboratory, Inc., Buffalo, N.Y.

January 13, 1958

In a recent paper,[1] Resler has provided a study of the characteristic, or sound, velocity of a gas out of thermodynamic equilibrium. This note is concerned with a related topic—namely, the detailed study of the dynamics of weak, or acoustic, disturbances in such a gas. Various authors[2, 3] have analyzed the behavior of an acoustic wave subject to both dissociation and vibration relaxation, finding results consistent with the well-known phenomenon of ultrasonic absorption which depends on relaxation of internal degrees of freedom in the gas.

It is interesting to consider the equation which, for a dissociated gas, replaces the usual acoustic wave equation. Assumption of a particular wave form—e.g., harmonic—will be avoided. For purposes of illustration, attention is restricted to the effect of dissociation of a diatomic gas, so that the internal energy and average gas constant may be written as†

$$E = [(7 - \alpha)/2]\, R_0 T + \alpha q_0 \quad (1)$$

$$R = (1 + \alpha) R_0 \quad (2)$$

For small departures from equilibrium, one may write that the dissociation rate is proportional to the difference between the actual temperature and the temperature at which the existing dissociation level would be in equilibrium:

$$\partial\alpha/\partial t = K[T - T_e(\alpha, \rho)] \quad (3)$$

where K is a positive reaction rate depending on the average state of the gas.

Using Eqs. (1)–(3) in conjunction with the linearized disturbance equations,

* The investigation upon which this note is based was sponsored by the Bell Aircraft Corporation.

† Notation in this note follows Resler.[1]

$$\bar{\rho}(\partial u/\partial t) + (\partial p/\partial \epsilon) = 0 \tag{4}$$

$$(\partial \rho/\partial t) + \bar{\rho}(\partial u/\partial \epsilon) = 0 \tag{5}$$

$$\bar{\rho}(\partial E/\partial t) + \bar{p}(\partial u/\partial \epsilon) = 0 \tag{6}$$

$$\bar{p} = \rho RT \tag{7}$$

(where bars represent mean properties in the absence of disturbance), one may derive the analog of the acoustic equation. The steps are (a) manipulating Eqs. (1), (2), and (4)–(7), obtain an equation involving only T and α; (b) further linearize Eq. (3) by writing

$$T_e = \bar{T} + (\partial T_e/\partial \alpha)_\rho \Delta\alpha + (\partial T_e/\partial \rho)_\alpha \Delta\rho \tag{8}$$

and (c) insert Eq. (8) into the equation obtained in (a) and its time derivative, combining the results in such a way as to give

$$(\partial/\partial t)\,[(\partial^2 T/\partial t^2) - a_f^2\,(\partial^2 T/\partial \xi^2)] + k[(\partial^2 T/\partial t^2) - a_e^2\,(\partial^2 T/\partial \xi^2)] = 0 \tag{9}$$

where

$$a_f^2 = \bar{R}\bar{T}\,[(9 + \bar{\alpha})/(7 - \bar{\alpha})] \tag{10}$$

which may be shown to be the "frozen" speed of sound (for a disturbance during which α would remain constant); where, defining $Q \equiv 2q_0/R_0\bar{T}$,

$$a_e^2 = \bar{R}\bar{T}\,\frac{(9 + \bar{\alpha})\,(\partial T_e/\partial \alpha)_\rho + \bar{\rho}\{Q - [8/(1 + \bar{\alpha})]\}(\partial T_e/\partial \rho)_\alpha + \bar{T}(Q + 1)}{(7 - \bar{\alpha})\,(\partial T_e/\partial \alpha)_\rho + \bar{T}(Q - 1)} \tag{11}$$

which may be shown to be the "equilibrium" speed of sound (for a disturbance during which the dissociation level follows its equilibrium relationship with the properties of state prevailing at each instant, i.e., $T = T_e$), and where k is a positive quantity

$$k \equiv K\{(\partial T_e/\partial \alpha)_\rho + [\bar{T}/(7 - \bar{\alpha})]\,(Q - 1)\} \tag{12}$$

By reference to Eq. (3), it is clear that k is essentially a reciprocal relaxation time, or a dissociation rate.

Eq. (9), it may be noted, has the same form as the equation derived by Morrison[4] for the propagation of elastic waves when a time lag exists between stress and strain.

From Eq. (9), which, for a dissociated gas, replaces the acoustic wave equation for temperature, certain conclusions may immediately be drawn regarding propagation of weak disturbances.

In general, both "frozen" and "equilibrium" processes are involved in a disturbance. In fact, the form of Eq. (9) implies that the frozen and equilibrium operators are out of phase during a periodic disturbance, so that the propagation speed must vary markedly during each cycle. Thus, a mechanism for wave-form distortion is apparent even in the linear approximation, in contrast to the usual distortion or steepening of an acoustic wave, which is a nonlinear effect.

For an oscillatory process, the presence of the extra time-derivative in the left-hand term may be replaced, in effect, by a frequency. If this frequency is large compared to the dissociation rate (k), then evidently the frozen wave equation dominates the motion, and if the frequency is small compared to k, the propagation is governed by the equilibrium wave equation. In fact, harmonic solutions of Eq. (9) may easily be obtained which show this change of sound speed with frequency, or "velocity dispersion," in the terminology of the literature of ultrasonic absorption, as well as the attendant energy absorption in the frequency range where the change in sound speed occurs.

In general, any given wave packet would include both low and high frequency constituents. Therefore, since the frozen sound speed is generally the higher, there would be a tendency for the high and low frequency components to be sorted out, with the high frequency waves running ahead at the frozen speed. In fact, recent shock-tube experiments[5] conducted at Cornell Aeronautical Laboratory in dissociated bromine and oxygen indicate that the head of a steep expansion wave does indeed travel at a sound speed frozen in respect both to molecular vibration and dissociation.

While the foregoing conclusions are substantially known,[2, 3, 6] it is perhaps noteworthy that they follow directly from the differential Eq. (9). Since relaxation times are long at low densities, the flow behind a shock during hypersonic flight at extreme altitudes would involve wave processes complicated by the considerations discussed herein. The present approach, further developed, might be helpful in formulating an aerodynamic theory of weak disturbances for such a situation.

References

[1] Resler, E. L., Jr., *Characteristics and Sound Speed in Nonisentropic Gas Flows With Nonequilibrium Thermodynamic States*, Journal of the Aeronautical Sciences, Vol. 24, No. 11, pp. 785–790, November, 1957.

[2] Chu, Boa Teh, *Wave Propagation and the Method of Characteristics in Reacting Gas Mixtures with Applications to Hypersonic Flow*, WADC TN-57-213, May, 1957.

[3] Lighthill, M. J., *Survey in Mechanics*, "Viscosity Effects in Sound Waves of Finite Amplitude," (G. I. Taylor 70th Anniversary Volume), Cambridge University Press, 1956.

[4] Morrison, J. A., *Wave Propagation in Rods of Voigt Material and Visco-Elastic Materials with Three-Parameter Models*, Quart. Appl. Math., Vol. 14, pp. 153–169, 1956.

[5] Treanor, C. E., Golian, T. C., Hertzberg, A., *Measurement of Flow Properties in a Dissociated Gas*, Paper presented at the Tenth Meeting of Am. Phys. Soc. (Fluid Mech. Div.), Bethlehem, Pa., November, 1957.

[6] Wood, W. W., and Kirkwood, J. G., *Characteristic Equations for Reacting Flow*, Jour. Chem. Phys., Vol. 27, No. 2, p. 596, 1957.

Faculty of Science of the University of Paris

Symposium on Rarefied Gas Dynamics and Aerothermodynamics

Centre Universitaire Méditerranéen, Nice, France, July 2–5, 1958

This Symposium will be mainly concerned with the present position in regard to research being carried out on Rarefied Gas Dynamics and Aerothermodynamics. It will include theoretical and experimental studies on (1) aerodynamic and thermodynamic phenomena in highly rarefied atmospheres; (2) fundamental physical values that occurred in the preceding investigations—that is, on the accommodation coefficient and exchange momentum coefficients; and (3) apparatus and methods of measurement that relate to the field already covered in previous investigations.

Participants should submit a title and brief outline of the proposed paper as soon as possible to the Secretary: *Dr. F. M. Devienne, Laboratoire Méditerranéen de Recherches Thermodynamiques, 2 Avenue Villebois Mareuil, Nice, France.*